UNIVERSITAT POLITÈCNICA DE CATALUNYA
BARCELONATECH
Escola d'Enginyeria de Telecomunicació
i Aeroespacial de Castelldefels

TREBALL DE FI DE GRAU

TFG TITLE: A preliminary study of space debris mitigation based on a swinging tether system

DEGREE: Bachelor's Degree in Aerospace Systems Engineering

AUTHOR: Ivan Carmona López

ADVISOR: Santiago Arias Calderón

DATE: October 28, 2021

Títol: Estudi preliminar de la mitigació de la brossa espacial basat en una lligadura balancejant

Autor: Ivan Carmona López

Director: Santiago Arias Calderón

Data: 28 d'octubre de 2021

Resum

Des dels inicis d'enviar satèl·lits a l'espai amb l'Sputnik 1 el 1957, la humanitat ha estat enviant repetidament i despreocupadament més i més naus i satèl·lits fora de l'atmosfera sense adonar-se'n al principi de les repercusions futures que tindria. Les escombraries o deixalles espacials són el que s'anomena a les restes de les missions inoperatives. L'augment de la quantitat no és només rellevant en el camp de l'exploració espacial, sinó que a la llarga és un problema que afectaria la nostra vida quotidiana i fins i tot al propi estat del planeta Terra.

Aquest no és un problema ignorat, ja que moltes agències espacials van començar a tractar amb aquest problema de manera indirecta fent les seves missions espacials amb parts blindades adicionals per estar segurs de que cap deixalla externa danyés les seves missions. A més a més, recentment s'han desenvolupat alguns mètodes per detectar les deixalles, així com lleis espacials que recomanen alguns passos addicionals en les missions espacials que s'afegeixen a la idea de prevenir i intentar no incrementar el nombre de deixalles en òrbita.

També es discuteix un enfocament més directe, on en aquest document es presentaran diverses solucions d'eliminació de deixalles i al final se'n seleccionará una: el sistema de lligadures. Posteriorment, es presentarà un esquema del sistema, s'obtindran les seves equacions de moviment i el punt més òptim per alliberar les deixalles a una òrbita més baixa perquè es desintegri serà l'objectiu principal d'aquest estudi.

Al final s'afegiran les condicions inicials del sistema i, amb això, es discutiran diversos gràfics i conclusions. Tres d'aquestes condicions inicials se sometran a algunes iteracions per veure el grau d'afectació en tot el sistema per aquestes variacions en els paràmetres d'entrada.

Title : A preliminary study of space debris mitigation based on a swinging tether system
Author: Ivan Carmona López

Advisor: Santiago Arias Calderón

Date: October 28, 2021

Overview

Since the very beginning of sending satellites into space with Sputnik 1 in 1957, humankind has been repeatedly and nonchalantly sending more and more spacecrafts outside the atmosphere without caring at first the future repercussions of that. Space junk or debris are what the remains of all the inoperative missions are called. The rise in quantity is not only relevant in the field of space exploration, but in the long run is a problem that would affect our daily lives and even the state of planet Earth.

This is not an unaware problem, as many space agencies started handling this issue in an indirect way by making their space missions with extra shielded parts to be positive that no external debris will damage their missions. Moreover, recently some space debris detection methods have been developed, as well as space laws that recommend some extra steps in space missions that add to the idea of prevention and to try not add to the number of orbiting debris.

A more direct approach is also discussed, where several debris removal solutions will be presented and at the end one of them is selected: the tether system. Thereafter, a schematic of the system will be presented, its equations of motion obtained, and the determination of the optimal point to release the debris into a lower orbit to disintegrate it will be the overall objective of this study.

At the end, the initial conditions for the system will be added, and with that several graphs and conclusions will be discussed. Three of these initial conditions will be subjected to some iterations to see to which degree the whole system is affected by those variations of the input parameters.

ACKNOWLEDGMENTS

I want to thank my family and friends that stood by my side and tried to cheer me up in the most difficult moments, and congratulated me as well when things were back on track after a mental block.

Moreover, a virtual thanks to all the people in the forums of Matlab for helping me endless times to find the exact answer to the issues I had while typing the code for this project. In the topic of thanking strangers, part of the interest of delving into this TFG topic comes from a TV show called ”Planetes”. Acknowledgments to the creative team.

Last but certainly not least, I would like to thank my advisor Santiago Arias Calderón for the effort and dedication that he put to guide me along this project. From the countless times that we met to solve any issues and looked for the path forward, to the many suggestions and corrections that he made over my work. I am truly grateful and could have not asked for a better advisor.

”We’re in very bad trouble
if we don’t understand
the planet we’re trying to save.”

Carl Sagan

CONTENTS

LIST OF FIGURES

LIST OF TABLES

INTRODUCTION

Once a space mission's operative life is over, the people responsible for it can take action in two ways: one of them is to have planned a re-entry maneuver to get the orbiting object back to Earth, but often those inoperative missions stay orbiting the Earth, with the objective of disintegrating them via the atmosphere in the long run. However, in the eyes of other operative satellites and missions, those forgotten objects are considered space debris. Those debris are typically pieces of space craft and rockets (result of the collision between them), inoperative satellites and flecks of paint from spacecrafts that keep increasing in number every year [1]. The amalgamation of space debris is a problem specially relevant in LEO orbits, where one could say that they have become an orbital graveyard. Figure 1 shows how the atmosphere is covered in this black layer composed of numerous black dots; the clutter in these low altitudes is caused by the over saturation of the orbit, as its closeness to the surface of the Earth allows the satellites to take images of higher resolution. In addition, telecommunication satellite constellations are usually deployed in LEOs to cover more regions in Earth as they would in higher altitudes [40].

If we jump into higher orbits as depicted in Figure 2, the over saturation in lower orbits becomes even more apparent. Moreover, the importance of geosynchronous orbits also emerge from observing it. That is because any object at that altitude orbits the Earth with a period of 24h, the same as the rotational motion of the Earth. Thus, the geosynchronous orbit is a valuable spot for monitoring weather, surveillance or communications over a specific area of the world [41].

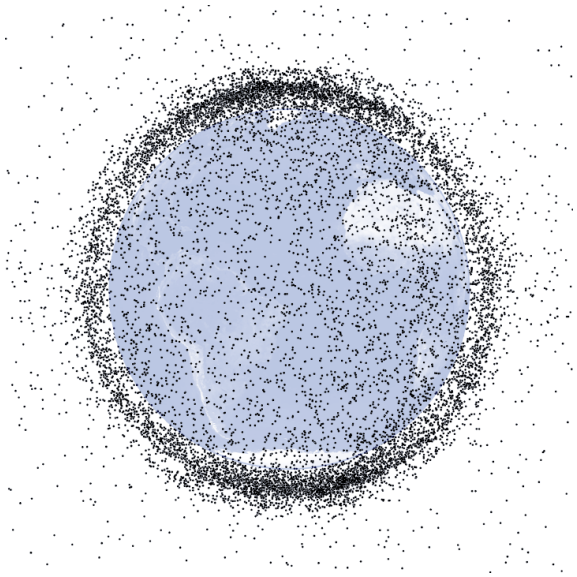

Figure 1: Low Earth Orbit debris illustration [2]

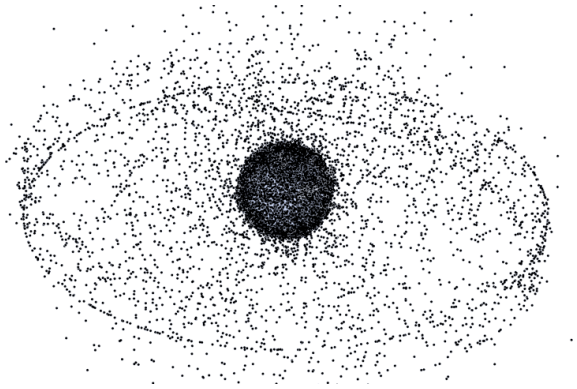

Figure 2: High Earth Orbit debris illustration [2]

To put into perspective the figures above, Table 1 depicts ESA's updated list of estimated data about debris and satellites in Earth orbits. The estimated objects go from 34000 objects greater than 10 cm to more than 128 million remains from between 1 mm and 1 cm; there is an exponential increase of debris as we keep decreasing their size.

Perhaps the most concerning fact about these data is that less than 30000 debris objects are fully tracked, which means that most of the times what can be done to avoid a potential collision with space debris is reactive avoidance, and not a proactive solution. This first chapter is about the way that current technology is able to detect those orbiting debris, and how each region of the world reacts to the space debris issue.

Launches since 1957	$\sim$ 6020 (excluding failures)
Satellites placed into orbit	$\sim$ 10680
Satellites still in space	$\sim$ 6250
Satellites still functioning	$\sim$ 3600
Tracked debris objects	$\sim$ 28210
Anomalies due to fragmentation	$>$550
Total mass of space objects	$>$9200 tonnes
Debris objects ($>$10 cm)	34000
Debris objects ($>$1 cm and $<$10 cm)	900.000
Debris objects ($>$1 mm and $<$1 cm)	128 million

Table 1: Latest estimated numbers about space debris (as of January 8th, 2021) [3]

CHAPTER 1. SPACE DEBRIS: RISKS AND MITIGATION

One of the first topics to be brought up in space debris history is the so called "Kessler Syndrome or Effect". That is a concept first proposed by Donald J. Kessler in 1978, one year before NASA began its official Orbital Debris Program, and it tells us that Earth's low orbit has so much density of objects that a single collision is enough to develop a cascade, in which each collision generates space debris that increases the likelihood of further collisions [4].

Since the discovery of that syndrome, currently it is still unknown formally that such cascade effect has occurred. What we do know is that the mass of the orbital population has increased by more than three hundred objects each year [4].

The increase in debris not only is worrying due to the congestion of space and consequent difficulty in doing tasks such as space exploration and astronomical observation, but also is dangerous for the existing satellites and modules already orbiting the Earth, as debris in a low earth orbit can achieve velocities of 8 km/s [5], making their collision with satellites a fatal accident.

1.1. Current detection methods

Nowadays there are more precise methods of detecting and extrapolating the number of debris orbiting the Earth. For instance, in Europe ESA has the Meteoroid and Space Debris Terrestrial Environment Reference (MASTER) and the Debris Environment Long-Term Analysis (DELTA) tools available [6].

MASTER uses the information derived from all the known generated debris, and determines impact flux information for a given satellite. It can cover sizes of debris of the order of micrometers, and predict their trajectories in the environment until 2050. Figure 1.1 is a screenshot of MASTER program; in the left the user inputs the thresholds and the desired time intervals to study, and then the program obtains the plot in the right side, which graphs a spatial density with respect to the altitude and declination (i.e., the angle from Earth's equator to a point north or south from that line) of the region of study. A mesh is created, where the peaks in the surface show the densest regions, in the case of Figure 1.1 being the cases of $\sim$ 800 km of altitude in the declinations of 80^{o} and -80^{o}.

This program will have an updated version that will also allow to assess the flux characteristics in Lagrange point orbits. These points are valued because they are the locations where the gravitational pull of two large masses equals the centripetal force required for a small object to move with them [42]. This means that any satellite sent there will remain in place.

Another tool that is used especially for long-term forecasts is DELTA, that examines different debris environment scenarios if we input some mitigation measures.

DELTA uses a semi-deterministic model that usually extracts the initial population from the previous program MASTER, then, it forecasts the evolution of the objects larger than a previously defined size, in low, medium and geosynchronous Earth orbits, for several decades.

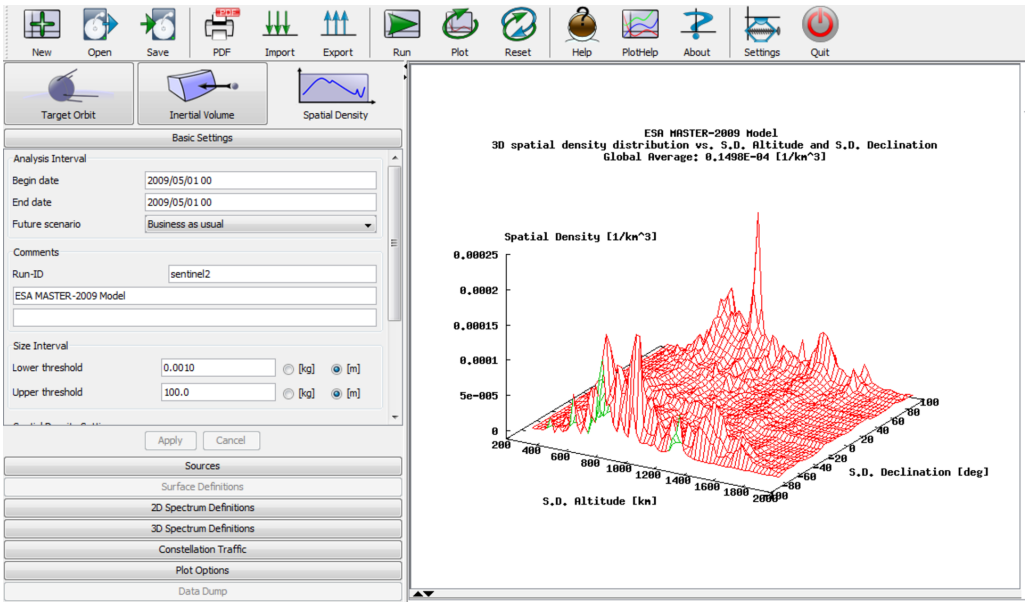

Figure 1.1: Screenshot of MASTER software tool [6]

The collisions between objects are first predicted with a tool that is target-centred to an object and it does the prediction stochastically. Then, it is computed via a model used by NASA: the EVOLVE 4.0 break-up model, that is a program that went through several iterations [7]; the last one added additional tracking and radar resources, perfected the estimations, as well as extended the time window period from which to observe the decay of objects.

Debris of an environment are fragmented due to explosions or collisions, and the number, size and mass of the fragments are estimated with results that are, with each iteration of EVOLVE, closer to reality as time flows.

1.2. Space regulation

Any space mission has its launch phase, where it tries to surpass Earth's gravitational pull. To do so it is more efficient that launch vehicles have several separate stages. Alas, it also means that whenever phase separations happen these elements will begin to roam around Earth's orbit, unless the stages come back to Earth [8], with a consequent chance of falling into Earth's surface while not being able to disintegrate fully.

The Inter-Agency Space Debris Mitigation Coordination Committee (IADC) is an international forum of governmental bodies for the coordination of activities related to debris in space. 13 space agencies are the members of this committee, including names such as NASA, ESA and JAXA. In 2002 the IADC created the Space Debris Mitigation Guidelines, which every mission should consider in every phase of an operation (launch, mission and disposal). This list, however, is not mandatory. Each country (regardless of it being a part of IADC or not) has the right to follow or to ignore some or all of these guidelines; a summary of the seven of them is described in Table 1.1.

IADC, in its guidelines document, also states that in case a space object needs to de-orbit and burn into the atmosphere, it should not take longer than 25 years to do so, to minimize the possible collisions it would produce [11].

The aforementioned rules are all referring to the mitigation solutions; the indirect approach; the prevention aspect of the problem. However, the Committee also tells us what to do when the objective is to launch a system to remove debris [10].

The theory states that if a space object damages one of another country, if the action can be proven, the culprit must take responsibilities. It is also stated that a country, currently, is not responsible for its own debris in outer space. In the future, though, when a series of countries will have their own space debris removal objects, it will be essential the co-operation between countries to allow the removal of other countries' debris, as well as to encourage each of them to control their debris and to remove them as much as possible.

Guideline	**Comments**
Limit debris released	If by design the not release is not feasible, at least the debris should be minimized.
Minimize the potential for break-ups	Failure modes that lead to accidental break-ups should be replaced with disposal and prevention measures.
Limit the probability of accidental collisions	The probability should be estimated and limited. If a potential collision is detected, an adjustment of the launch time should be considered.
Avoid intentional destruction	If intentional break-ups are necessary, they should be conducted at low altitudes to limit the lifetime of the resulting fragments.
Minimize post-mission break-ups resulting from stored energy	All on-board sources of stored energy should be depleted when they are no longer required for mission operations.
Limit the long-term presence of stages in LEO region after a mission's end	Low Earth Orbit graveyards should only be planned as long as the disposed objects have a short-term presence.
Limit the long-term presence of stages in GEO region after a mission's end	Leaving objects in orbits above the GEO region should be considered, to avoid future potential collisions near the GEO region.

Table 1.1: Main guidelines proposed by the IADC in Vienna, 2010 [9]

1.3. Prevention and mitigation

As seen before with the space debris guidelines, the focus right now is on the mitigation of debris with upcoming missions, not in removing the existing ones.

Apart from the aforementioned IADC, each individual space agency around the world is trying, each one with its own differences, methods to try to decrease the amount of debris created, or procedures to avoid them.

Russia for instance, alongside the previous guidelines, kept track of the detected objects with distances less than 50 km from each mission, as well as also tracking the events with distances less than 10 km. Finally, they focused on one of their missions, the Express AM-11, and they performed the necessary correction maneuvers to then extract some conclusions that later would be proposed as additions to the already established IADC guidelines [12], as seen in Table 1.2.

Project Title	**The Proposal**
Unmanned spacecraft, estimating mass of remaining usable propellant	Measurements of fuel remainders should be included as reference
Management for Debris Mitigation	To harmonize the Standard with STSC Space Debris Mitigation Document
Disposal of Satellites Operating at Geosynchronous Altitude	The Standard should be based on the ≪IADC Space Debris Mitigation Guidelines≫

Table 1.2: Russian proposals for space debris mitigation [12]

ISRO, the Indian Space Research Organisation, initiated in 2019 Project NETRA [13], which is a warning collision system in LEO orbits for their satellites, and it can track and catalogue objects as small as 10 cm. Although their priority is to develop that tracking system to be able to detect collisions in GEO orbits and also to protect their satellites from other's countries range, the focus on mitigating space debris to protect their missions is also there.

Although the majority of countries in the world meet and even expand the Space Debris Mitigation Guidelines, there are some countries that opt for not following them to some degree. That could be due to, for instance, the space agency determining that other mission requirements are more important, and leaving the debris mitigation in a lower position within the priority list.

This is the case of China: in April of this year 2021 they launched a rocket, the Long March 5B, which was not programmed to make a reentry into the Earth and land properly. Instead, they planned to let the rocket fall and disintegrate into the atmosphere. However, as the rocket was out-of-control, in practice it was considered as space debris [14]. The European Space Agency estimated a "risk zone" that affected several countries, but in the end the debris landed south of India in the sea, as can be seen in the estimated area of landing of Figure 1.2.

Figure 1.2: Estimated area of landing of the Chinese rocket Long March 5B [14]

NASA and other space agencies criticized China for not planning a so-called ”graveyard orbit” to place their rocket once its usage was over, or try and effectuate a controlled reentry mission, where the rocket would be re-used as the ones Space-X creates. This shows that although the guidelines are optional, that does not mean that this issue can be taken lightly, as many political issues and human lives are taken into account in this regard. And as time passes those regulations will tend to be less and less optional due to the problem of space debris being increasingly more worrying.

CHAPTER 2. ACTIVE REMOVAL SOLUTIONS

Besides prevention and mitigation, there are some Agencies such as JAXA in Japan with its Debris Removal Satellite ELSA planned to be tested [15], and SpaceX with its Starship mission [16], that are already looking up a direct approach to clean up space debris using their missions. In that regard, NASA proposed a classification of the active debris removal methods and their viability in the nearby future [17].

It must be noted that the methods listed in this classification are not the only ones currently being studied. Methods such as solar sails and solid rocket propulsion modules could also be listed, but they will not be considered due to the lack of information and higher complexity with respect to the other solutions.

All the technologies aiming to remove space debris ideally would want to clear the higher amount of objects possible, i.e., the smaller ones. That is because the number of them is several orders of magnitude higher, as seen in Table 1. However, with our current technology, the removal of the small-sized debris is out of the scope of any solution. That is why all the listed removal methods focus on the larger objects: because they are easier to be detected, are more stable in their shape, and their number is several orders of magnitude less than the smaller debris objects.

2.1. Lasers

Lasers emit light through a process of optical amplification, that is based on the stimulation of electromagnetic radiation. That process is the reason why the beam of light can be so focused in a point. In the case of aiming to space debris with it, the intention of destroying a large debris object with it would not be feasible, as the laser would need to be steadily and slowly disintegrating every inch of the object. Instead, letting the beam deviate or displace debris from its original orbit would be an easier task, and it would reduce the application time of the laser.

The physics behind this deviation phenomenon are the following: the beam would add an extra force to the equations of motion of the irradiated piece of debris; that addition would result in a modification in the semi-major axis of the debris, lowering or raising it depending on the orientation of the beam at the moment of the application. While it is true that the most interesting solution would be to lower debris orbits to eventually cease the trajectory of the object, the act of raising a target's orbit could be used as a way to, in short terms, bring that debris into a space region less cluttered and with less risk of colliding with another object.

The laser methodology is depicted in Figure 2.1, where from a given point in space, and throughout a certain arc of the trajectory, the laser keeps applying a net force to the target, that at the end results in the debris raising (or in this case, lowering) the altitude of its orbit.

This beam solution is quite troublesome because it interferes with space law and generates possible conflicts with the potential shooting of an undesired space object property of another country. Nevertheless, the debris contemplated in the methodology are large enough to be tracked without any possible mistake. The same could not be said if instead, the laser was aimed towards a smaller-sized debris, which would result in a higher chance of accidentally impacting another object.

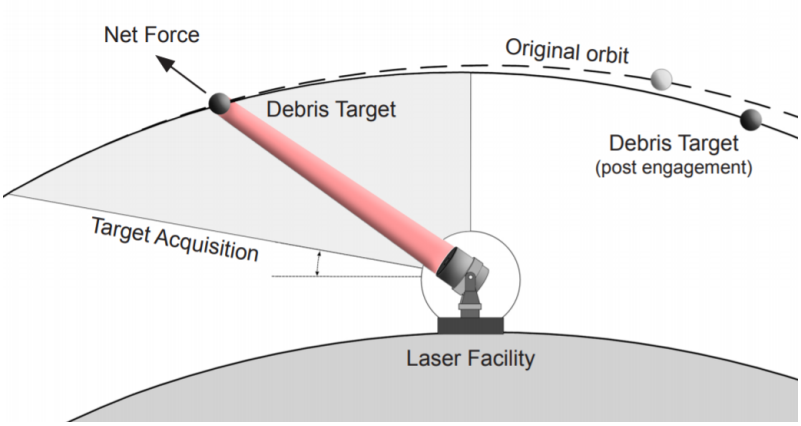

Figure 2.1: Schematic of a laser facility operating onto a debris target [18].

A study has been made that evaluated how a 5 kW and 10 kW beam deviated debris in Antarctica, the ideal location to install a facility that contained the laser, as that location has the maximum engagement opportunities with debris thanks to being situated in a pole, as well as due to the reduction of atmospheric beam losses and turbulence effects [18]. However, due to the unfeasibility of installing a laser in a harsh-environmental place such as the Antarctica, 3 other feasible locations were tested.

The *modus operandi* of this experiment is the following: the beam would be assigned to one target at a time for an average time of 103 minutes per day. Moreover, it would only be operative to engage an average of 10 objects per day, which makes the system one that still needs more research and optimizations to cope with the sheer amount of debris in low earth orbits.

Table 2.1 shows the locations and their altitude in the globe, for each power level of the laser; success rates are defined then to each of these scenarios. They are the number of space objects deviated from 50 to 1000 meters away. Objects deviated 50 to 100 meters have a mass of more than 100 kg, thus being comparatively less affected in their trajectory as opposed to the smaller-sized debris, which comprises from 200 m to 1 km of deviation. These smaller debris sizes vary from locations, but the smallest size to be detected is around 10 cm in diameter.

	Site Parameters		**Success Rates**				
Power	**Location**	**Altitude**	**50 m**	**100 m**	**200 m**	**500 m**	**1000 m**
5 kW	PLATO, Antarctica	4.09 km	74	56	43	13	5
5 kW	AMOS, Hawaii	3.00 km	30	13	5	4	2
5 kW	Mt. Stromlo, Australia	0.77 km	11	4	4	3	0
5 kW	Eielson AFB, Alaska	0.50 km	31	12	5	4	2
10 kW	PLATO, Antarctica	4.09 km	89	74	56	34	13
10 kW	AMOS, Hawaii	3.00 km	42	30	13	5	4
10 kW	Mt. Stromlo, Australia	0.77 km	29	12	4	4	3
10 kW	Eielson AFB, Alaska	0.50 km	48	31	12	4	4

Table 2.1: Success rates of a debris-deviating beam in several locations [18]

Targets are all approximately sun synchronous and that explains why the results differ so much between the Antarctica and the other locations: because space objects elsewhere are more difficult to track. Moreover, the results show that the increase in double the power in the beam does not turn out in an increase in double the debris displaced, but rather an improvement of +25% of the objects deviated with 5 kW of power. The results in Amos, Hawaii and Eielson, Alaska turn out to be rather similar but for different cases: Alaska thanks to it being in a high latitude and Hawaii because the altitude of the laser placement is nearly as much as in Antarctica.

2.2. Web capture

A web capture system would be optimal for the small and medium sized debris scattered around low earth orbits. These webs would be made of zylon, a very strong and thermally stable material which is used for instance in tennis racquets and some of the Martian rovers [19]. The negative part about this model is that these webs cannot handle the enormous velocities of the medium and small sized debris objects, so they are mostly suited for large objects.

As shown in Figure 2.2, a web capture would intentionally deform the strings from which the web is composed of. That would decelerate the debris velocity and thus creating a reaction force that the web's material must endure. Moreover, the shape of the grid also impacts on the capabilities of repulsion.

The simulation was made by assuming an initial target velocity of 100 m/s and a kinetic energy of 1.6 MJ. In Figure 2.2, it is depicted the different shapes that were considered in the design of the web that would catch the debris and, similar to the way spiders use octagonal shapes to build their cobwebs, the space web shape that is more resilient to impacts is the octagonal one, as opposed to a squared shape.

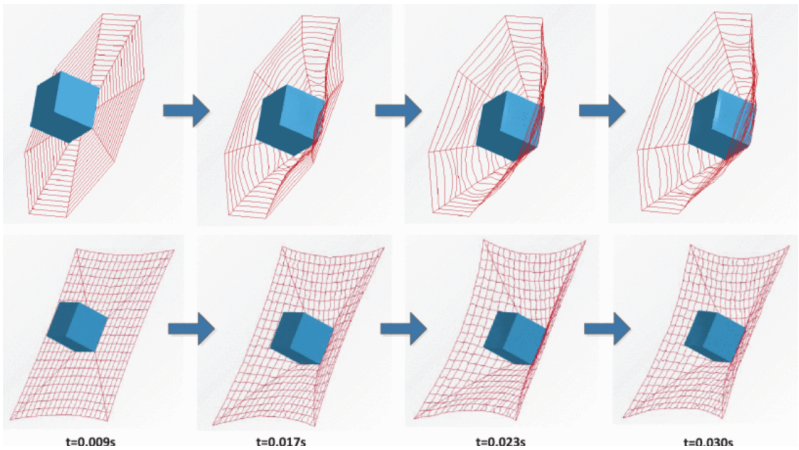

Figure 2.2: Deformation of two webs with an object of 1x1x1m with a velocity of 100 m/s [19]

Once the catch were successful, the object or objects would be wrapped up by the web, that ideally thanks to the material's strength and high energy absorption properties would not create a hole in the mesh and instead would continue to close on itself until the ends of the web would be tied up, as visually represented in the following Figure.

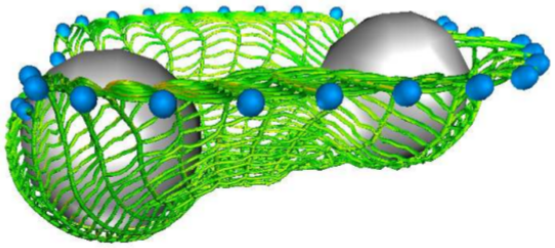

Figure 2.3: Wrapping process of the web around the target objects [20]

The wrapping process, when simulated [20], showed a strong dependency with the shape of the debris, the number of simultaneous catches, relative velocities and rotational angular velocities. Therefore, achieving a perfectly orthogonal catch (i.e., the velocity vector of the moving debris form a 90^{o} angle with the spread-out web) with an almost perfectly round target seems very unlikely.

This technology has already been tested in SpaceX [21], that contemplates to send the Falcon 9 with a Japanese Experiment Module inside. This mission, removeDEBRIS, would have a harpoon with a net to capture targets and also drag sails that would deploy to make the experiment fall into the atmosphere. The tests are already in place, where in 2018 they secured a 20 cm cube of a bit more than 1 kg. Two more tests were performed, the most recent one happening in march 2019, where two more cubes were secured successfully. However, this mission still has to be able to reduce its velocity (and thus, its orbital altitude) by deploying its drag sails to burn in the atmosphere upon re-entry.

2.3. Metal claws

A similar device to a web capture device is a claw-shaped one. The motion of the capture wouldn't be reactive as it is in the web solution, but instead would need to actively close its claws to the right position to capture the target.

ESA signed at the end of 2020 a contract alongside a Swiss start-up named ClearSpace S.A., which states the intention of launching the debris removal mission ClearSpace-1 in 2025 [22]; This would be ESA's first space debris removal mission.

The mission is expected to be launched initially to an orbit of 500 km and then to begin the rendezvous maneuver to reach a payload adapter that was used by the Vega launcher in 2013, and since then has been wandering in space. This payload adapter has a diameter of 1 m, a mass of 112 kg and an orbital altitude of around 600 and 800 km. The target is catalogued as a small size satellite, thus enabling the metal claws to correctly close on themselves further securing the target as opposed of a hypothetically larger object, where the same claws would be more loose.

Once the target is secured (depicted in Figure 2.4), both the metal claws and the satellite would start descending into the atmosphere to disintegrate steadily. This means that the claw debris removal system, at least conceptually, would involve a one-use-time usage. ESA's plan is to use those types of missions not only to remove space debris, but also to allow in-orbit refuelling and servicing of other satellites, extending their life-span [22].

Figure 2.4: ClearSpace-1 simulation where it captures Vega's payload adapter [23]

2.4. Spaceblower

Similar to lasers, another technology whose intention is to deviate debris and not erase them is the Spaceblower [24]. It consists in a rocket that would be sent once we knew a collision between two satellites would happen no matter what. To avoid that, and with the mindset of not wanting to generate even more debris, a three-phase rocket would be deployed.

The procedure of the Spaceblower, once it was about a hundred kilometers away from the target, would be to rotate itself so that the nozzle of the Spaceblower pointed towards the incoming debris object. Then, it would spray out a cloud of particles of around 5 microns across, made of materials abundant in Earth such as copper [24]. This spray would collide with the debris in question, deviating the object of its current trajectory or, by spraying the object in the opposite direction of the movement of the debris, decelerating the object's motion enough to avoid any potential collision.

A visual representation of the moment of the spraying is depicted in Figure 2.5, where the arc in the bottom illustrates the current phase at which the mission is at the moment, the ejection of particles is during a 10 second time-window, at a distance from the target in that instant of 100 m, and an altitude of 800 kilometers. The debris in question is around 12 meters in diameter, so at the moment the project is aiming to deviate the largest orbiting objects. The particles ejected by the nozzle would slow down the debris velocity by 10 cm/s, then to let the Spaceblower fall into the atmosphere once its goal has been completed.

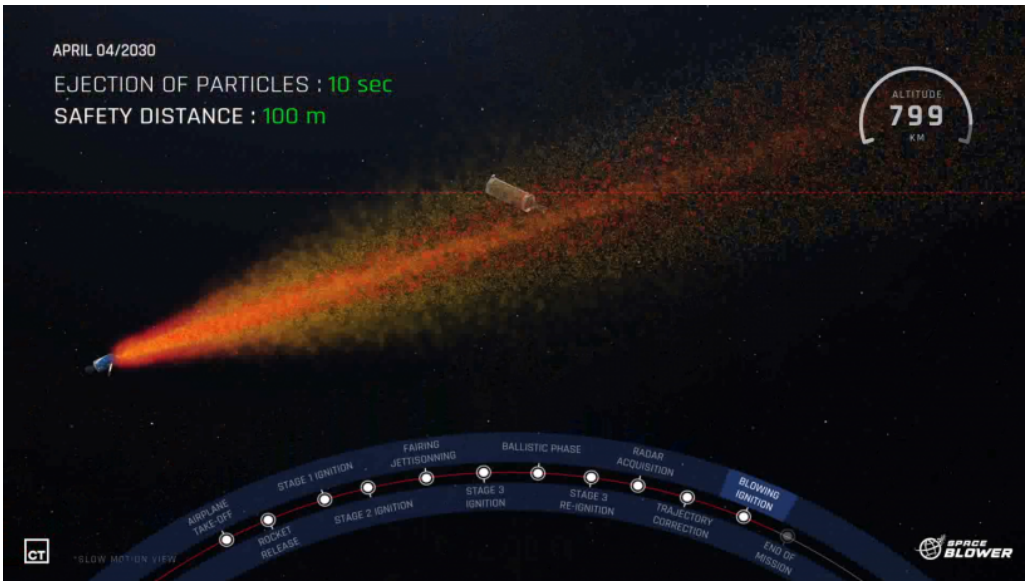

Figure 2.5: CNES' Spaceblower ejecting particles to deviate the debris' trajectory [24]

CNES, the French Space Agency behind the design of the Spaceblower, is aiming to have the first two stages of the mission reusable, with an estimated cost, after 5 or 6 launches testing it out, of 2 to 3 million euros. This technology, however, would only be deployed in gaps of 5 years or so, where a major debris collision would be detected and would be desirable to avoid, and their first testing is expected to happen in 2030.

2.5. Tethers

The last type of active debris removal technology in this classification is the Space Tether. It consists in a rope or thread that connects two end masses, where one of them is the payload (debris in this scenario), and the other end mass is the tether's main body, which could be a satellite or simply act as a counter mass with no usage outside of that.

The most interesting part about space tethers is their capability of staying in orbit while acting as a debris removal system: if the tether's main body is connected to an object with a lower orbit, the release of it would cause the payload to fall into a lower altitude (given that the bond with the main body resulted in the payload losing the speed it should have at that altitude). At the same time, that release would result in the rise of the orbit of the tether's main body. The same could be said in the opposite case, if the target were to be in a higher orbit than the tether's body, the bonding and then release of the object would result in the target reaching higher altitudes than before, and the main body having a lower orbit than before.

This principle, consequence of the conservation of momentum, enables the tether to have a multiple usage: on one hand, extending the rope into a lower object, that in all cases will be debris, would result in it falling into a lower orbit and thus falling and burning in the atmosphere. On the other hand, higher-altitude objects could also be targeted given that the release of debris would rise the orbit of our tether. By grabbing and then releasing other satellites that could need a higher orbit, our tether could once again reach a lower altitude and continue its operation of removing debris in a cycle of rising and lowering its orbit.

Figure 2.6 depicts an example of tether, where the main body is a satellite and it is tied to a debris object, which in the image is being burned up as a consequence of entering the atmosphere. The next step in this representation would be to release the object with the consequence being the rise of the satellite. Moreover, the rope would need to be reeled up to then be extended on the other side of the satellite. Then, by picking up and then releasing any on-demand satellite that could need an uplift, the tether would return to its initial orbit.

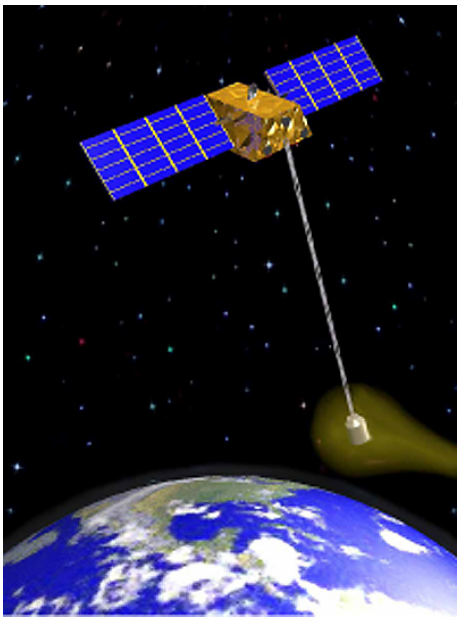

Figure 2.6: Space tether representation [25]

Space tethers can be modified or enhanced to complement autonomously the methodology described above. The simplest type of tether is the so called **hanging** tether, where the rope of the system is always in the direction of the gravity, and it does not spin whatsoever.

An upgrade in the efficiency if we want to optimize the debris removal part of the system would be the second type of space tether: the **swinging** one. This time the system will keep oscillating as a result of an initial perturbation of one of the end masses, as for instance a pendulum clock would do. This oscillation is beneficial if for example the payload is released at the point in the arc swing which the velocity of the end mass is minimal, or maximum. The method of obtaining that swinging initial condition will not be discussed in this TFG, as it will be assumed that as soon as the tether is fully joined, the swing will begin. Regardless, to be able to start the oscillations an external perturbation would need to be the catalyst in this type of tether.

The last space tether that could be designed is the so called **spinning** tether. The name is often interchangeable with the last tether type but the main difference is that this time the swing does not follow a pendulum-like trajectory, but rather a full 360º rotation, apart from the one that the tether performs around the Earth. To be able to achieve that constant spin an engine needs to be implemented in the center of mass of the tether, so that the extra push that the system would need to keep rotating is added and thus the full 360º spin is reached.

The concept of space tethers comes from a refinement of another idea, first proposed by Konstantin Tsiolkovsky in 1895: the space elevator. It would be a tower constructed tall enough to reach into space, and be held together by the Earth's rotation motion. Nevertheless, that concept required an unrealistic amount of resources to be implemented. The idea of joining objects of space to the Earth remained, though, as the next iteration of the idea was a concept proposed by Jerome Pearson in 1970: the moon elevator, that conceived an elevator that could go between the Moon and points at a given distance from it. After some more improvements over the idea, the concept was conceived not as means to join something to the Earth or the Moon, but to an artificial satellite. It was at that moment, in 1979, when NASA started to examine the feasibility of tethers that connected satellites to other objects such as other satellites, space probes or other astronomical objects, and the idea of space tethers were finally conceived.

Tether systems are currently being tested and researched. One example is the ESTCube-1, as depicted in Figure 2.7. It is one of the three satellite payloads that the VEGA launch vehicle brought to space in 2013. It is a cubic satellite developed by Estonia that once deployed extends a conductive tether for testing electric solar wind technologies [26]. This satellite happens to be the first in the world that used that technology, and is one of the several examples of satellites that use tethers in space with the objective of testing or analyzing, or as it is called, they use tethers as probes.

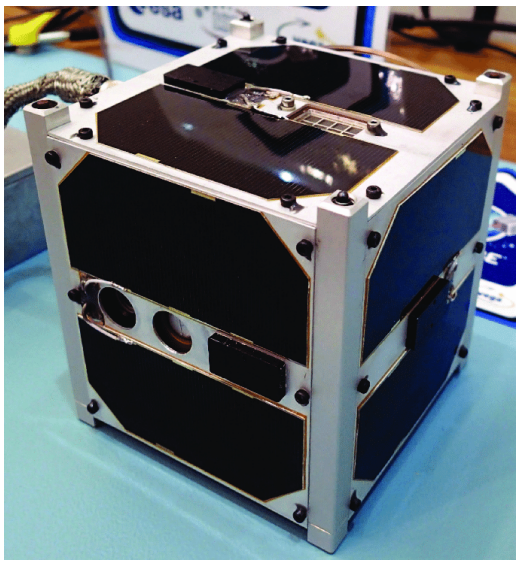

Figure 2.7: Assembled ESTCube-1 at the Guiana Space Centre [27]

In addition to the base idea of space tethers, they could be attached not to the desired debris object but to an adhesion compartment instead. In this regard NASA proposes space tugs that would be attached in between the target and the end rope, the other end being the tether's main body, such as a satellite [29]. This addition to the base idea of a tether would allow to de-orbit objects from further away orbits, as well as to gain a much powerful grabbing force to make sure that the debris does not detach the tether.

In this classification, tethers are not considered as a probe, but as a pendulum. This means that the objective in mind is not to deploy the tether's rope and take measurements with it, but rather to connect the other end of the rope and with that achieve some kind of motion. This is the methodology behind the space debris removal with tethers, as they are based on momentum exchange between both ends of the rope to, for instance, lower the orbit of the payload attached to the tether, at the expense of the system gaining altitude [28]. On the other hand, it could also drop the payload into a higher orbit, causing the tether's main body to lose altitude. This concept is the key idea of the space tether and this TFG objective.

The swinging tether has been chosen over the other two types of tether because the pendulum movement that it provides is a direct improvement from the hanging tether and and it is not too complicated to implement it. Nevertheless, due to the increase in complexity due to the addition of an engine, the spinning tether will not be considered. The reasons why the tether system as a whole is also picked over the other aforementioned debris removal solutions are listed in Table 2.2.

Laser technologies would be around 1 or 2 million dollars in overall cost, would be reusable as the laser would always remain in the same place in Earth, with enough precision it could deviate objects of 10 cm in diameter but always one at a time, to prevent undesired laser impacts to other countries' satellites.

In the case of the web capture, if we use the definition of the kinetic energy $K = \frac{1}{2}MV^2$ and apply it to the simulation values of a kinetic energy of $1.6 \cdot 10^6$ Joules and a target velocity of 100 m/s, we get a target mass of 320 kg. Furthermore, multiplying that value by the average of 10000$ that costs launching a 1 kg object to a low Earth orbit [30], we obtain a launch cost of 3.2 M$, to which we should also add the costs of the zylon web construction. Depending on the nature of the debris and the objective in deploying the web, instead of burning into space the wrapped target could be reeled back into a space station, making the deploy of another web possible and, thus, accounting for re-usability. Moreover, various small enough debris could be captured at the same time making the multi-target capture a reality.

The metal claws target is a satellite of 112 kg of mass, which implies a cost to be sent into space of 1.2 M$, plus the construction of the claws cost. The designers at ESA are already working on the design of space claws that could embrace more than one object.

Spaceblower already has an estimated cost of 2 to 3 million dollars, but the debris that is intended to be deviated is of 12 m of diameter, making the targets of this solution the largest in the classification.

Tethers are the most difficult to predict cost-wise, because they can be of several types, one of them incorporating a motor in its center of mass, that would add to their cost. However, what can be said about tethers is that they can be reusable by altering their altitude via rising and lowering space objects on the other end of the rope.

For this reason, space tethers are the only solution that could also be applied to rise other satellites orbits, as well as to remove debris, of course. Hanging tethers have been tested by testing and checking space conditions via a probe in one end of the tether's rope, although a test in a swinging tether in order to remove debris is yet to come.

This TFG has chosen the tether because, among the solutions that feature re-usability (the most attractive characteristic in order to seize the launch of an object to space), tethers were the ones that had other applications while keeping their objective of removing space debris. With that exchange, fuel cost once the system is already orbiting would be none, as opposed to other removal systems. Proper tethers, though, would be the spinning type, so that their other application of rising other satellites to maintain the tether's orbit would not be necessary; but as previously stated it is considered the swinging type of tether, the one without an engine in its rope that instead relies on the pendulum-swing of the end masses of the rope to boost the debris to the atmosphere.

	Laser	**Web capture**	**Metal claws**	**Spaceblower**	**Tethers**
Operational cost	1-2 M$	3.2 M$ + web construction	$\sim$1.2 M$ + claw construction	2-3 M$	Variable
Debris' sizes available	$>$ 10 cm	$>$ 1 m	$>$ 3 m	$>$ 12 m	Order of meters
Re-usable	Yes	Kinda	No	Kinda	Yes
Already tested	No	Kinda	No	No	Kinda
Other applications	No	No	Yes	No	Yes
Multi-target capabilities	No	Yes	Yes	No	No

Table 2.2: Summary of the characteristics of each active debris removal solution.

CHAPTER 3. THE TETHERED SYSTEM

This chapter analyses the physics behind a tethered system, from which a series of expressions will be deduced and validated in order to interpret and characterize them.

3.1. Mechanical principles and elliptical parameters

Before jumping into the equations of motion that our swinging tether will have, this first part of the section sets the hypothesis that will be assumed in regards of the tethered system.

The rope that joins each end masses will be considered rigid, that is, the tether does not bend, undergo torsion or change in length once it connects both ends. Moreover, despite not happening in reality, in order to simplify the otherwise much complex problem, the end masses and the rope that ties them will be mass-less, with no moments of inertia.

Another hypothesis made to reduce the complexity of this analysis is to limit the tether's movement in a single spatial plane: it will be a two-dimensional study. This simplification changes the number of equations of motion from 2 to 1, and it reduces the complexity of the expressions at the expense of lacking the third dimension study. The number of equations may change, but the conclusions of this study will not differ with or without that extra parameter.

The last consideration comes from assuming the tether as a conservative system; this means that its mechanical energy will always remain constant. It also means that aerodynamic drag, solar radiation, electrodynamic forces and gravitational perturbations are neglected. This idea can be applied to obtain expressions based on the conservation of energy and momentum. But because those equations will be based on an ellipse, the first step is to define the parameters and expressions of the type of orbit that our tether will have: an elliptic one.

3.1.1. Elliptical orbit expressions

The parameters of an ellipse are shown in Figure 3.1, that depicts a given ellipse, where the Earth is one of the ellipse's focus. Those are defined such as the sum of the distances between both foci and a given point in the ellipse is constant. Instead of a constant radius, in an ellipse it is defined a semi-major axis (a in the representation), and a semi-minor axis (b in Figure 3.1). The parameter r in this scenario is the distance between one of the focus (the Earth in this case) and a given point set on the elliptic trajectory. Finally θ is the angle that the point has along the trajectory (or that object's direction): the true anomaly. To obtain an expression for r two more elliptical parameters are needed.

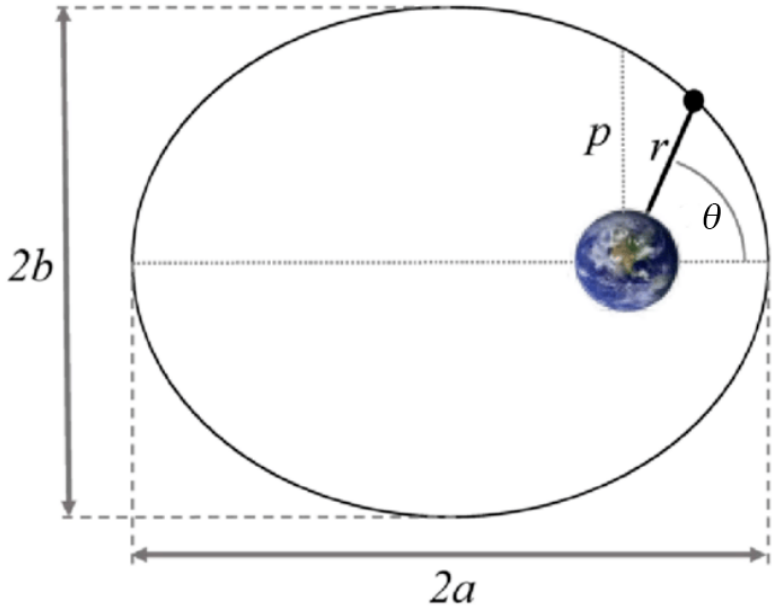

Figure 3.1: Visual representation of the parameters of an ellipse [32]

The first one is the eccentricity of an orbit, which characterizes the shape of the ellipse: whether it is more or less flattened. It is defined by a relation of the ellipse axis, where c is the distance from the center of the ellipse to one of its focus,

$$e = \frac{c}{a} = \frac{\sqrt{a^2 - b^2}}{a} \tag{3.1}$$

The other parameter that is needed is the semi-latus rectum p (already depicted in Figure 3.1) . It is the distance (perpendicular to the semi-major axis) from a focus to a point of the curve. It is a consequence of the system being ruled by Kepler's laws [37], and its expression is a result of the Pythagoras theorem application. It can be defined in multiple ways, depending on which parameter is more desirable: the semi-major axis a, the periapsis (shortest distance from the trajectory to the focus) R_{per}, or the apoapsis (longest distance to the focus) R_{apo}. In all cases the definition depends on the eccentricity of the orbit.

$$p = a(1 - e^2) = R_{per}(1 + e) = R_{apo}(1 - e) \tag{3.2}$$

With both p and e parameters defined, an expression for the (changing) radius of a point following an elliptical path as in Figure 3.1 is the following.

$$r = \frac{p}{1 + e \cdot cos(\theta)} \tag{3.3}$$

Expression 3.3 gives a way to obtain the trajectory of all the parts of the tether. However, an expression for the angular velocity $\dot{\theta}$ is missing, and to obtain it, the principles of conservation of energy and momentum are introduced.

3.1.2. Conservation of energy and momentum

Our tether system can be simplified as one object that, while it keeps subject another object (the debris), it is being attracted by the Earth, but as the tether is orbiting around the planet (or infinitely falling to it) in an elliptic trajectory, its mechanical energy is conserved [31]. This is equivalent to stating that the sum of the system's potential and kinetic energy at any point in the orbital trajectory will be the same. Equation 3.4 states this equivalence, where E, T and U are the mechanical, kinetic and potential energy, respectively. By substituting each energy with its definition, other parameters come to light, such as G, the gravitational constant consequence of connecting the gravitational force between two bodies; m and M, the masses of both objects; V, the total velocity of m; and r, the distance from the focus of the ellipse (the Earth) to the orbiting object.

$$E = T + U = \frac{1}{2}mV^2 + \left(-\frac{GMm}{r}\right) = constant \tag{3.4}$$

We can equal the mechanical energy for two points in the trajectory, for instance the apoapsis and periapsis, as well as changing the energy to a specific one (i.e., energy by unit of mass), which from rearranging gets us to expression 3.5. The subscript "apo" corresponds to the apoapsis parameters and "per" to the periapsis ones.

$$\frac{V_{apo}^2}{2} - \frac{V_{per}^2}{2} = \frac{GM}{r_{apo}} - \frac{GM}{r_{per}} \tag{3.5}$$

An absence of external momentum in a system equals to a constant angular momentum with respect to an arbitrary point [33]. With that in mind, a procedure similar to the conservation of energy can be made, where the specific angular momentums (H) in the apoapsis and periapsis of the elliptic trajectory are equal, obtaining with that an expression for the velocity at the periapsis,

$$H = r_{per} \cdot V_{per} = r_{apo} \cdot V_{apo} = constant => V_{per} = \frac{r_{apo}}{r_{per}} \cdot V_{apo} \tag{3.6}$$

Given that the apoapsis is the furthest distance from the focus of the ellipse and the periapsis the closest one, from Figure 3.1 an equivalence can be made,

$$2a = r_{per} + r_{apo} \tag{3.7}$$

By substituting expressions 3.6-3.7 into 3.5 the so called vis-viva equation is obtained [32]. It gives the orbital velocity of any point following an ellipse in its trajectory.

$$V^2 = GM\left(\frac{2}{r} - \frac{1}{a}\right) \tag{3.8}$$

3.1.3. Particularizing parameters

Going from the general case of an ellipse to our particular case of the swinging tether, prior to particularize the expressions to our tether, the rendezvous maneuver must be done, to connect the tether's main body to the orbiting debris. This TFG will not get an in-depth look into this procedure, as the initial point of the calculations is set when the tether is created. Nevertheless, there are some considerations regarding the rendezvous process.

The condition to rendezvous between the two objects is such as the distance from the tether to the target is much lower than the distance from Earth's center to the desired debris [36]. Figure 3.2 depicts both debris and tether when the rope would be deployed and the two end masses joined (indicated by the thick dotted line). At that moment a center of mass is created in the rope that will define the tether's orbiting trajectory as a whole. Each end mass has its own orbital radius and system of reference (depicted by the subscripts "tet" for tether and "deb" for debris), and those references have (in this section and across all the parametric study) their x-component following the direction of Earth's gravity, and the y-component being perpendicular and following the direction of the orbital motion. As soon as the system is created both distances from the center of the Earth to each end mass R_{tet} and R_{deb} will change their trajectories and it is at that moment that our parametric analysis will begin.

As previously stated the trajectory of the chosen debris is assumed to be close-to-circular. However, as soon as the tether is formed, that trajectory will become an elliptic one, similar to the tether's main body orbit but with its respective orbital parameters.

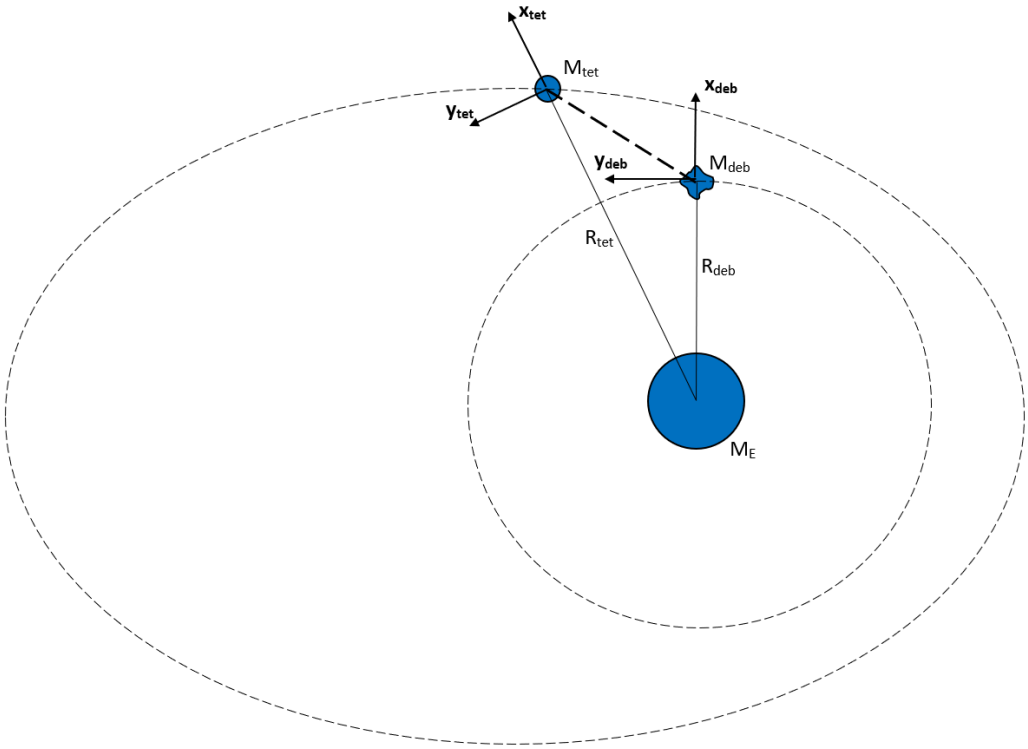

Figure 3.2: Diagram of the desired rendezvous maneuver

Targets in this study will be debris large enough to resemble the size of the main tether's body. That is due to the numerous debris of smaller size having a larger range of orbit altitudes, inclinations and eccentricities; debris of larger sizes (above 10cm in diameter) are more stable in their size and characteristics, including their close-to-circular orbits [35]. This is because the smaller sized debris are known by the breakup models that are primarily a result of fragmentation or collisions between larger debris objects, making their orbits more random and harder to predict. Clear concentrations and the best approximations that verify the close-to-circular patterns of large debris can be seen in less than 2000 km orbits (LEO), around 20000 km (semi-synchronous orbits, i.e., where objects have a period of rotation of 12 hours), and at 36000 km (GEO) [43]. This TFG analyses debris in LEO orbits as these are the closest ones to Earth and also because debris at lower altitudes have the benefit of being able to burn down into the atmosphere; an action that cannot be done at GEO altitudes.

When the tether is formed, the system's movement is ruled by the center of mass, that keeps the whole tether in place. Nevertheless, apart from that point the two end masses will be swinging as the tether orbits around the Earth. This means that our system should be perceived as three independent points, which happen to be united. However, as soon as the tether's rope is cut, all the elliptic parameters (eccentricity, semi-major axis, etc.) that we previously had and could consider as a whole are now separated intro three new packs of values: the ones of the new debris orbit, the new tether's main body orbit and the new center of mass (now imaginary) orbit.

With the expressions brought up due to the elliptical trajectory, and the tether already set and orbiting, the next step is to reach a parametric model that explains how the system moves and behaves.

3.2. Parametric model

The goal of this parametric model is to arrive to the equations of motion that the system has, and with them to obtain the velocities of each of the tether's parts along their trajectories. The swings that will affect the tether's behaviour are explained by the equations of motion that will be obtained.

3.2.1. Equations of Motion

If we took a picture of the swinging tether at any point in the trajectory, adding the angles and velocities that will be needed, Figure 3.3 would be the result of it.

This picture is divided into three sections, each one of them being the angles and velocities corresponding to either the tether's main body (subscript "tet"), the center of mass (subscript "CoM") and the debris (subscript "deb"). Each of these system sections has the parameters that fix their position in the plane of space: a radial component R and an angular component θ, each one with the corresponding subscripts. The only variable θ that will be considered along the study is that of the CoM, because neither that of the debris nor that of the tether's body is brought up in the upcoming expressions. This is the reason why that angle will not have any subscript at all.

Apart from θ, the other key angle in this study will be ψ, which is related to the pendulum-swinging of the tether, and is defined as the angle between the x-axis of the center of mass and the tether's rope. Therefore, when ψ is equal to 0, the sections debris-CoM-tether's body are aligned with the local gravity. Other angles that appear in Figure 3.3 are ϕ and λ; however, they are arbitrary angles needed in some calculations later in the chapter and will not take part in obtaining the equations of motion. At the same time, the three kinds of velocities (represented by the colors orange, green and violet) depicted in the figure will be useful afterwards, and will be brought up in the Release section.

The tether's center of mass CoM separates the original rope's length into two shorter L's: the one in the tether's side and the one in the debris' side. These lengths of the rope do not change, as initially stated, the tether's rope will not vary its length once it joined both tether and debris. They also meet the condition that the end masses and lengths are related such as $L_{deb} \cdot M_{deb} = L_{tet} \cdot M_{tet}$. This means that the relation between the two rope section lengths will be given by the relation of the masses of the tether's body and the debris.

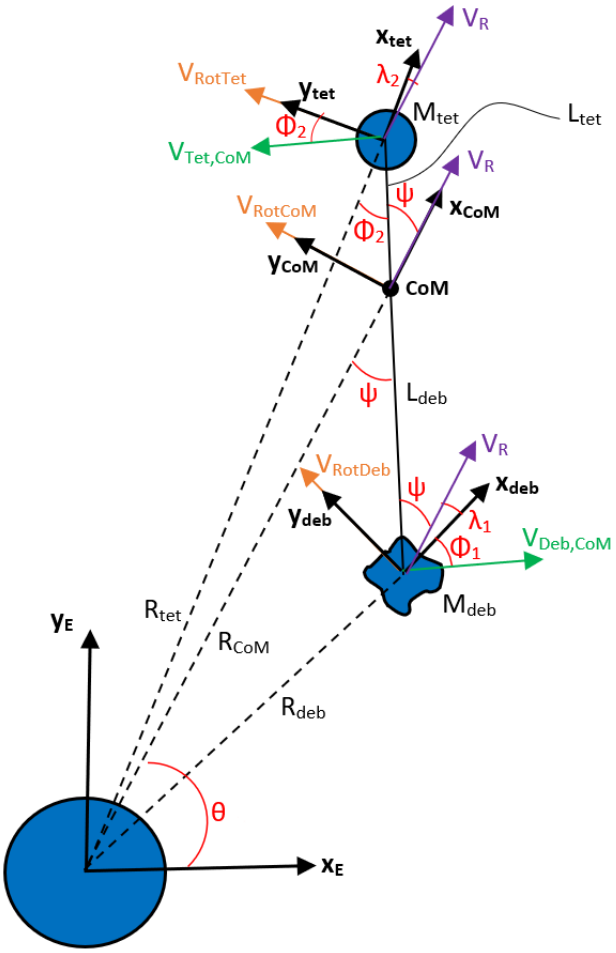

Figure 3.3: Geometry of a swinging tether in 2D

The initial elliptical trajectory of the tether system is given by two parameters: the varying radius that the center of mass has along the orbit R_{CoM}, and the angular velocity it achieves while doing that motion $\dot{\theta}$. The first parameter comes from equation 3.3, but with the addition that in the definition of this radius, the definition of p that will be taken is the one in expression 3.2, that has the periapsis as an input. Knowing that the Earth will be the focus of our elliptic trajectory, from now on the periapsis and apoapsis will be called perigee and apogee, respectively. That is, the planet Earth is the focal point of the ellipse.

$$R_{CoM} = \frac{R_{per}(1+e_{CoM})}{1+e_{CoM}\cdot cos(\theta)} \tag{3.9}$$

The time derivative of R_{CoM} is also defined as it will be relevant in later calculations.

$$\dot{R}_{CoM} = R_{per}(1+e_{CoM})\cdot \frac{e_{CoM}\cdot sin(\theta)\cdot\dot{\theta}}{[1+e_{CoM}\cdot cos(\theta)]^2} \tag{3.10}$$

The expression of the angular velocity of an elliptical object comes from equating the gravitational force and the centripetal force of the object along the orbit [45], but because it is an elliptical and not circular orbit, the term $(1+e\cdot cos(\theta))$ is added to compensate that at each point in the elliptical trajectory the orbital velocity will be different [46]. In the following equation, we also take into account that our desired angular velocity $\dot{\theta}$ is equal to the instantaneous velocity V over the radius of the orbit R_{CoM}. A new parameter μ is added in this equation, which is equal to the gravitational constant G times the Earth's mass M. The other mass m relates to the mass of the smaller object (the tether system in our case), but that parameter becomes irrelevant, as the only mass that is relevant in the angular velocity of an orbiting object is the one at the focus of the ellipse (the Earth, this time).

$$F_c = F_g[1+e\cdot cos(\theta)] => \frac{mV^2}{R_{CoM}(\theta)} = G\frac{Mm}{R^2_{CoM}(\theta)}[1+e\cdot cos(\theta)] => \dot{\theta} = \sqrt{\frac{\mu[1+e\cdot cos(\theta)]}{R^3_{CoM}(\theta)}} \tag{3.11}$$

With the main schematic introduced and the center of mass' expressions defined, the equations of motion will be now derived based on Lagrangian mechanics. The requirements to follow that formulation include having the expressions of the Cartesian coordinates of both the tether's body and the debris, as well as having obtained R_{deb} and R_{tet}.

By applying trigonometry in Figure 3.3, the Cartesian coordinates of the tether system end masses are the following:

$$x_{tet} = R_{CoM}\cdot cos(\theta) + L_{tet}\cdot cos(\psi+\theta) \tag{3.12}$$

$$y_{tet} = R_{CoM}\cdot sin(\theta) + L_{tet}\cdot sin(\psi+\theta) \tag{3.13}$$

$$x_{deb} = R_{CoM}\cdot cos(\theta) - L_{deb}\cdot cos(\psi+\theta) \tag{3.14}$$

$$y_{deb} = R_{CoM}\cdot sin(\theta) - L_{deb}\cdot sin(\psi+\theta) \tag{3.15}$$

The time derivatives of the previous equations with respect to time are relevant enough to be listed as follows:

$$\dot{x}_{tet} = \dot{R}_{CoM} \cdot cos(\theta) - R_{CoM} \cdot \dot{\theta} \cdot sin(\theta) - L_{tet} \cdot (\dot{\psi} + \dot{\theta}) \cdot sin(\psi + \theta) \tag{3.16}$$

$$\dot{y}_{tet} = \dot{R}_{CoM} \cdot sin(\theta) + R_{CoM} \cdot \dot{\theta} \cdot cos(\theta) + L_{tet} \cdot (\dot{\psi} + \dot{\theta}) \cdot cos(\psi + \theta) \tag{3.17}$$

$$\dot{x}_{deb} = \dot{R}_{CoM} \cdot cos(\theta) - R_{CoM} \cdot \dot{\theta} \cdot sin(\theta) + L_{deb} \cdot (\dot{\psi} + \dot{\theta}) \cdot sin(\psi + \theta) \tag{3.18}$$

$$\dot{y}_{deb} = \dot{R}_{CoM} \cdot sin(\theta) + R_{CoM} \cdot \dot{\theta} \cdot cos(\theta) - L_{deb} \cdot (\dot{\psi} + \dot{\theta}) \cdot cos(\psi + \theta) \tag{3.19}$$

Although R_{CoM} in Figure 3.3 is already defined in expression 3.9, we also need to express R_{tet} and R_{deb}. Using expressions 3.12-3.15 an equation for both distances can be obtained.

$$R_{tet} = \sqrt{x_{tet}^2 + y_{tet}^2} = \sqrt{L_{tet}^2 + R_{CoM}^2 + 2 \cdot L_{tet} \cdot R_{CoM} \cdot cos(\psi)} \tag{3.20}$$

$$R_{deb} = \sqrt{x_{deb}^2 + y_{deb}^2} = \sqrt{L_{deb}^2 + R_{CoM}^2 - 2 \cdot L_{deb} \cdot R_{CoM} \cdot cos(\psi)} \tag{3.21}$$

From this point forward, Lagrangian mechanics will be used, therefore, the next step is to express the kinetic and potential energy of our system in order to put their derivatives in Lagrange equation. The upcoming method is a practical application of the conservation of energy principle from expression 3.4.

$$T = \frac{1}{2} M_{tet} [(\dot{x}_{tet})^2 + (\dot{y}_{tet})^2] + \frac{1}{2} M_{deb} [(\dot{x}_{deb})^2 + (\dot{y}_{deb})^2] \tag{3.22}$$

If we put expressions 3.16-3.19 into equation 3.22 we get the kinetic energy that the tether system will possess:

$$T = \frac{1}{2}(M_{tet} + M_{deb})(\dot{R}_{CoM}^2 + R_{CoM}^2 \cdot \dot{\theta}^2) + \frac{1}{2}(M_{tet} \cdot L_{tet}^2 + M_{deb} \cdot L_{deb}^2)(\dot{\psi} + \dot{\theta})^2 \tag{3.23}$$

By applying the expression of the potential energy present in equation 3.4, but to our swinging tether; as well as by substituting the radius expressions of 3.20 and 3.21, we get equation 3.24.

$$U = -\frac{\mu \cdot M_{tet}}{R_{tet}} - \frac{\mu \cdot M_{deb}}{R_{deb}} = -\frac{\mu \cdot M_{tet}}{\sqrt{L_{tet}^2 + R_{CoM}^2 + 2 \cdot L_{tet} \cdot R_{CoM} \cdot cos(\psi)}} - \frac{\mu \cdot M_{deb}}{\sqrt{L_{deb}^2 + R_{CoM}^2 - 2 \cdot L_{deb} \cdot R_{CoM} \cdot cos(\psi)}} \tag{3.24}$$

Expression 3.25 is Lagrange's equation; it gives the equations of motion by partially differentiating Lagrange's function with respect to q, where these finite number of q represent each independent variable of our system [38]. Lagrange's equation is equal to the term that accounts for the non conservative forces that act on a system F_{NC}.

$$\frac{d}{dt}[\frac{\partial L}{\partial \dot{q}_i}] - \frac{\partial L}{\partial q_i} = F_{NC}, \qquad i = 1,2,...,N \tag{3.25}$$

Once the extended expressions of the kinetic and potential energy are set, we put them into Lagrange's function (expression 3.26), keeping in mind that we only need one equation, the one that gives us the tether's rotation angle ψ, because as stated earlier this study will be two-dimensional. Thus, the parameter q_1 will be our only variable in the expression: ψ. Moreover, in our scenario F_{NC} is equal to 0 because one of our initial assumptions was that no non-conservative forces act on the tether.

$$L(q_i, \dot{q}_i, t) = T(q_i, \dot{q}_i, t) - U(q_i, t) \tag{3.26}$$

Once expression 3.26 is set, substituting this L into equation 3.25 gives us the equation of motion of the swinging tethered system, keeping in mind the assumptions previously stated. This expression 3.27 tells us how the system will be moving alongside time.

$$\begin{aligned} \ddot{\psi} + \ddot{\theta} + \frac{\mu \cdot R_{CoM} \cdot sin(\psi)}{L_{tet} + L_{deb}} [(R_{CoM}^2 + L_{deb}^2 \\ -2 \cdot R_{CoM} \cdot L_{deb} \cdot cos(\psi))^{-\frac{3}{2}} - (R_{CoM}^2 + L_{tet}^2 + 2 \cdot R_{CoM} \cdot L_{tet} \cdot cos(\psi))^{-\frac{3}{2}}] = 0 \end{aligned} \tag{3.27}$$

However, from this point on-wards we consider the variables as a function of the true anomaly θ. This way, we are able to reduce its complexity by assuming the orbit to remain in a Keplerian orbit. Such transformations are listed the following expressions, where the quotation marks represent the derivative with respect to θ.

$$\dot{\psi} = \frac{d\psi}{d\theta}\frac{d\theta}{dt} = \dot{\theta}\psi' \tag{3.28}$$

$$\ddot{\psi} = \frac{d}{dt}(\dot{\theta}\psi') = \dot{\theta}^2\psi'' + \dot{\theta} \cdot \dot{\theta}' \cdot \psi' \tag{3.29}$$

Some extra simplifications have been made to expression 3.27. The first one is to consider the tether lengths negligible in comparison with the orbital radius [38]. The other comes from chapter 3.2.1, where the assumption $L_{deb} \cdot M_{deb} = L_{tet} \cdot M_{tet}$ was set. If we apply those simplifications to the potential energy expression 3.24, and change the current time derivatives to theta derivatives from the previous expressions, we get a simplified version of the equation of motion:

$$\psi'' - \left[\frac{2 \cdot e_{CoM} \cdot sin(\theta)}{1 + e_{CoM} \cdot cos(\theta)}\right](\psi' + 1) + \frac{3 \cdot sin(2\psi)}{2[1 + e_{CoM} \cdot cos(\theta)]} = 0 \tag{3.30}$$

With the knowledge of our ψ, the velocities of the tether system end masses will be obtained. Afterwards, the optimal point of release in the trajectory will be found, with the objective of rising the orbit of the tether's body and lowering the one of the debris.

3.2.2. Release

Once the debris is dropped, it will decrease its orbit, and we want to take advantage of that. For reference, any orbital object orbiting at 600 km, normally falls into Earth within several years; in orbits around 800 km its decay time is measured in decades and in orbits over 1000 km is measured in centuries [5]. The objective of the tether would be to lower as much as possible the debris' orbit to minimize the time it is orbiting the Earth and disintegrating over time. At the same time, the tether would increase its orbit to compensate the payload loss and to keep the same angular momentum in our system.

Figure 3.4 shows the desired maneuver, where the payload goes into a lower orbit and the tether increases its orbital radius by a certain amount. This release ideally will happen around the apogee of our orbit, because that way we force that the reduction of the semi-major axis a_{Deb} will happen at the perigee of the orbit, making the debris closer to the surface of the Earth. If instead we released the payload at the perigee, we would maintain the same perigee and instead make the reduction of a_{Deb} in the apogee, and that would not benefit our objective of lowering the debris' closer to the Earth, to begin the process of disintegration.

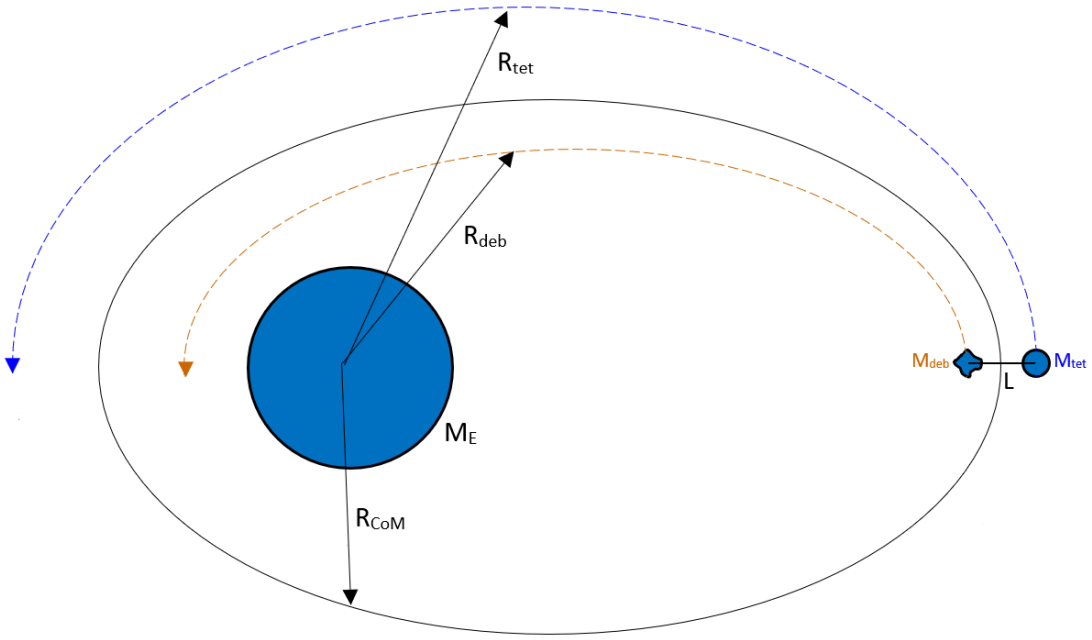

Figure 3.4: Trajectory of the released debris as well as the tether's body

The velocities that each part of the swinging tether possesses at the moment of the cut will dictate how their trajectories will change. In order to introduce every velocity that takes place, Figure 3.3 will be separated in two parts to explain how the velocities come to be in the first place.

Figure 3.5 shows a separation between the tether's mass-side of the tether system and the debris-side of the system. Distances and velocities will be considered in their vector form along this demonstration.

Both plots have the center of mass in common, and its distance to the center of the Earth $\vec{R}_{CoM}$, in pink. The distance from the latter to the tether's body and the debris are, respectively, $\vec{R}_{tet}$ and $\vec{R}_{deb}$. The whole length of the tether's rope is split into two, where in the left drawing is the distance CoM-tether's body ($\vec{R}_{tet,CoM}$), and the right plot is the distance debris-CoM ($\vec{R}_{deb,CoM}$). That way, the total longitude from the debris to the tether's body would be the vector sum $\vec{R}_{deb,CoM} + \vec{R}_{tet,CoM}$.

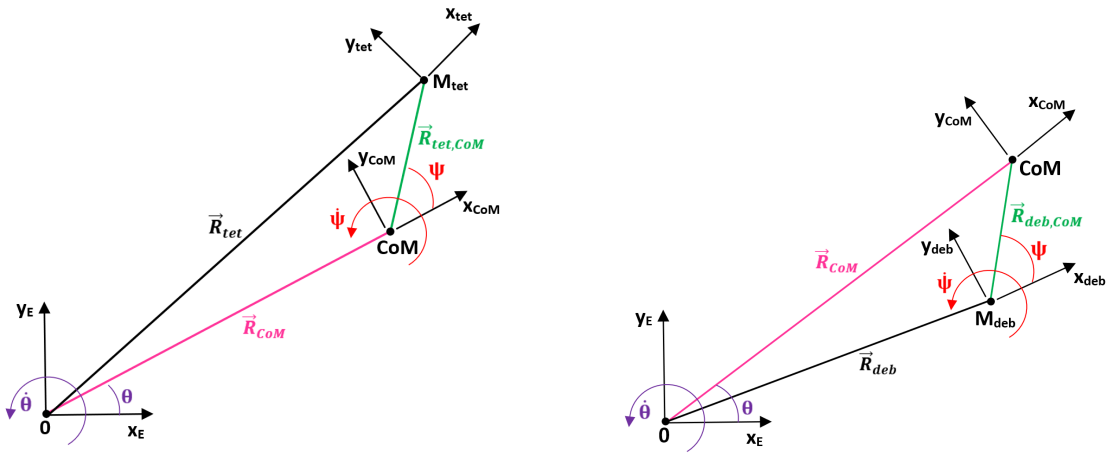

Figure 3.5: Distances in vector form and angles regarding the main body-side of the tether (left figure) and the debris-side (right figure)

If we focus firstly on the tether's body sketch (left side), the expression of the velocity of the tether's body with respect to the Earth $\vec{V}_{tet}$ will be given by three components: the velocity of the CoM with respect to the Earth $\vec{V}_{CoM}$, the relative velocity of the tether with respect to the CoM $\vec{V}_{tet,CoM}$ and the effect of the rope orbiting along with the system $\vec{\omega}_{CoM,Earth} \wedge \vec{R}_{tet,CoM}$.

Equations 3.31, 3.32 and 3.33 develop the terms described previously. $\vec{V}_{CoM}$ has a component consequence of the elliptical path changing the radius of the orbit $\dot{\vec{R}}_{CoM}$ and the part accounting for the CoM orbiting around the Earth, which equals to the cross product of the angular velocity of the CoM $\dot{\vec{\theta}}$ times the vector $\vec{R}_{CoM}$. The term $\vec{V}_{tet,CoM}$ is defined by the rotational velocity of the tether itself, i.e., $\dot{\vec{\psi}}$.

$$\vec{V}_{CoM} = \dot{\vec{R}}_{CoM} + \dot{\vec{\theta}} \wedge \vec{R}_{CoM} \tag{3.31}$$

$$\vec{\omega}_{CoM,Earth} \wedge \vec{R}_{tet,CoM} = \dot{\vec{\theta}} \wedge \vec{R}_{tet,CoM} \tag{3.32}$$

$$\vec{V}_{tet,CoM} = \dot{\vec{\psi}} \wedge \vec{R}_{tet,CoM} \tag{3.33}$$

Once these components are defined, adding all of them gives expression 3.34: the total velocity of one end of the tether, its main body. In this expression it is merged together the terms with $\dot{\vec{\theta}}$, and their vector sum result in the new term $\dot{\vec{\theta}} \wedge \vec{R}_{tet}$. That is because, from Figure 3.5, $\vec{R}_{tet} = \vec{R}_{tet,CoM} + \vec{R}_{CoM}$.

$$\vec{V}_{tet} = \vec{V}_{CoM} + \vec{V}_{tet,CoM} + \vec{\omega}_{CoM,Earth} \wedge \vec{R}_{tet,CoM} = \vec{\dot{R}}_{CoM} + \vec{\dot{\psi}} \wedge \vec{R}_{tet,CoM} + \vec{\dot{\theta}} \wedge \vec{R}_{tet} \quad (3.34)$$

The same process can be made but to the right side of Figure 3.5 to obtain the total velocity of the debris. Definitions for the components of the total debris velocity are listed in equations 3.35 and 3.36.

$$\vec{\omega}_{CoM,Earth} \wedge \vec{R}_{deb,CoM} = \vec{\dot{\theta}} \wedge \vec{R}_{deb,CoM} \quad (3.35)$$

$$\vec{V}_{deb,CoM} = \vec{\dot{\psi}} \wedge \vec{R}_{deb,CoM} \quad (3.36)$$

Due to the debris being closer to Earth than the CoM, the total velocity for the debris is not the sum of its components. This is because this time $\vec{R}_{deb} = \vec{R}_{CoM} - \vec{R}_{deb,CoM}$.

$$\vec{V}_{deb} = \vec{V}_{CoM} - \vec{V}_{deb,CoM} - \vec{\omega}_{CoM,Earth} \wedge \vec{R}_{deb,CoM} = \vec{\dot{R}}_{CoM} - \vec{\dot{\psi}} \wedge \vec{R}_{deb,CoM} + \vec{\dot{\theta}} \wedge \vec{R}_{deb} \quad (3.37)$$

Previously in Figure 3.3 some velocities were shown, and each of them relate to the previous vector components of the tether velocities.

V_R is parallel to the x_{CoM} axis and it tells how the orbital radius varies along the elliptical trajectory. It is the modulus of $\vec{\dot{R}}_{CoM}$ of expression 3.31.

V_{DebCoM} is perpendicular to the distance from Earth's center and the debris R_{deb}, and is the modulus of the terms of expression 3.36. If we change the notation from vector to only modulus form, and to the same one as Figure 3.3, we get that the distances $\vec{R}_{deb,CoM}$ and $\vec{R}_{tet,CoM}$ become L_{deb} and L_{tet}, respectively.

V_{Rot} coincides with the direction of the y component of each system of reference (debris, tether's body and CoM), and is the term accounting for the rotation due to the orbital velocity $\dot{\theta}$. It is the last term of expression 3.34 for the debris and the last of expression 3.37 for the tether's body, while the definition for the CoM is the distance R_{CoM} times the angular velocity $\dot{\theta}$.

Table 3.1 classifies the previously described velocities. However, it must be noted that this table lists the modulus of the velocities, and in order to know the total velocity that both tether's main body and debris have, those velocity components need to be split to every radial component on one side and every normal component on the other one.

Definition	**Notation**
Radial Velocity	$V_R = \dot{R}_{CoM}$
CoM rotation velocity due to $\dot{\theta}$	$V_{RotCoM} = R_{CoM} \cdot \dot{\theta}$
Debris' rotation velocity due to $\dot{\theta}$	$V_{RotDeb} = R_{deb} \cdot \dot{\theta}$
Debris' rotation velocity due to CoM	$V_{DebCoM} = L_{deb} \cdot \dot{\psi}$
Tether's rotation velocity due to $\dot{\theta}$	$V_{RotTet} = R_{tet} \cdot \dot{\theta}$
Tether's rotation velocity due to CoM	$V_{TetCoM} = L_{tet} \cdot \dot{\psi}$

Table 3.1: All the velocities that take part in the motion of the tether (in modulus)

Those radial and normal components will be with respect to each respective system of reference: velocities that belong to the debris' end of the tether will be radial and normal to that system of reference and the tether's main body velocities will be referenced through that system of reference instead. Using trigonometry in Figure 3.3, we classify the velocities of the debris in the x_{deb} and the y_{deb} axis. An important thing to consider in expressions 3.38 and 3.39 is that the term $V_{deb,CoM}$, due to the distance $\vec{R}_{deb,CoM}$ being defined opposite from the one corresponding to the tether's body, it carries a negative sign that changes the trigonometry analysis of this velocity.

$$V_{RadDeb} = -V_{DebCoM} \cdot cos(\phi_1) + V_R \cdot cos(\lambda_1) \tag{3.38}$$

$$V_{NormDeb} = V_{RotDeb} + V_{DebCoM} \cdot sin(\phi_1) + V_R \cdot sin(\lambda_1) \tag{3.39}$$

$$V_{RadTet} = -V_{TetCoM} \cdot sin(\phi_2) + V_R \cdot cos(\lambda_2) \tag{3.40}$$

$$V_{NormTet} = V_{RotTet} + V_{TetCoM} \cdot cos(\phi_2) - V_R \cdot sin(\lambda_2) \tag{3.41}$$

Angles λ_1, λ_2, ϕ_1 and ϕ_2 are obtained again from the same figure. First apply the sine rule to get ϕ_1:

$$\frac{R_{CoM}}{sin(\frac{\pi}{2} + \phi_1)} = \frac{R_{deb}}{sin(\psi)} \tag{3.42}$$

$$\phi_1 = arcsin\left(\frac{R_{CoM} \cdot sin(\psi)}{R_{deb}}\right) - \frac{\pi}{2} \tag{3.43}$$

Then we can know the value of λ by doing:

$$\lambda_1 = \frac{\pi}{2} - \phi_1 - \psi = \pi - arcsin\left(\frac{R_{CoM} \cdot sin(\psi)}{R_{deb}}\right) - \psi \tag{3.44}$$

Repeating the process for the other end of the tether (main body), the difference is the trigonometry used to obtain the respective orbital and rotational velocity, as the radial one is the same. In order to obtain the expressions, two new angles λ_2 and ϕ_2 are introduced (present in Figure 3.3), and going along the same procedures, we get expressions 3.45 and 3.46 for the radial and normal components of the tether's body, and the definitions of the new angles in 3.47 and 3.48.

$$V_{RadTet} = -V_{TetCoM} \cdot sin(\phi_2) + V_R \cdot cos(\lambda_2) \tag{3.45}$$

$$V_{NormTet} = V_{RotTet} + V_{TetCoM} \cdot cos(\phi_2) - V_R \cdot sin(\lambda_2) \tag{3.46}$$

$$\phi_2 = arcsin\left(\frac{R_{CoM}}{R_{tet}} \cdot sin(\pi - \psi)\right) \tag{3.47}$$

$$\lambda_2 = \psi - \phi_2 \tag{3.48}$$

At some point in the trajectory the goal is to detach the debris from the tether. The equation that hints where that release point should be comes from isolating a from equation 3.8. In order to lower the debris as much as we can, the new semi-major axis of that object a_{Deb} must be as low as possible. Expression 3.49 shows that in order to do so, two conditions must be met. The first one is that the total velocity of the debris must be minimal, to make the denominator larger. That moment of less total velocity of the debris, which is defined as $\sqrt{V_{NormDeb}^2 + V_{RadDeb}^2}$, occurs in the apogee. This information is given to us by equation 3.11: the larger R_{CoM} is, the lower $\dot{\theta}$ will become. The second condition is that R_{deb} must be minimal, and that occurs at the perigee. However, by releasing the debris at the perigee we would get a reduction in the height of the apogee, contrary of what we want. Thus, the optimal release point will be the instants of our trajectory where those two conditions align and result in the lowest a_{deb} values possible.

We will simulate several orbits, to then pick from the multiple minimums of a_{deb}, the one with the best balance of being the lowest value possible but also being close to the apogee, to make the change in semi-major axis influence the height of the debris' perigee, lowering it.

$$a_{Deb} = \frac{\mu \cdot R_{deb}}{2\mu - V_{TotDeb}^2 \cdot R_{deb}} \tag{3.49}$$

The final step will be to calculate the new orbital radius of the debris. Prior to that expression, the new eccentricity e_{Deb} and semi-latus rectum p_{Deb} are defined.

On one hand, from equation 3.2 an expression for the eccentricity that our debris will have can be derived.

$$e_{Deb} = \sqrt{1 - \frac{p_{Deb}}{a_{Deb}}} \tag{3.50}$$

On the other hand, to know the semi-latus rectum p_{Deb}, we can use the definition of that distance in terms of the specific angular momentum H.

$$p_{Deb} = \frac{H^2}{\mu} = \frac{(V_{NormDeb} \cdot R_{deb})^2}{\mu} \tag{3.51}$$

By inserting equations 3.49, 3.50 and 3.51 into equation 3.3, the expression of the new radius of the debris is obtained. Note that we must add $\theta_{Release}$ to the iterative values of θ in the expression of the new radius; this new parameter is the true anomaly the debris had at the moment of the release, and this addition will result in the new orbit starting at the moment the rope is cut.

An equivalent process but changing the subscripts "deb" to "tet" can be made to obtain the expressions from 3.49 to 3.52 respective to the tether's body.

$$R_{NewDeb} = \frac{p_{Deb}}{1 + e_{Deb} \cdot cos(\theta + \theta_{Release})} \tag{3.52}$$

3.3. Validations

This section will validate the equations of motion used in chapter 3.2. Nevertheless, in order to check them a new parameter must be added into the equations, as the doctorate that was used to obtain the equations of motion uses a swinging tether in three dimensions [38]. In this case, presented by Ziegler in 2003, the motion of the tether is not restricted to a plane, and instead is a more generic scenario. Figure 3.6 shows how the geometry of the tether changes, as now an angle accounting for the degree of inclination in the orbit plane needs to be defined: α. In our study this angle was 0, due to always working in a 2D orbital plane.

Figure 3.6 has θ and ψ the same way as before, R as our R_{CoM}, the subscripts 1 and 2 as deb and tet, and the system of reference $x_0 - y_0 - z_0$ as the one of the center of mass. On top of that, the angle α is the inclination of the tether with respect to the orbital plane, and is defined as the angle between that plane and the tether's rope L_1 (or L_2).

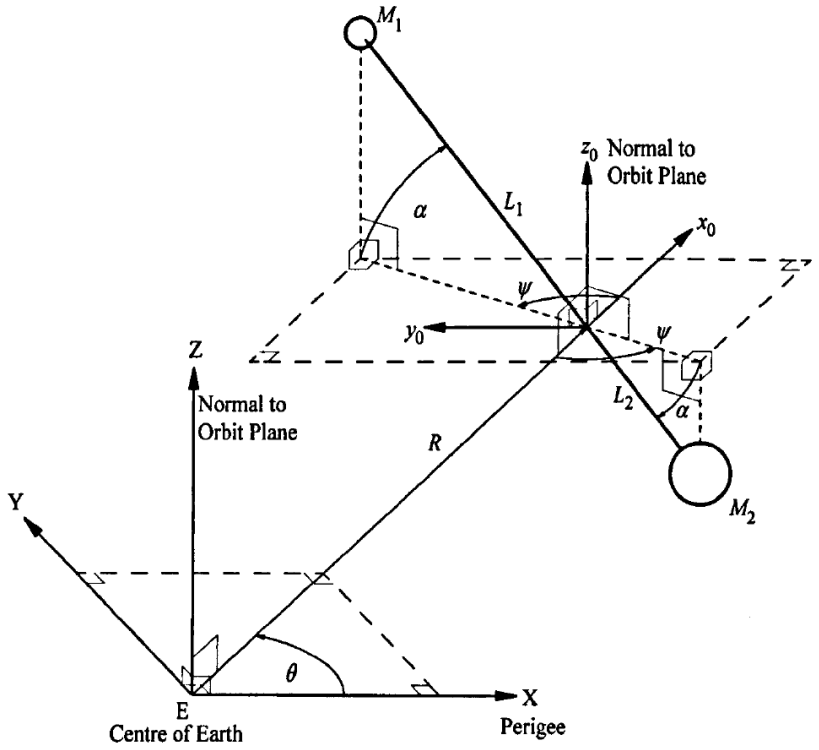

Figure 3.6: Geometry of an out-of-plane tether [38]

From this point, a study equivalent to the one done in chapter 3.2 can be made, where the Cartesian coordinates of each mass are defined, and the Lagrangian function is found, this time with the alpha parameter in the equations. All the related information about the process can be found in Ziegler's document [38]. Equations 3.53 and 3.54 are what result from following that process and making the same simplifications as the ones made before. In this case the equations of motion are two, as now the tether's self-rotation angle can happen both in the plane $x_0 - y_0$ (being that angle ψ) and the plane $y_0 - z_0$ (being in this other case the angle α).

$$\psi'' - \left[2 \cdot \alpha' \cdot tan(\alpha) + \frac{2 \cdot e \cdot sin(\theta)}{1 + e \cdot cos(\theta)}\right](\psi' + 1) + \frac{3 \cdot sin(2\psi)}{2[1 + e \cdot cos(\theta)]} = 0 \tag{3.53}$$

$$\alpha'' - \frac{2 \cdot e \cdot sin(\theta)}{1 + e \cdot cos(\theta)}\alpha' + \frac{1}{2}sin(2\alpha)\left[(\psi' + 1)^2 + \frac{3 \cdot cos^2(\psi)}{1 + e \cdot cos(\theta)}\right] = 0 \tag{3.54}$$

Ziegler in his doctorate plotted a couple graphs showing the variation of ψ and α angles with respect to the number of orbits, given the initial conditions shown in Table 3.2. He considered a several kilometers long tether with both end masses of 1 tonne, with a radius of the perigee of 7000 km (or a height of 629 km, if we subtract the radius of the Earth). The only initial condition different from 0 is $\alpha(0)$.

M_{tet}	M_{deb}	L_{tet}	L_{deb}	e	R_{per}	$\psi(0)$	$\dot{\psi}(0)$	$\alpha(0)$	$\dot{\alpha}(0)$
1000 kg	1000 kg	10 km	10 km	0.25	7000 km	0 rad	0 rad/s	0.1 rad	0 rad/s

Table 3.2: Initial conditions of Ziegler's scenario

Given the initial conditions in this scenario, and solving equations 3.53 and 3.54 with them, Ziegler in his doctorate obtains the left side of Figure 3.7, which shows the rotation angle ψ with respect to the number of orbits. To test the validity of those equations of motion (a set of more complete equations than our main case, which has α = 0), expressions 3.53 and 3.54 were solved in Matlab, with the initial conditions in Table 3.2, and the right plot of Figure 3.7 resulted from it. Both graphs are a match, and they show that the angle the tether rotates with, ψ, never tilts the end masses more than 0.4 radians.

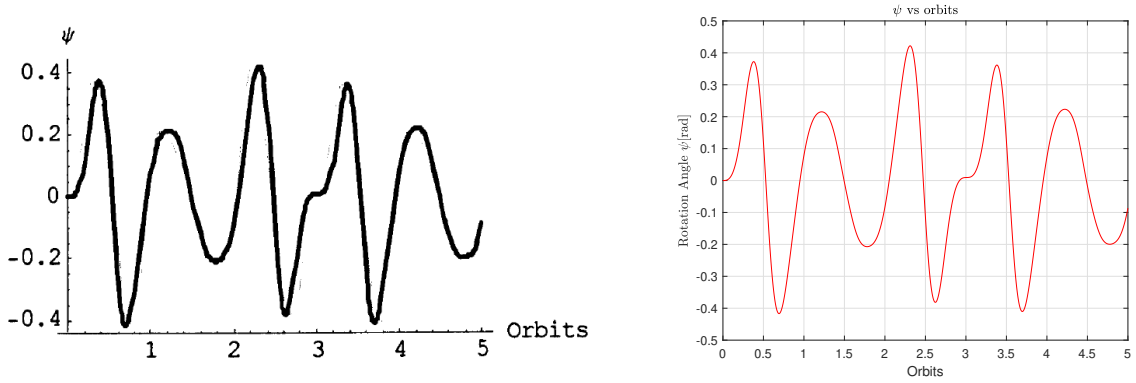

Figure 3.7: Graphs of rotation angle ψ along 5 orbits. Left side is Ziegler's sketch and right side is the Matlab output

In addition, the same validation process was made with angle α in Figure 3.8. The result is again the same plot, and we observe that α never goes beyond 0.15, which reflects that the orbital plane does not vary that much. However, it shows a more periodical and clearer pattern than the previous angle.

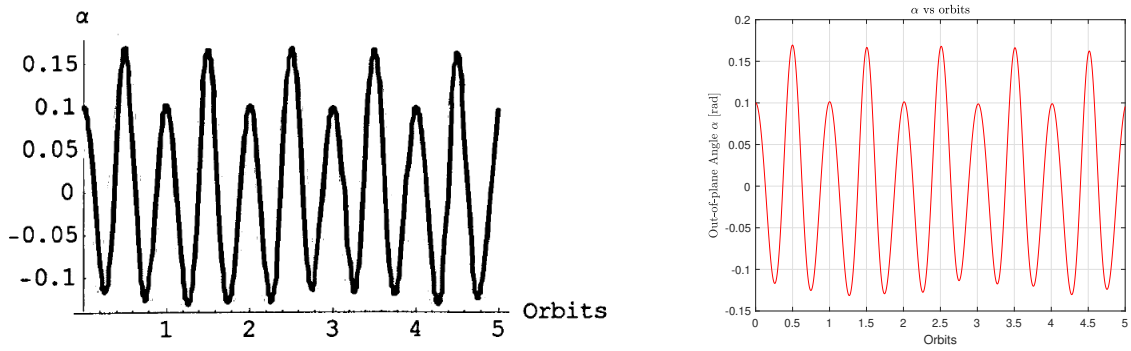

Figure 3.8: Graphs of α angle in this scenario; left side Ziegler's plot, right side Matlab verification

In the following comparisons with Ziegler's results will not be possible, as the doctorate did not add more Figures, but the ones that will be shown here will expand the information that he had.

Equation 3.9 showed how the radius of the center of mass of the swinging tether changed along the elliptical trajectory. If we plot it with the eccentricity and perigee radius of the initial conditions of Table 3.2 we get the increase in radius of the orbit (Figure 3.9). Instead of the radius, it is plotted the orbit height, which is the distance not to the center of the Earth, but the Earth's surface. We can see that at each apogee (every half an orbit), the CoM reaches a height of almost 10 times the value it had at the perigee. This is due to the high eccentricity, which makes the difference between the distances of the perigee (valleys) and apogee (peaks) significant.

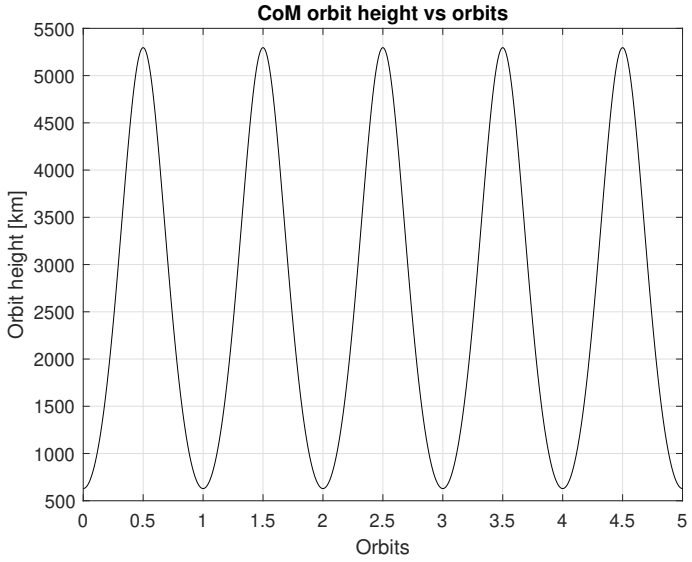

Figure 3.9: Variation of the CoM orbit height along the trajectory

A similar plot to the one in Figure 3.9 is to plot how the true anomaly θ changes as the orbits go by. The next figure shows that for each orbit θ goes from 0 to 2π radians, to then repeat the cycle.

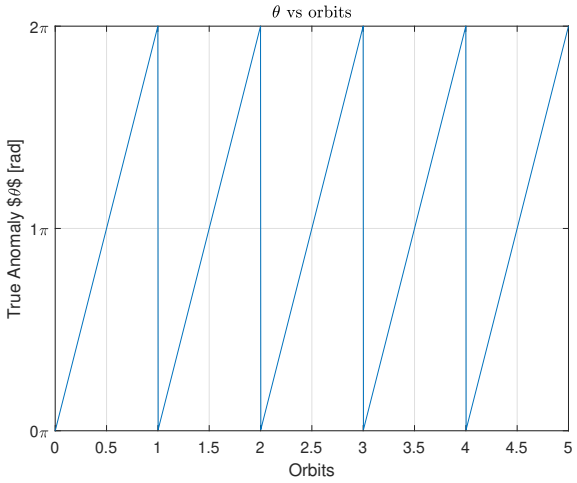

Figure 3.10: Variation of the true anomaly θ along the trajectory

Another graph that could be shown is the difference between the total velocity of the tether's body and the debris along the orbits. Nevertheless, we cannot use the velocity expressions that we deduced in the previous chapter, as they are only valid with a restricted orbital plane.

To calculate the total velocities, we will start from Figure 3.6, and deduce each Cartesian component of the velocity of the tether's body and the debris. Expressions 3.55 to 3.60 are the new equations that need to be used this section. Note that this time a z-component is added, as we are now in 3D.

$$x_{deb} = R_{CoM} \cdot cos(\theta) - L_{deb} \cdot cos(\alpha) \cdot cos(\psi + \theta) \tag{3.55}$$

$$y_{deb} = R_{CoM} \cdot sin(\theta) - L_{deb} \cdot cos(\alpha) \cdot sin(\psi + \theta) \tag{3.56}$$

$$z_{deb} = -L_{deb} \cdot sin(\alpha) \tag{3.57}$$

$$x_{tet} = R_{CoM} \cdot cos(\theta) + L_{tet} \cdot cos(\alpha) \cdot cos(\psi + \theta) \tag{3.58}$$

$$y_{tet} = R_{CoM} \cdot sin(\theta) + L_{tet} \cdot cos(\alpha) \cdot sin(\psi + \theta) \tag{3.59}$$

$$z_{tet} = L_{tet} \cdot sin(\alpha) \tag{3.60}$$

Afterwards, we will apply the time derivative to each equation, to then use the definition of total velocity $V_{Tot} = \sqrt{\dot{x}^2 + \dot{y}^2 + \dot{z}^2}$, adding the corresponding subscript for the debris "deb" and the tether's body "tet".

If we plot the two total velocities that we obtain, Figure 3.11 is what we get. Note that the velocities oscillate almost 10 km/s from peaks to valleys due to the high eccentricity value given at the beginning. Another interesting result is that the tether's body and the debris velocities seem mirrored from one each other: when the debris is at a peak value of total velocity, the tether is at a valley and vice-versa.

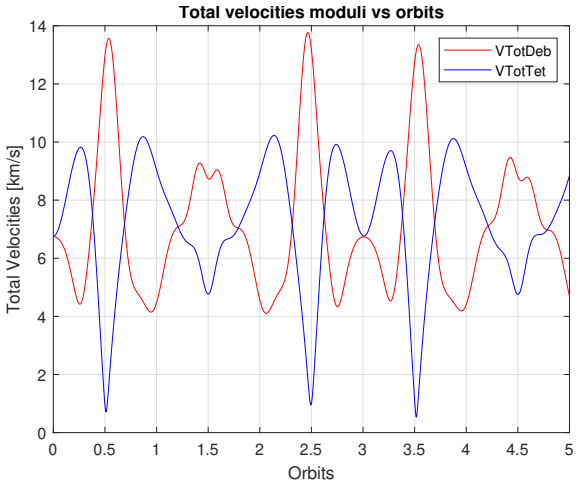

Figure 3.11: Total velocities of the debris and the tether's body in Ziegler scenario

All the graphs of this section were generated using the three-dimensional version of the equations of motion. However, for the final chapter of the TFG, we will start from the simplified equation of motion in expression 3.30, as our scenario has the orbital plane fixed.

CHAPTER 4. RESULTS AND DISCUSSION

In this final chapter we will give similar results as the ones shown in section 3.3, but now with the equations of motion found in section 3.2 (i.e., without the parameter α). The initial conditions used are fixed values, but tests will be made where each time one of these parameters is going to vary. Those variations will bring the main results that can be obtained in this study, regarding the removal of space debris.

The initial values from which the variations and calculations this section are based on are listed in Table 4.1. As opposed to the previous scenario, values such as the tether's rope length and the eccentricity are reduced, while the radius of the perigee is at a higher point. R_{per} is set at 9371 km (or 3000 km of height) because we will consider a hypothetical debris that orbits around that height.

Moreover, the tether's main body will be 10 times heavier than the debris. This is to add to the pendulum effect that we want to occur, because due to the identity $M_{tet} \cdot L_{tet} = M_{deb} \cdot L_{deb}$, that difference in mass is equivalent to having a rope where the debris-part length (L_{deb}) is 10 times longer than the tether's, which means that the debris will swing with more intensity than the other end of the rope. The system will begin with an initial ψ different from zero, because otherwise the pendulum motion would not occur.

M_{tet}	M_{deb}	L_{tet}	L_{deb}	e	R_{per}	$\psi(0)$	$\dot{\psi}(0)$
1000 kg	100 kg	120 m	1200 m	0.1	9371 km	0.2 rad	0 rad/s

Table 4.1: Initial conditions of the swinging tether to study

The parameters of this table that will vary are the eccentricity of the initial orbit e, the length of the tether's side of the rope L_{tet} (and consequently L_{deb}), and the radius of the CoM perigee R_{per}. The former parameter has an effect on the atmospheric drag that will act on the debris once it is in a low enough orbit: If we have an excessively eccentric orbit, drag will be acting mostly in the perigee of the trajectory, and the orbit will tend to circularize itself, while the radius of the perigee will tend to remain the same [44]. If instead, we have an orbit with the same value of perigee, but a low value of eccentricity, the orbit will have an atmospheric drag acting almost constantly along the trajectory, and the orbit will keep decreasing its altitude in an homogeneous way.

The released debris needs to end up in an orbit with a low enough altitude so that it can begin its process of disintegration. This process is given by the exponential increase in atmospheric drag as we approach the Earth's surface. Table 4.2 gives an estimation of the density of the atmosphere depending on the altitude that an object has in an elliptic trajectory. At 1000 km the density is, comparatively to the largest numbers in the table, almost negligible, but is sufficient enough to, in the long run, keep decreasing the debris altitude. With that, we will set the threshold of the lowest point in the new debris' orbit in 1000 km, to guarantee that the released debris will eventually disintegrate.

Altitude [km]	100	200	300	400	500
Density [g/km^3]	497.4	255-316	17-35	2.2-7.5	0.4-2.0
Altitude [km]	600	700	800	900	1000
Density [g/km^3]	0.08-0.64	0.02-0.22	0.007-0.08	0.003-0.04	0.001-0.02

Table 4.2: Approximated values of atmospheric density at different altitudes [44]

4.1. Varying the orbit's eccentricity

The first modification of the initial conditions of Table 4.1 will be to vary the tether's center of mass eccentricity e. The starting value will be 0 and each iteration the value will increase by 0.05 up to 0.15.

Solving the equation of motion 3.30 with the initial values gives how the rotation angle changes over time. In this first case the eccentricity is a parameter that affects the outcome of the angles so Figure 4.1 shows the result of the first eccentricity (e=0), and then Figure 4.2 all of the eccentricities combined. Starting from the simpler graph, in it the ψ angle in blue and its time derivative $\dot{\psi}$ in orange are represented. Both of these parameters are plotted versus time, or more specifically, the number of orbits. When the rotation angle reaches a maximum or minimum value, its velocity is 0, checking that the time derivative is working as intended. ψ spans between 0.2 and -0.2 radians, while the rotation velocity $\dot{\psi}$ goes from 0.34 to -0.34 radians per second, approximately.

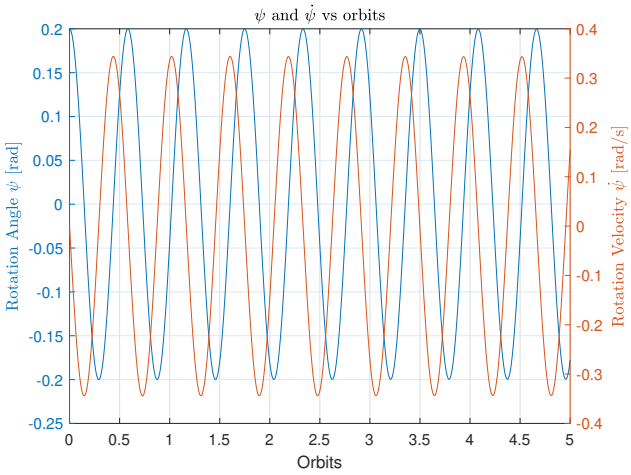

Figure 4.1: Variation of the rotation angle ψ and its time derivative $\dot{\psi}$ alongside the trajectory with $e = 0$

If we now take into account not only the first value of eccentricity, but all four of them, we obtain Figure 4.2. The multiple curves manifest that the eccentricity is a parameter that alters the values of the rotation angle ψ. The higher the eccentricity, the more abrupt the changes between the peaks and valleys are.

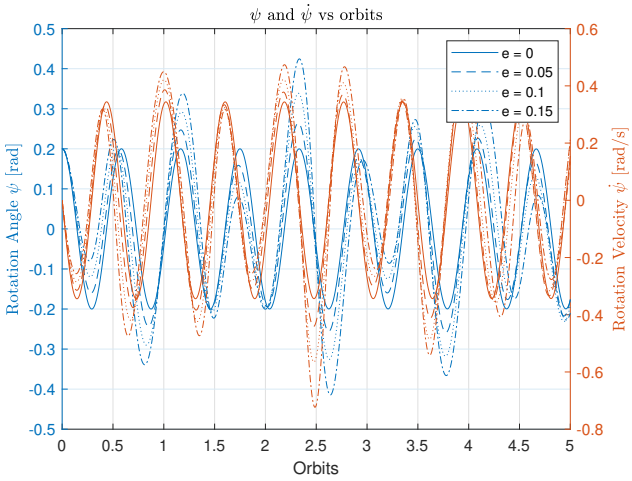

Figure 4.2: Variation of the rotation angle ψ and its time derivative $\dot{\psi}$ with $e = [0, 0.05, 0.1, 0.15]$

Before going into the velocities, we can graph equation 3.9, the radius of the center of mass, with respect to the number of orbits, depicted in Figure 4.3. There we can see that the higher the eccentricity, the higher the value of the apogee (at every peak) will be. This is because we impose from the start that the radius of the perigee will be 9371 km, so the apogee is the distance that keeps increasing instead. The y-axis of the graph is the orbit height, instead of radius. If we subtract the radius of the Earth (6371 km) to the initial 9371 km of perigee radius, we get the orbit height of the center of mass instead: 3000 km in the case of the perigee. Hereafter, and for the sake of clarity, all the radius-related values will be in terms of the height (distance with respect to the Earth's surface).

If we were to plot the orbit height graphs for the debris and tether's body, we would see that both of them would be almost identical to the CoM one, because initially the only difference between the three distances are the rope lengths; distances almost irrelevant next to the magnitudes of thousands of kilometers that are displayed in this Figure 4.3.

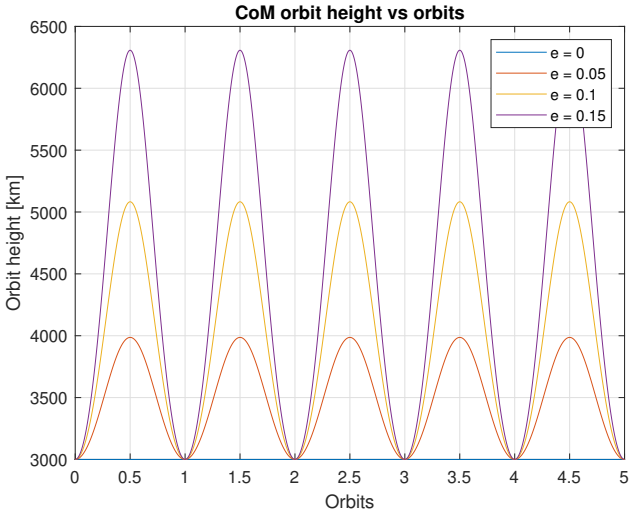

Figure 4.3: Orbit height of the center of mass of the tether system throughout the trajectory with $e = [0, 0.05, 0.1, 0.15]$

Figure 4.4 depicts the modulus of the velocities that were shown in Figure 3.3, each one with their own corresponding color. V_{Rot} and V_R are the same in both plots, the former being the predominant velocity with around 6 km/s that keeps oscillating more the higher e is, and the latter centered in 0 and also deviating more as the eccentricity increases. V_{DebCom} and V_{TetCom} are the differential factor in these plots since they are the velocities that come from the end masses being attached to a center of mass, which means that they are proportional to L_{deb} and L_{tet}. In our case those lengths are different by an order of magnitude of 10. The difference in both green curves explains how in the pendulum-effect, the debris-side of the tether is the one swinging the most, while the other side keeps its ups and downs in velocity in a less pronounced way. The direction of the black arrows indicates how each velocity changes as we keep increasing the eccentricity e, with the effect of varying more the maximum and minimum values of every velocity.

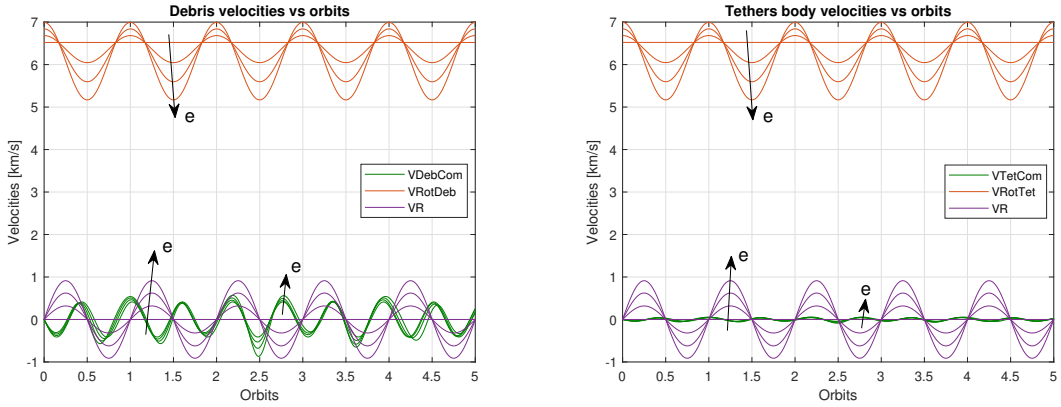

Figure 4.4: Modulus of the velocity components of the debris (left) and the tether's body (right) with the CoM eccentricity $e = [0, 0.05, 0.1, 0.15]$

The graph that depicts the radial and normal components of the previously shown velocities is Figure 4.5. Apart from those components, the total velocity is also added in this plot. It can be seen that the left plot is much more erratic in its behaviour than the right one, and that is due to V_{DebCom} having more impact in the debris than its counterpart in the tether's body. Another interesting aspect to highlight is V_{RadDeb}, that is inverted with respect to its tether's body counterpart. This behaviour is explained by the initial conditions of ψ, where that initial push results in the debris swinging with a radial component inwards (i.e., towards the Earth), making the initial motion negative in this component, as opposed to the tether that initially keeps increasing its radial component as it moves towards the apogee.

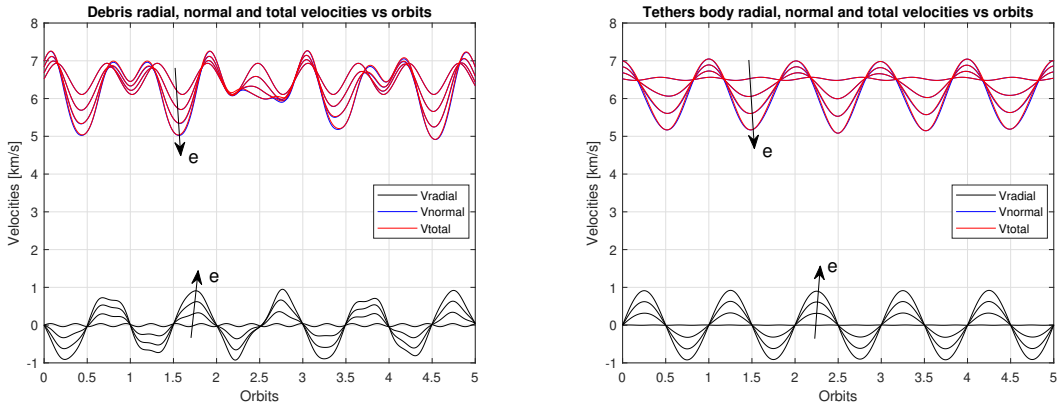

Figure 4.5: Radial, normal and total velocity of the debris (left) and the tether's body (right) with respect of time with $e = [0, 0.05, 0.1, 0.15]$

Before the release, both the tether's body and the debris have a semi-major axis equal to the one of the center of mass. Nevertheless, we can make a plot of the infinite possible values of a_{Deb} that we would have if we released the debris at any point in the trajectory.

The thin curves of Figure 4.6 result from plotting expression 3.49 for each iteration of eccentricities. On the other hand, the thick horizontal lines represent the actual values of the debris after the release maneuver (and that value becomes constant along the orbits because the debris exits the restriction of being in a tether system and instead now follows a typical elliptical orbit, with a single value of semi-major axis).

To check that our debris does in fact have a constant a_{Deb} value after release, we can obtain the total velocity it will have at each point in the new trajectory. Similar to the components of our CoM of the tether system, this time we know that the debris will have a radial component $V_{RNewDeb} = \dot{R}_{NewDeb}$ and a normal one $V_{RotNewDeb} = R_{NewDeb} \cdot \dot{\theta}_{NewDeb}$. Total velocity values are obtained by the squared sum of these two components, which then are iterated along all the values of R_{NewDeb}, substituted in Equation 3.49 and plotted in the left plot of Figure 4.6, giving constant values of a_{Deb} after the release. Those values keep increasing as the initial eccentricity increases as well.

Those new a_{Deb} values will intersect with the minimum values of one of the valleys of the curves of the same figure. Out of the eight valleys we can see for each e, we need to choose the one that best suits these conditions: the first one is to be as close as possible to an apogee (which happens at the middle of every orbit); by doing so, we will reduce the semi-major axis by lowering the distance of the perigee, and not the apogee. The second condition is that whenever possible we must choose the valley that is the minimum among all of them (and this with every eccentricity).

This first scenario, we will choose the 8th valley, the one around 4.5 orbits. This is because we will prioritize a bit more that out of all of the valleys, this is the closest one to its respective apogee. However, an equally valid reasoning would be to choose the 6th valleys before 3.5 orbits, which are more deviated from the apogee, but give lower values of a_{Deb}.

The right plot of Figure 4.6 zooms in the spot of release of this scenario, where the values shown are the minimum of each respective curve. Upon iterating the new values of total velocity into equation 3.49, the new values of a_{Deb} are the same as each respective minima graphed in Figure 4.6 (right). Note that as we keep increasing the eccentricity of our orbit, the release point will be every time a bit more to the right.

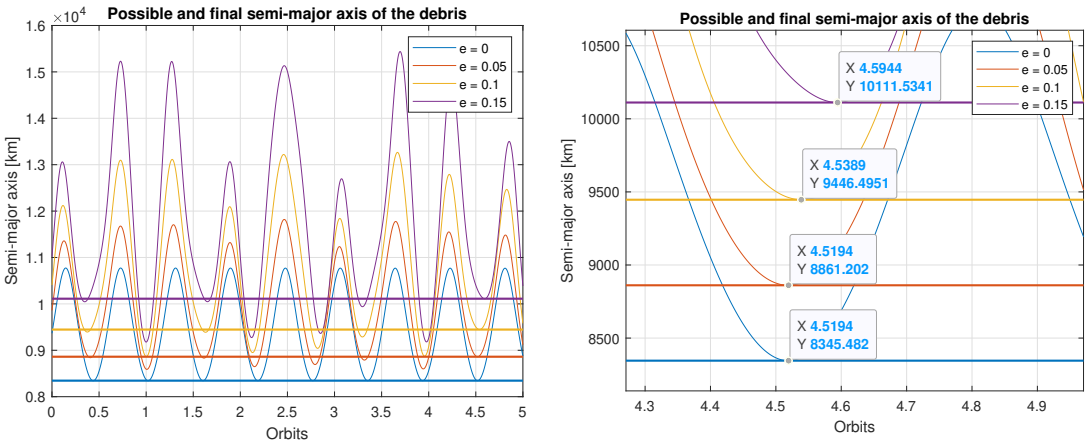

Figure 4.6: Possible and final semi-major axis values for the debris (left) and a zoom in the release spot (right) with $e = [0, 0.05, 0.1, 0.15]$

The same process is repeated for the tether's body, and in doing so we can see a left plot with less oscillations, signifying a less intense pendulum-like motion as opposed to the previous figure. Also, note that each curve is mirrored from their corresponding counterpart in Figure 4.6: when the tether's body has a valley, the debris has a peak.

The right plot of Figure 4.7 tells us that a minimum value of a_{Deb} not necessarily equals to the maximum one of a_{Tet}, as in this case we see that all four points of the new axis of the tether's body happen after the maximum value of a_{Tet}. In some cases the difference in the maximum and the chosen value will be closer together than others. In this scenario, for instance, as we increase e, that difference seems to increase as well.

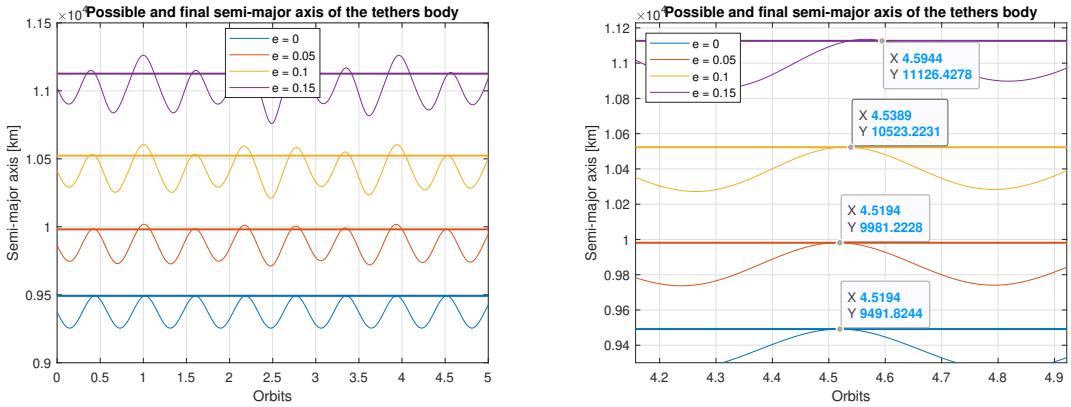

Figure 4.7: Possible and final semi-major axis values for the tether's body (left) and a zoom in the release spot (right) with $e = [0, 0.05, 0.1, 0.15]$

In order to obtain the new values of semi-major axis the debris had, we needed R_{NewDeb}. We can iterate expression 3.52 through all the values of θ (the starting point being the release of the debris) and then plot the result in order to obtain Figure 4.8. There the resulting new orbits of the debris for the four cases of eccentricity are shown in terms of height, and their starting point is their respective moments of release. As we can corroborate in the zoom plot of the new perigees in the right, the higher the eccentricity, the earlier we arrive at the new perigees, and the higher they are.

All four cases reduced the perigee of the debris. However, our valid cases are the first three eccentricities, as the case of $e = 0.15$ does not achieve a perigee close to our threshold value of 1000 km. The third case does not achieve that value either, but taking into account the variations in the atmospheric density due to solar cycles, debris at that height could also be pulled into the atmosphere and eventually disintegrated, so we will count the case of $e = 0.1$ as a valid one.

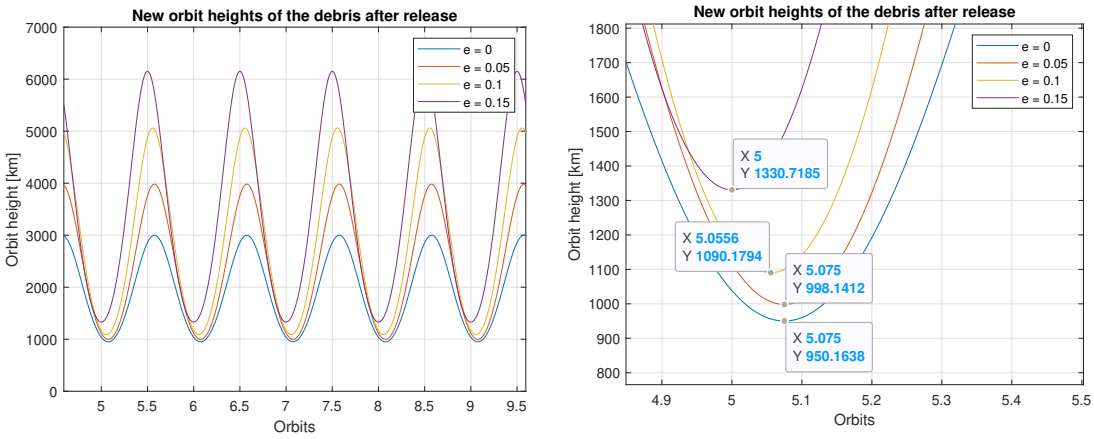

Figure 4.8: New orbital trajectory of the debris after release (left) and a zoom in the new perigee (right) with $e = [0, 0.05, 0.1, 0.15]$

On the other hand, the tether's main body in Figure 4.9 results in an orbit that instead of decreasing, has increased its perigee from when it was tied to the debris. We observe in the right plot that similar to the debris' case, the higher we set the eccentricity, the earlier the new orbit will reach its perigee. However, it can be seen that as we increase e, we will get lower values of height, which in this case is not desirable, as we want to also increase the tether's body height as much as we can. The exception here is the case of $e = 0$, which due to the prior orbit having a perigee and apogee of the same distance, it limits how much the tether's body can go up in its new perigee.

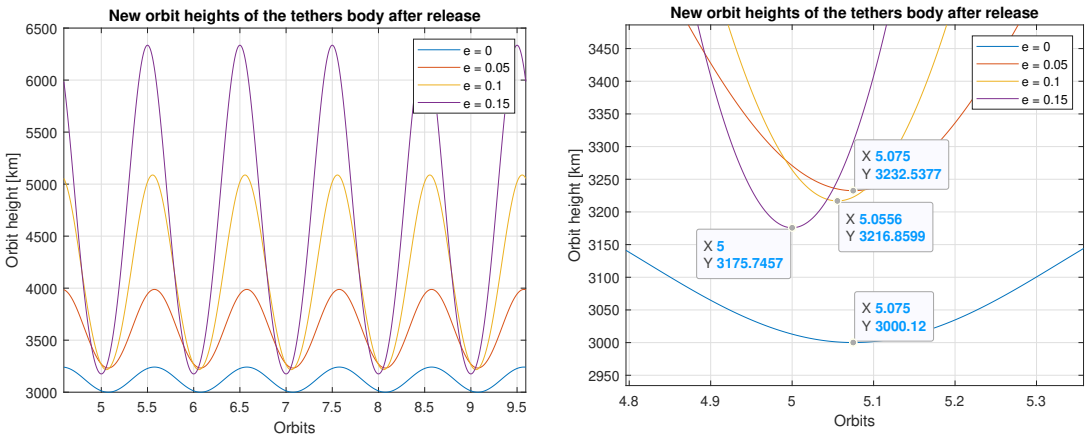

Figure 4.9: New orbital trajectory of the tether's body after release (left) and a zoom in the new perigee (right) with $e = [0, 0.05, 0.1, 0.15]$

4.2. Varying the length of the tether

This time the varying parameter will be the length of both ends of the tether system: L_{deb} and L_{tet}. A previously stated hypothesis guaranteed us the center of mass of our tether was in place: $L_{tet} \cdot M_{tet} = L_{deb} \cdot M_{deb}$. If we want to change the lengths of the tether, that identity must be true. The length of the tether body's side of the rope will increase from an initial value of 80 m with intervals of 20 m each iteration, and thanks to the previous identity we know that the other side of the rope will be 10 times longer, as a consequence of the values of mass that are written in Table 4.1.

The reason why the varying values are the lengths and not the masses is that in reality we can know better the masses of a certain target and our own tether's body, instead of a theoretical rope that will be extended a certain amount of meters.

The variation in ψ and its time derivative along the orbits is different from the previous case, but that is because this time the eccentricity plotted is 0.1, the initial condition of the table, instead of 0 (the initial value from the previous section). Moreover, in sections 4.2 and 4.3, ψ will only have one curve, because unlike before with the eccentricity, the tether's length or the radius of the perigee, unless we set them to 0, do not vary the values of ψ. In this second scenario, Figure 4.10 shows a more abrupt difference between the higher and lower points of the curves, result of increasing the initial eccentricity of the system.

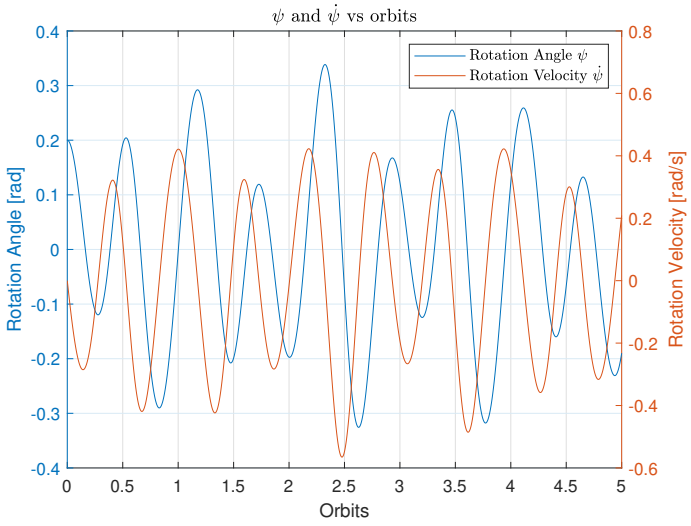

Figure 4.10: Variation of the rotation angle ψ and its time derivative ψ̇ alongside the trajectory

The orbit the center of mass follows at the beginning is given in the following Figure 4.11. It can only be seen a single curve, which tells us that changing the tether's length does not have an impact in the orbit of the CoM, opposite of what happened if we changed e previously.

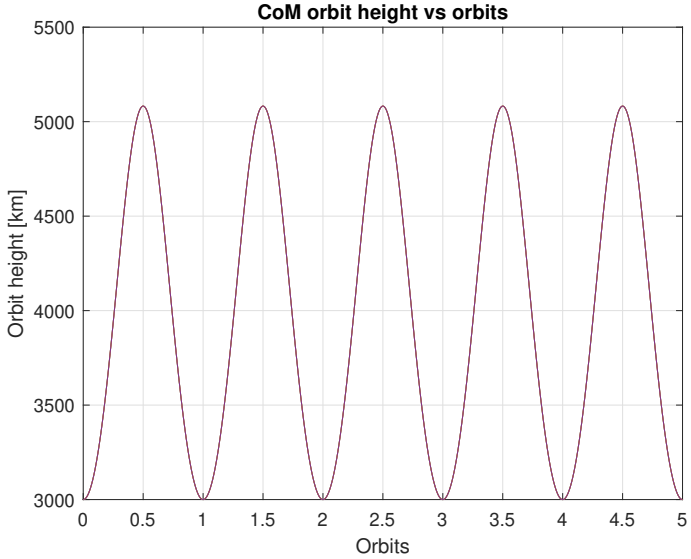

Figure 4.11: Orbital height of the center of mass of the tether system with respect to the number of orbits

In this second scenario the modulus of the velocities behave in a similar way to varying the eccentricity, with the difference that this time V_{Rot} velocities are much closer to each other (because we are not varying the eccentricity in this scenario). V_{DebCom} and V_{TetCom} are still different because the values of their respective lengths of the rope differ in one order of magnitude. In addition to that, the more we increase the tether's length, the more intense the variations in V_{DebCom} (and V_{TetCom}) are.

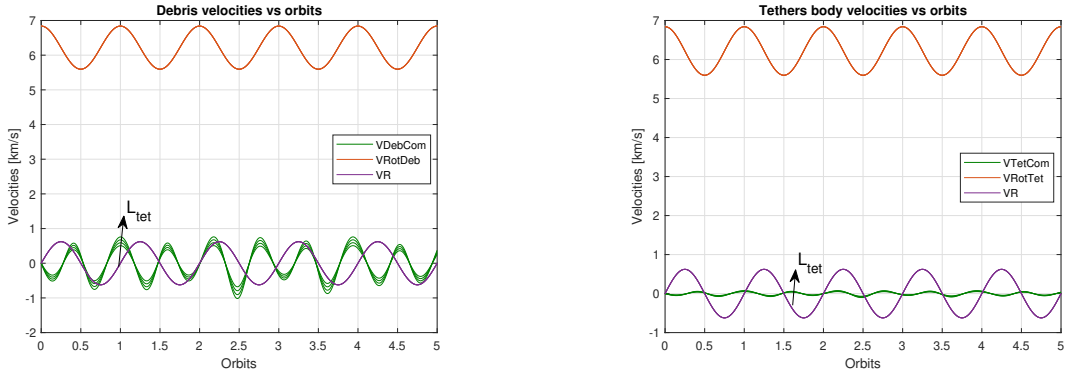

Figure 4.12: Modulus of the velocity components of the debris (left) and the tether's body (right) with $L_{tet} = [80, 100, 120, 140]m$ and $L_{deb} = [800, 1000, 1200, 1400]m$.

Figure 4.13 shows us that the radial, normal and total components of the debris velocities depict more variance as opposed to the much stable behaviour of the tether's body velocities. Nevertheless, varying the lengths of the tether's rope seems to bring a set of velocities much closer to each other for the normal velocities and specially for the radial ones, again due to the eccentricity being fixed this time. This is because varying the tether's length does not affect as much velocity-wise as changing the eccentricity. Moreover, in the graph we can see that as the tether's length increases, all the velocities will remain almost constant except for the normal (and thus total) components for the debris, that will have higher maximums and lower minimums in their values.

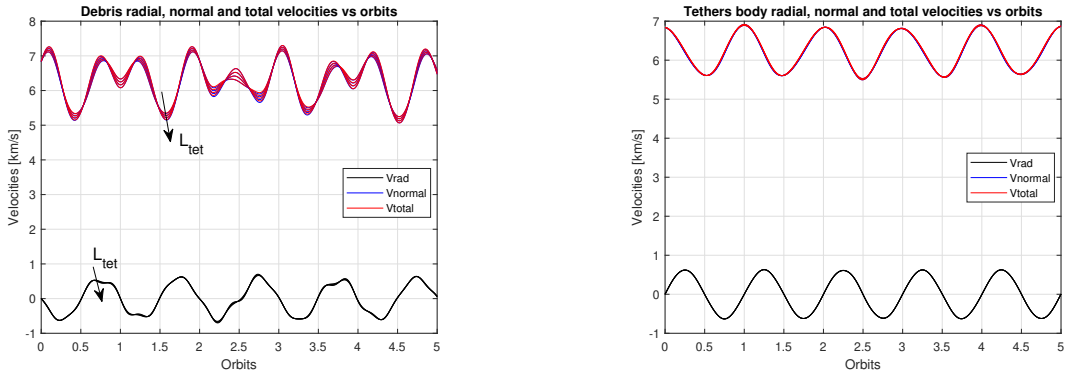

Figure 4.13: Radial, normal and total velocity of the debris (left) and the tether's body (right) with respect of time with $L_{tet} = [80, 100, 120, 140]m$ and $L_{deb} = [800, 1000, 1200, 1400]m$.

The possible semi-major axis the debris will have after release, and the actual values, are given in the next figure.

Similar to the previous scenario, we should find the lowest values of a_{Deb} while being sufficiently close to the apogee. In this second scenario, we will choose the 5th valley of the curves, at around 2.8 orbits. This is because now we will prioritize the fact of being a valley as low as possible (but not so much as to choosing the second or seventh valley, as they are very much situated at the perigee).

By selecting that spot as our release window, a zoom can be seen in the right plot of Figure 4.14, where the minimum values of a_{Deb} are depicted. Additionally, as we increase the tether's length, we get slightly earlier release spots and lower semi-major axis values.

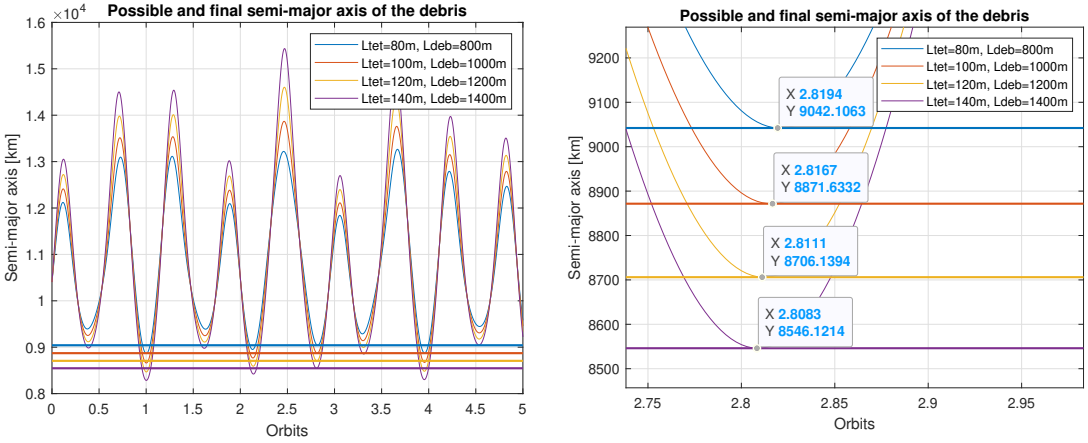

Figure 4.14: Possible and final semi-major axis values for the debris (left) and a zoom in the release spot (right) with $L_{tet} = [80, 100, 120, 140]m$ and $L_{deb} = [800, 1000, 1200, 1400]m$

The semi-major axis values in the case of the tether's body are depicted in Figure 4.15, where the oscillations of the possible values of a_{Tet} are less intense than the debris', and more importantly, the release spots deduced earlier get us close-to-maximum spots for the semi-major axis of the tether's body. The right plot show that even though we are not at the maximum value that we could obtain in rising our tether's body height, we are close enough. The longer we set our tether's rope is beneficial in this case as well, because it gets us higher values of a_{Tet}.

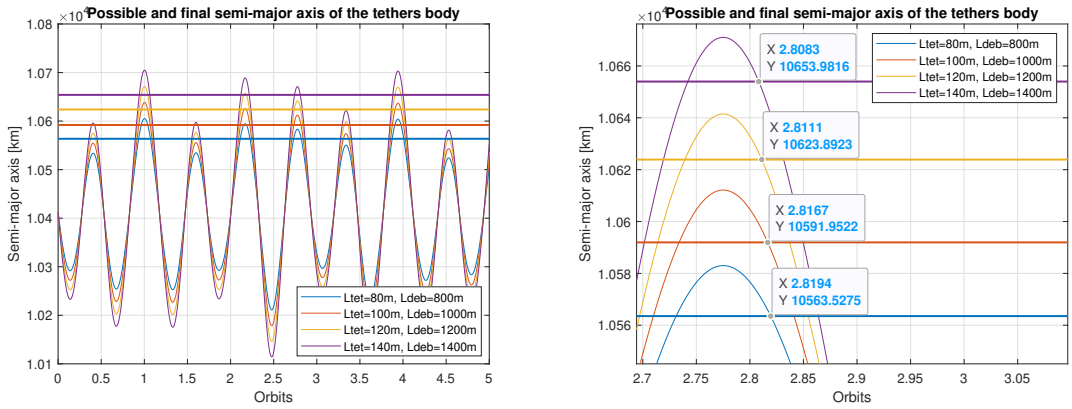

Figure 4.15: Possible and final semi-major axis values for the tether's body (left) and a zoom in the release spot (right) with $L_{tet} = [80, 100, 120, 140]m$ and $L_{deb} = [800, 1000, 1200, 1400]m$

Arguably the most important graphs in each scenario are plots such as 4.16, which shows the new trajectories that the debris has once released. This time we do not start at almost the apogee, but afterwards, because we chose not to be as close to the apogee as we did the first scenario. This is also reflected in the values of the new apogees, that will vary from each value of L_{tet}. The two first tether lengths give us perigee heights of more than 1000 km, our threshold value, and thus are not good enough for our goals. Note that the instant we get to the new perigees is slightly earlier as we decrease the tether's length.

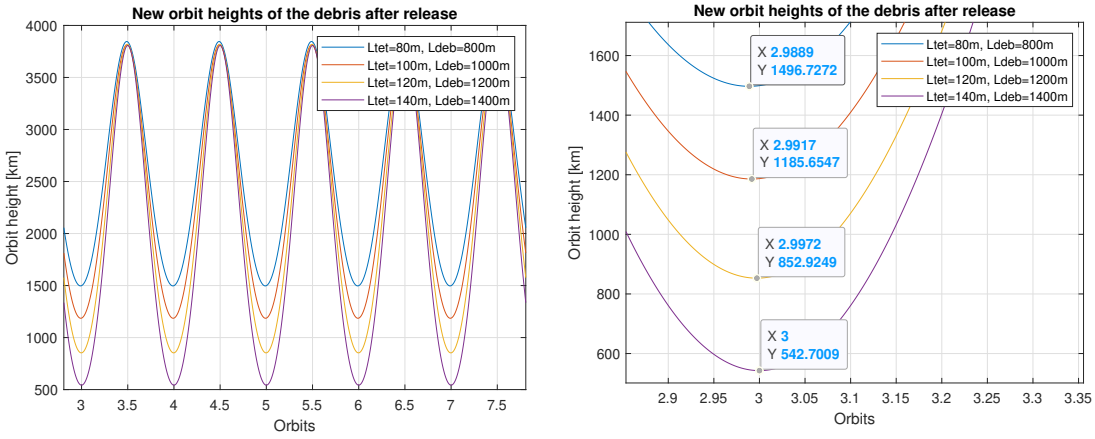

Figure 4.16: New orbital trajectory of the debris after release (left) and a zoom in the new perigee (right) with $L_{tet} = [80, 100, 120, 140]m$ and $L_{deb} = [800, 1000, 1200, 1400]m$

Figure 4.17 depicts the new trajectory of the tether's body, which goes from a height of 3100 km to around 5400 km in the apogee. It can be seen that all four cases start at almost the same height, and the difference between the new perigees are not as significant as the last figure. All four tether lengths give us higher perigees than we had before, but due to the debris not achieving its desirable height in the first two tether lengths, we cannot have them as valid here either. As we increase L_{tet} and L_{deb}, we get higher values of the perigee at a slightly delayed instants.

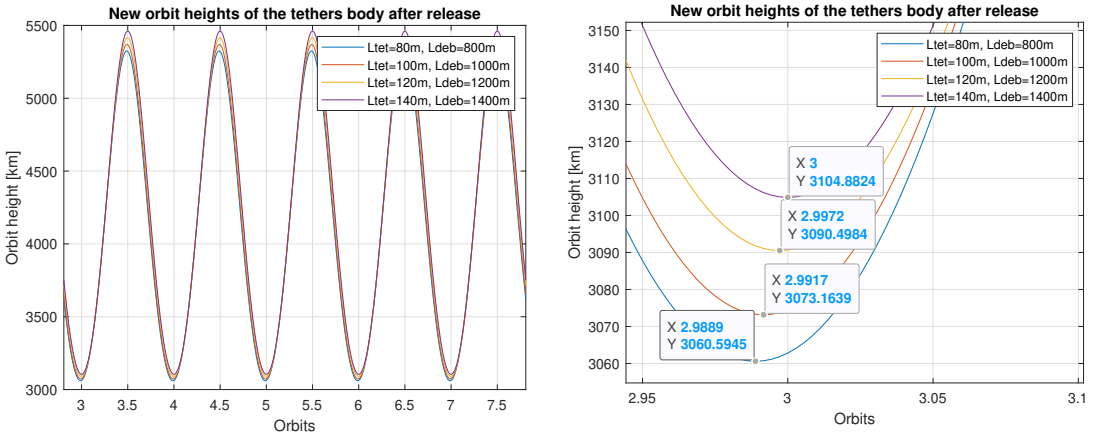

Figure 4.17: New orbital trajectory of the tether's body after release (left) and a zoom in the new perigee (right) with $L_{tet} = [80, 100, 120, 140]m$ and $L_{deb} = [800, 1000, 1200, 1400]m$

4.3. Varying the radius of the perigee

The last variation that will be done to the initial conditions set at the beginning of the chapter is to change the radius of the initial perigee of the CoM orbit. The iteration starts at 2000 km of height (8371 km in terms of radius, adding the radius of the Earth) and keeps increasing 1000 km to reach a final height of 5000 km in the perigee, or h_{per} notation-wise.

The graph corresponding to ψ is the same as the previous case, because neither the tether's length nor the radius of the perigee affects the outcome of the equation of motion that gives us the rotation angle ψ.

In order to interpret the new orbits of the debris and tether's body, 4.18 shows the initial CoM orbit heights along time. It is relevant to note the 4 curves one on top of each other as we keep increasing the perigee. The valleys of each curve represent each of the values of h_{per} that we stated at the beginning of this third scenario.

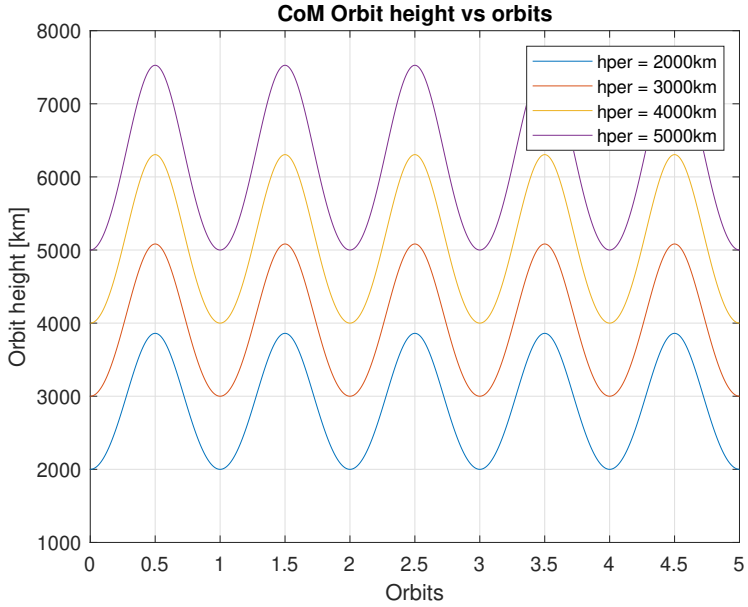

Figure 4.18: Orbital height of the center of mass of the tether system with the conditions of $h_{per} = [2000, 3000, 4000, 5000]km$

The graphs of the modulus of the different velocities of the debris and tether's body are next. As represented in Figure 4.19, V_{RotDeb} and V_{RotTet} can be distinguished from each other, because this time the radius (the most significant variable of V_{Rot}) varies in every iteration. As we keep increasing the height of the initial perigee, the values of V_{Rot} and V_R decrease all-together: their peaks and valleys are reduced.

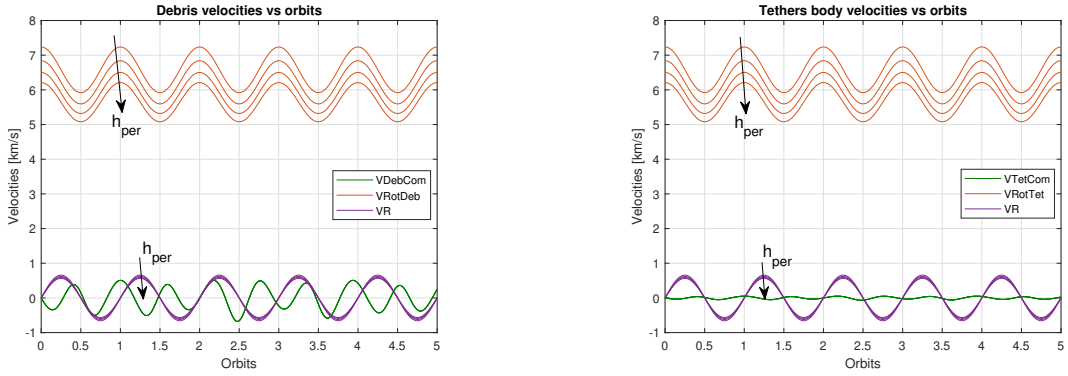

Figure 4.19: Modulus of the velocity components of the debris (left) and the tether's body (right) with $h_{per} = [2000, 3000, 4000, 5000]km$

For the third time, differentiating between radial and normal components, as well as plotting the total component, Figure 4.20 is created. Same as before, the radial component of the debris mirrors the tether's body's radial component. As we keep increasing the radius of the perigee, V_{Norm} will be slower in both end masses. The same outcome can be seen, but in a more subtle way, in the values of V_{Rad}, as we increase h_{per}.

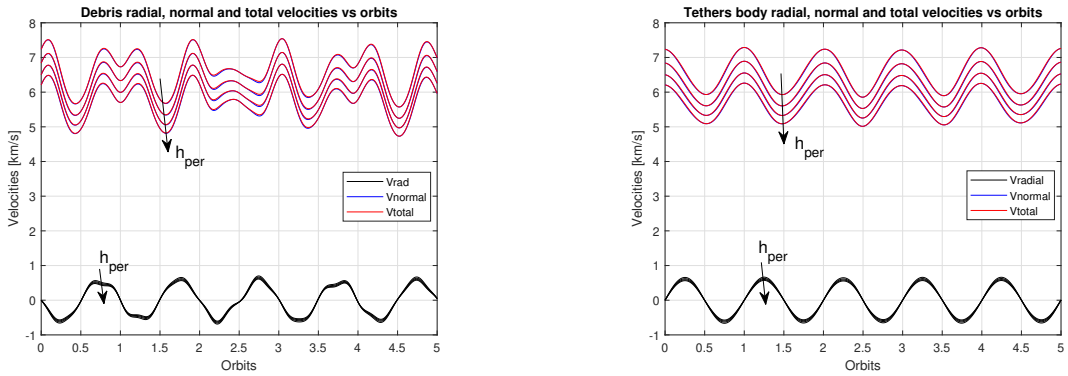

Figure 4.20: Radial, normal and total velocity of the debris (left) and the tether's body (right) with respect of time with $h_{per} = [2000, 3000, 4000, 5000]km$

From the orbital height of the CoM and the total velocity of the debris, the graph of its potential (and final) semi-major axis values are plotted here as well.

Naturally, as we increase the height of the perigee, the virtual semi-major axis while we are in the tether system will increase as well. Out of the eight valleys that we have, in this scenario we will pick the 3rd one, the one after 1.5 orbits. The eighth valleys are closer to their apogee, but since the third ones have a lower value of a_{Deb}, we will go with them.

The right plot of Figure 4.21 shows that as we keep increasing h_{per}, and in order to obtain the minimum values of a_{Deb}, we will get the instants for release slightly sooner each iteration.

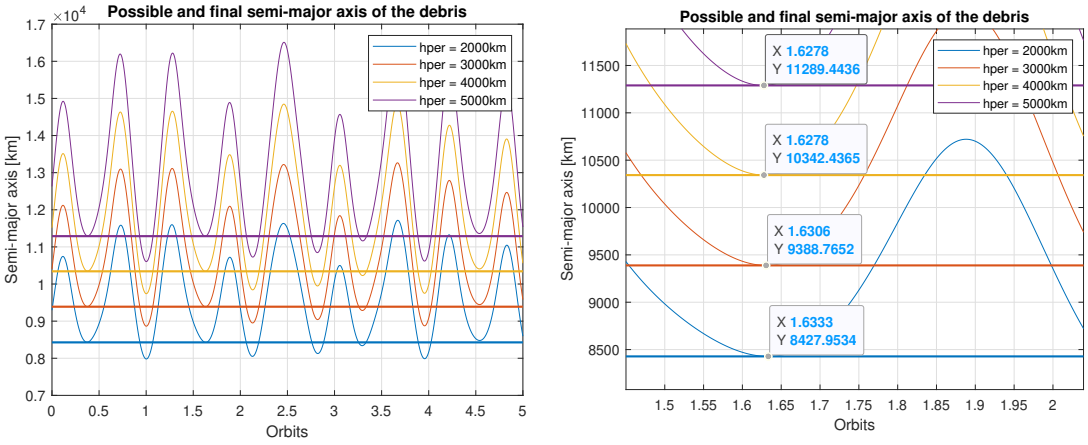

Figure 4.21: Possible and final semi-major axis values for the debris (left) and a zoom in the release spot (right) with $h_{per} = [2000, 3000, 4000, 5000]km$

The possible semi-major axis values of the tether's body a_{Tet} are displayed in Figure 4.22 on the left, with a zoom in the release window on the right plot. A less oscillating behaviour tells us the less intense motion nature of our tether's body in every swing. Same as before, an increase in h_{per} result in an increase of the possible, as well as final, semi-major axis.

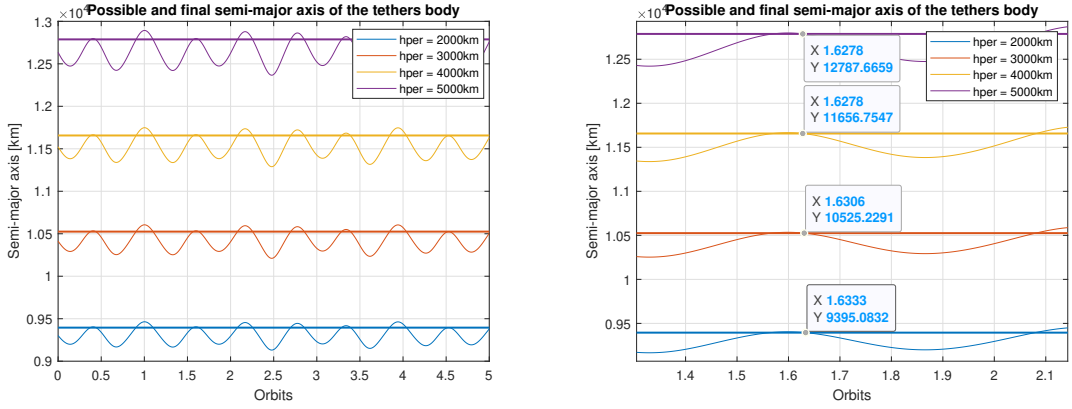

Figure 4.22: Possible and final semi-major axis values for the tether's body (left) and a zoom in the release spot (right) with $h_{per} = [2000, 3000, 4000, 5000]km$

The new orbit of the debris in this scenario starts at the moment of each respective release, and at their respective heights, as seen in Figure 4.23.

By doing the same zoom as before, the right plot of the same figure shows that the new values of the debris' perigee occur at practically the same time, with a slight tendency of delaying the instant of the lowest point in the curve as we increase h_{per}. Moreover, as we keep decreasing this initial condition, we will get closer to Earth values of the perigee.

That being said, the only valid value of h_{per} is when it is equal to 2000 km, because the other ones do not achieve our new perigee threshold of 1000 km, even though all of them succeed in lowering the orbit of the debris from when it was tied to our tether.

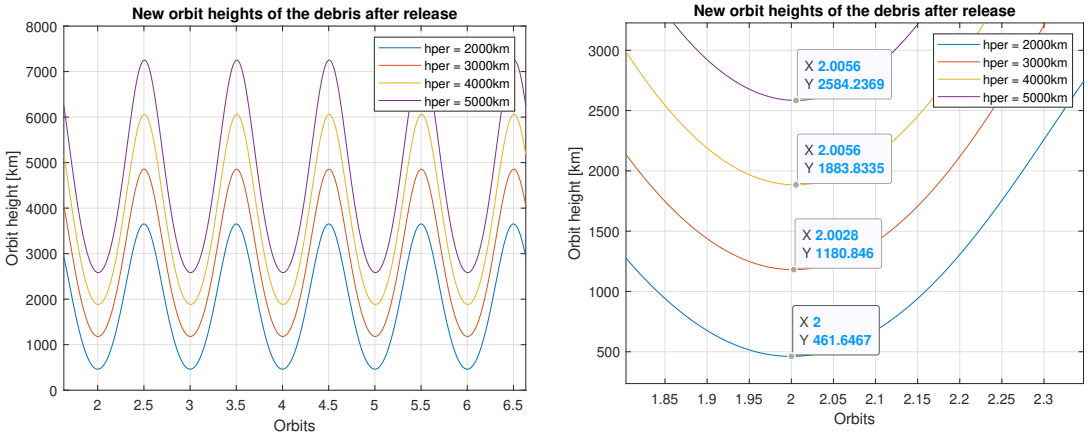

Figure 4.23: New orbital trajectory of the debris after release (left) and a zoom in the new perigee (right) with $h_{per} = [2000, 3000, 4000, 5000]km$

Finally, doing the same procedures for the tether's body, Figure 4.24 shows curves that for every iteration succeeds in rising the lowest point the tether's body had previously: above 2000 km in the blue curve, above 3000 km in the orange one and so on, as seen in the zoomed out plot in the right. The increase in height is every time more significant as we keep increasing h_{per}.

Nevertheless, we can only pick the blue curve as the valid one, because the other three did not achieve our objective of lowering enough the debris.

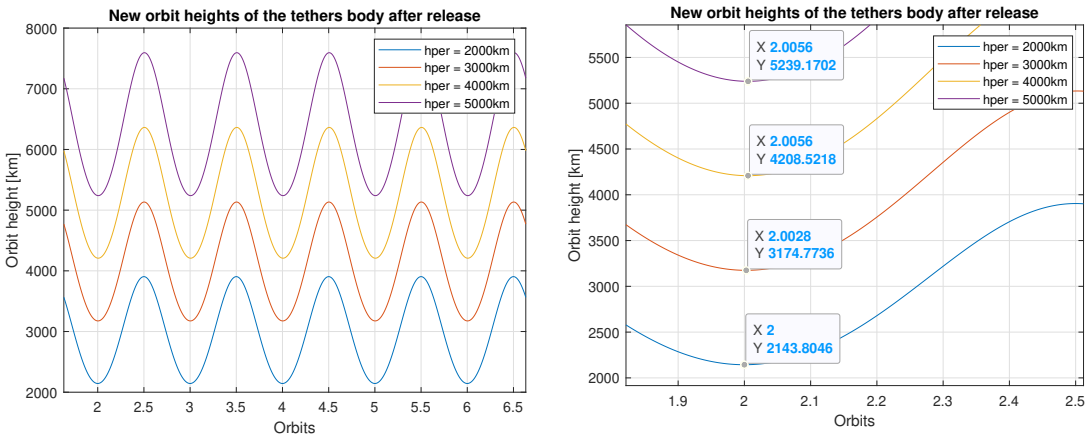

Figure 4.24: New orbital trajectory of the tether's body after release (left) and a zoom in the new perigee (right) with $h_{per} = [2000, 3000, 4000, 5000]km$

CONCLUSIONS

After stating the situation of space debris nowadays, choosing the space tether as the active debris removal system to be studied, and giving the main equations to take results from, we arrived at the graphs of chapter 4.

From Table 4.1, we iterated the parameters of the 3rd column (which in essence was the same as altering the 1st, 2nd and 4th one), the 5th column and the 6th column. Those are, naturally, the length of the tether's body-side of the rope L_{tet}, the initial eccentricity e and the radius of the perigee R_{per}, respectively.

In the first scenario where we varied the eccentricity of our orbit, we chose the moment of release very close to the 4.5 orbits. The resulting graphs of the new orbits showed that increasing e too much meant that our debris would not reach our threshold of 1000 km, but keeping $e = 0$ resulted in our tether's body rising, but not a significant amount. In order to obtain good enough values, we need to set an eccentricity as low as possible, in our case $e = 0.05$ or $e = 0.1$, but keeping it different than 0.

For the tether's length case we chose to prioritize a lower value of a_{deb} even if it deviated more from the apogee, at 2.8 orbits. The results in the new orbit height plots were that the more length we gave to our tether, the lower our debris got in its new perigee and the higher it got in the case of the tether's body. For our initial conditions, lengths below 120 m for the tether's body-side, resulted in the debris not reaching our threshold value in the perigee.

Lastly, for the case of increasing the radius of the perigee, we set the release spot at the valley of semi-major axis that was at 1.6 orbits, and it meant a decrease of the debris in all cases, but the one corresponding to h_{per} = 2000 km was the only valid curve, for the same reasons as before. Nevertheless, as we increased the radius of the perigee, we got difference in heights that were more significant each iteration: debris got increasingly lower values of perigee, comparatively; and the tether's body had risen each iteration more kilometers than before.

From these three scenarios we get that in order to place debris into a low enough orbit (1000 km in the perigee) we must get the lowest a_{deb} possible at release, and also be as close as possible to an apogee in that instant. This, however, is a problem with different answers, as the release point chosen can vary if we prioritize different aspects. All in all, the result from varying the three parameters that we chose was that in order to de-orbit debris to 1000 km, we need the lowest possible (different than 0) eccentricity, as much length of tether's rope as we can, and to set a low value of the initial perigee (the closer this value is to 1000 km, the better).

This leads us to the final thought, which is that once the debris reaches its final value of the perigee, it would start disintegrating, while the tether's body, at which that point would have rose its height from before, could attach to a satellite at a higher orbit to then proceed with another release maneuver, where this time the tether's main body would aim for a lower orbit, and the attached satellite a higher orbit. Future projects could develop that release maneuver to end up placing our tether's body at the same orbital height it had at the beginning of this project. Moreover, a study of the tether system and its release maneuvers in 3D could also be developed, to have a more complete insight on how the pendulum motion of the tether works in three dimensions, the angle α accounting for that.

BIBLIOGRAPHY

[1] Space Debris - NASA. https://www.nasa.gov/centers/hq/library/find/bibliographies/space_debris. On-line (04/2021) 1

[2] Orbital Debris Program Office - NASA's Earth Observatory. https://earthobservatory.nasa.gov/images/40173/space-debris. On-line (04/2021) xi, 1, 2

[3] Space debris by the numbers - ESA. https://www.esa.int/Safety_Security/Space_Debris/Space_debris_by_the_numbers. On-line (04/2021) xiii, 2

[4] The Kessler syndrome - Louis de Gouyon Matignon. https://www.spacelegalissues.com/space-law-the-kessler-syndrome/. On-line (04/2021) 3

[5] FAQs: Orbital Debris - NASA. https://www.nasa.gov/news/debris_faq.html. On-line (05/2021) 3, 28

[6] Analysis and Prediction of Space Debris - ESA. https://www.esa.int/Safety_Security/Space_Debris/Analysis_and_prediction. On-line (05/2021) xi, 3, 4

[7] NASA's new breakup model of evolve 4.0 - N.L.Johnson, P.H. Krisko, J.C.Liou, P.D.Anz-Meador. https://www.sciencedirect.com/science/article/abs/pii/S0273117701004239. On-line (05/2021) 4

[8] Falcon 9 First Stage Landing - SpaceX's Youtube channel. https://www.youtube.com/watch?v=rvsP-mPh9hY. On-line (05/2021) 4

[9] Space Debris Mitigation Guidelines - United Nations. https://orbitaldebris.jsc.nasa.gov/library/space-debris-mitigation-guidelines_copuos.pdf. On-line (05/2021) xiii, 5

[10] Space Law and Hazardous Space Debris (page 12) - International Institute of Space Law https://oxfordre.com/planetaryscience/view/10.1093/acrefore/9780190647926.001.0001/acrefore-9780190647926-e-70?print=pdf. On-line (05/2021) 5

[11] Orbital debris mitigation guidelines still useful, if complied with - Jeff Foust (Space News) https://spacenews.com/orbital-debris-mitigation-guidelines-still-useful-if-complied-with/. On-line (06/2021) 5

[12] Activity of Russian Federation on Space Debris Problem - Federal Space Agency of Russia http://www.unoosa.org/pdf/pres/stsc2007/tech-26.pdf. On-line (06/2021) xiii, 6

[13] ISRO initiates 'Project NETRA' to safeguard Indian space assets from debris and other harm - Madhumathi D.S. (The Hindu) https://www.thehindu.com/sci-tech/science/isro-initiates-project-netra-to-safeguard-indian-space-assets-from\-debris-and-other-harm/article29497795.ece. On-line (06/2021) 6

[14] NASA criticizes China's handling of rocket re-entry as debris lands near Maldives - Jackie Wattles (CNN) https://edition.cnn.com/2021/05/08/app-international-edition/china-space-debris-long-march-rocket-reentry-scn/index.html. On-line (07/2021) xi, 6, 7

[15] Harnessing the Power of the Private Sector to Clean Up Space Junk - JAXA https://global.jaxa.jp/article/2017/special/debris/okada.html. On-line (07/2021) 9

[16] SpaceX's Starship may help clean up space junk - Mike Wall (Space.com) https://www.space.com/spacex-starship-space-junk-cleanup. On-line (07/2021) 9

[17] Space Debris Removal methods classification (pages 29-30) - NASA https://www.nasa.gov/pdf/692076main_Orbital_Debris_Management_and_Risk_Mitigation.pdf. On-line (07/2021) 9

[18] Orbital Debris-Debris Collision Avoidance - James Mason, Jan Stupl, William Marshall, Creon Levit https://arxiv.org/pdf/1103.1690.pdf. On-line (06/2021) xi, xiii, 10

[19] Bionic Design and Experimental Study for the Space Flexible Webs Capture System - Boting Xu, Yueneng Yang, Bin Zhang, Ye Yan, Zhiyong Yi https://ieeexplore.ieee.org/document/9022992?denied=. On-line (06/2021) xi, 11

[20] Dynamics of the Net Systems, Capturing Space Debris (page 7) - Pavel M. Trivailo, Hirohisa Kojima https://www.jstage.jst.go.jp/article/tastj/14/ists30/14_Pr_57/_pdf. On-line (06/2021) xi, 12

[21] Swiss technology hunting space debris - Mehdi Atmani (House of Switzerland) https://www.houseofswitzerland.org/swissstories/science-education/swiss-technology-hunting-space-debris. On-line (07/2021) 12

[22] ESA purchases world-first debris removal mission from start-up - ESA https://www.esa.int/Safety_Security/ESA_purchases_world-first_debris_removal_mission_from_start-up. On-line (07/2021) 12

[23] ESA's debris removal mission - ESA's Youtube channel https://www.youtube.com/watch?v=il5cvSzYMfE&feature=emb_title. On-line (07/2021) xi, 13

[24] Spaceblower: A Rocket to Combat Space Debris - CNES https://sciences-techniques.cnes.fr/en/space-blower-rocket-combat-space-debris. On-line (06/2021) xi, 13, 14

[25] The Terminator Tether Aims to Clean Up Low Earth Orbit - Bill Christensen (Space.com) https://www.space.com/537-terminator-tether-aims-clean-earth-orbit.html. On-line (06/2021) xi, 15

[26] Europe's Vega launch vehicle - Anatoly Zak (Russian Space Web) http://www.russianspaceweb.com/vega_lv.html. On-line (08/2021) 16

[27] ESTCube-1 nanosatellite for electric solar wind sail in-orbit technology demonstration - Silver Lätt, Andris Slavinskis, Erik Ilbis, Mart Noorma https://www.researchgate.net/figure/Assembled-ESTCube-1-satellite-at-the-Guiana-Space-Centre-in-French\-Guiana_fig1_262821715. On-line (07/2021) xi, 16

[28] Space Transportation with a Twist - NASA https://www.nasa.gov/vision/universe/roboticexplorers/tethered_spacecraft.html. On-line (07/2021) 17

[29] Design and Analysis of Preload Control for Space Debris Impact Adhesion Capture Method - Zhengyou Xie, Xinlong Chen, Yajing Ren, Yangyang Zhao https://ieeexplore.ieee.org/document/9252955?denied=. On-line (06/2021) 17

[30] Applications of Tethered Space Systems in Spacecraft Propulsion (page 12) - Brandon Copp https://www.colorado.edu/faculty/kantha/sites/default/files/attached-files/final_report_copp.pdf. On-line (06/2021) 17

[31] Mecánica newtoniana (page 68) - Joan Josep Martínez Benjamín (2001). 21

[32] Vis-viva equation - (The Space Techie) https://www.thespacetechie.com/vis-viva-equation/. On-line (08/2021) xi, 20, 21

[33] Mecánica newtoniana (page 63) - Joan Josep Martínez Benjamín (2001). 21

[34] Tethered Satellites - Forces And Motion (1994) - AIRBOYD https://www.youtube.com/watch?v=tsEKGxoMGdA. On-line (08/2021)

[35] Orbital Debris: A Technical Assessment (page 70) - Committee on Space Debris https://www.nap.edu/read/4765/chapter/670. On-line (08/2021) 23

[36] Orbital Mechanics for Engineering Students (pages 338-340) - Howard Curtis (2005). 22

[37] Semilatus Rectum - Mathworld (Wolfram) https://mathworld.wolfram.com/SemilatusRectum.html. On-line (08/2021) 20

[38] The Rigid-body Dynamics of Tethers in Space (pages 34-38)- Spencer Wilson Ziegler (2003). xi, 27, 33

[39] Modern Astrodynamics (pages 210-225) - Pini Gurfil (2006)

[40] LEO details - ESA https://www.esa.int/ESA_Multimedia/Images/2020/03/Low_Earth_orbit. On-line (08/2021) 1

[41] What Is a Geosynchronous Orbit? - Elizabeth Howell (Space.com) https://www.space.com/29222-geosynchronous-orbit.html. On-line (08/2021) 1

[42] What is a Lagrange Point? - Neil J. Cornish (NASA Science) https://solarsystem.nasa.gov/resources/754/what-is-a-lagrange-point/. On-line (08/2021) 3

[43] Orbital Debris: A Technical Assessment (page 63) - Committee on Space Debris (1995) https://www.nap.edu/read/4765/chapter/6. On-line (08/2021) 23

[44] Mecánica newtoniana (page 162) - Joan Josep Martínez Benjamín (2001). xiii, 39, 40

[45] Kepler's Laws of Planetary Motion - LumenCandela https://courses.lumenlearning.com/suny-osuniversityphysics/chapter/13-5-keplers-laws-of-planetary-motion/. On-line (09/2021) 25

[46] Orbital Velocity Formula - Vedantu https://www.vedantu.com/formula/orbital-velocity-formula. On-line (09/2021) 25

APPENDICES

APPENDIX A. MATLAB CODE

ZIEGLER FUNCTION

```
function dxdt = DifferentialZiegler(t,x,e)
    dxdt(1) = x(2);
    dxdt(2) = (2 * x(4) * tan(x(3)) + (2*e*sin(t))/(1 + e * cos(t
       ))) * (x(2) + 1) - (3 * sin(2*x(1)))/(2 * (1+e*cos(t)));
    dxdt(3) = x(4);
    dxdt(4) = (2*e*sin(t))/(1 + e * cos(t)) * x(4) - (sin(2*x(3))
        / 2) * ((x(2) + 1)^2 + ((3 * (cos(x(1)))^2)/(1+e*cos(t)))
       );
    dxdt = dxdt';
end
```

MAIN FUNCTION

```
function [dxdt] = Differential(t,x,e)
        dxdt(1) = x(2);
        dxdt(2) = ((2 * e * sin(t))/(1 + e * cos(t))) * (x(2) +
           1) - (3 * sin(2 * x(1))) / (2 * (1 + e * cos(t)));
        dxdt = dxdt';
end
```

ZIEGLER SCENARIO

```
clc;clear;close all;
syms y(x) w(x);
%THETA = x, PSI = y, ALPHA = w

G = 6.674e-11;
Me = 5.972e24;
mu = G * Me;
rad = pi/180;
Re = 6371000;

%ORBIT INTERVAL
x0 = 0;
xf = 5 * 2*pi;
xinterval = (x0:rad*1:xf);

%INITIAL ANGLES
y0 = 0;
w0 = 0.1;
dy0 = 0;
dw0 = 0;
```

```
21 initialconditions = [y0; dy0; w0; dw0];
22
23 %RADIUS PERIGEE
24 rp = 7000000;
25
26 %MASSES AND LENGTHS
27 Md = 1000;
28 Mt = 1000;
29 Ld = 10000;
30 Lt = 10000;
31
32 %ECCENTRICITY
33 e = 0.25;
34
35 %VELOCITIES
36 [theta, Y] = ode45(@(theta, Y) DifferentialZiegler(theta,Y,e),
       xinterval,initialconditions);
37 psi = Y(:,1);
38 dpsi = Y(:,2);
39 alpha = Y(:,3);
40 dalpha = Y(:,4);
41
42 for i=1:length(theta)
43     Rcom(i) = (rp*(1+e))/(1+e*cos(theta(i)));
44     dtheta(i) = sqrt((mu/(1+e*cos(theta(i)))) / ((Rcom(i))^3));
45     dRcom(i) = rp * (1+e) * (1 / (1+e*cos(theta(i)))^2) * (e*sin(
           theta(i)))*dtheta(i);
46     Rtet(i) = sqrt(Lt^2+(Rcom(i))^2+2*Lt*Rcom(i)*cos(alpha(i))*
           cos(psi(i)));
47     Rdeb(i) = sqrt(Ld^2+(Rcom(i))^2-2*Ld*Rcom(i)*cos(alpha(i))*
           cos(psi(i)));
48
49     dxtet(i) = dRcom(i)*cos(theta(i)) - Rcom(i)*dtheta(i)*sin(
           theta(i)) + Lt*(-dalpha(i)*sin(alpha(i))*cos(psi(i)+theta(
           i)) + cos(alpha(i))*(dpsi(i)+dtheta(i))*-sin(psi(i)+theta(
           i)));
50     dytet(i) = dRcom(i)*sin(theta(i))+Rcom(i)*dtheta(i)*cos(theta
           (i)) + Lt * (-dalpha(i)*sin(alpha(i))*sin(psi(i)+theta(i))
            + cos(alpha(i))*(dpsi(i)+dtheta(i))*cos(psi(i)+theta(i)))
           ;
51     dztet(i) = Lt * dalpha(i)*cos(alpha(i));
52
53     dxdeb(i) = dRcom(i)*cos(theta(i))-Rcom(i)*dtheta(i)*sin(theta
           (i)) - Ld * (-dalpha(i)*sin(alpha(i))*cos(psi(i)+theta(i))
            + cos(alpha(i))*(dpsi(i)+dtheta(i))*-sin(psi(i)+theta(i))
           );
54     dydeb(i) = dRcom(i)*sin(theta(i))+Rcom(i)*dtheta(i)*cos(theta
           (i)) - Ld * (-dalpha(i)*sin(alpha(i))*sin(psi(i)+theta(i))
```

```
        + cos(alpha(i))*(dpsi(i)+dtheta(i))*cos(psi(i)+theta(i)))
       ;
    dzdeb(i) = - Ld * dalpha(i)*cos(alpha(i));

    VTotTet(i) = sqrt(dxtet(i)^2 + dytet(i)^2 + dztet(i)^2);
    VTotDeb(i) = sqrt(dxdeb(i)^2 + dydeb(i)^2 + dzdeb(i)^2);
end

%PSI PLOT
figure;
plot(theta/(2*pi),psi,'r');  grid on;
xlabel('Orbits'); lg = ylabel('Rotation Angle $\psi$[rad]');
tl = title('$\psi$ vs orbits');
set(lg, 'Interpreter', 'latex'); set(tl, 'Interpreter', 'latex');

%ALPHA PLOT
figure;
plot(theta/(2*pi),alpha,'r'); grid on;
xlabel('Orbits'); lg = ylabel('Out-of-plane Angle $\alpha$ [rad]'
   );
tl = title('$\alpha$ vs orbits');
set(lg, 'Interpreter', 'latex'); set(tl, 'Interpreter', 'latex');

%RADIUS PLOT
figure;
plot(theta/(2*pi),Rcom / 1000 - (Re / 1000),'k'); grid on;
xlabel('Orbits'); ylabel('Orbit height [km]');
title('CoM orbit height vs orbits');

%THETA PLOT
figure;
plot(theta/(2*pi),wrapTo2Pi(theta)); grid on;
xlabel('Orbits'); ylabel('True Anomaly $\theta$ [rad]');
lg = title('$\theta$ vs orbits');
pmin = min(theta);
pmax = max(theta);
pimin = floor(pmin/pi);
pimax = ceil(pmax/pi);
ylim([0 2*pi])
yticks((pimin:pimax) * pi);
yticklabels( string(pimin:pimax) + "\pi" )
set(lg, 'Interpreter', 'latex'); set(tl, 'Interpreter', 'latex');

%VELOCITIES PLOT
figure;
plot(theta/(2*pi),VTotDeb / 1000,'r'); hold on;
plot(theta/(2*pi),VTotTet / 1000,'b'); grid on;
legend('VTotDeb', 'VTotTet');
```

```
100 xlabel('Orbits'); ylabel('Total Velocities [km/s]');
101 title('Total velocities moduli vs orbits');
```

MAIN SCENARIO

```
1  %------- Varying eccentricity -------
2
3  clc;clear;close all;
4  syms y(x);
5  %THETA = x, PSI = y
6
7  G = 6.674e-11;
8  Me = 5.972e24;
9  mu = G * Me;
10 rad = pi/180;
11 Re = 6371000;
12
13 %ORBIT INTERVAL
14 x0 = 0;
15 xf = 5 * 2*pi;
16 xinterval = (x0:rad*1:xf);
17
18 %INITIAL ANGLES
19 y0 = 0.2;
20 dy0 = 0;
21 initialconditions = [y0; dy0];
22
23 %RADIUS PERIGEE
24 rp = 3000000 + Re;
25
26 %MASSES AND LENGTHS
27 Md = 100;
28 Mt = 1000;
29 Lt = 120;
30 Ld = (Mt / Md) * Lt;
31
32 %ECCENTRICITY
33 e = 0;
34 for k=2:4
35     e(k) = e(k-1) + 0.05;
36 end
37
38 %VELOCITIES
39 for k=1:length(e)
40     [theta, Y] = ode45(@(theta, Y) Differential(theta,Y,e(k)),
          xinterval,initialconditions);
41     psi(:,k) = Y(:,1);
42     dpsi(:,k) = Y(:,2);
```

```
    for i=1:length(theta)
        Rcom(i,k) = (rp * (1 + e(k))) / (1 + e(k) * cos(theta(i)));
        dtheta(i,k) = sqrt( (mu*(1 + e(k)*cos(theta(i)))) / (Rcom(i,k)^3) );
        dRcom(i,k) = rp * (1+e(k)) * (1/(1+e(k)*cos(theta(i)))^2) * (e(k)*sin(theta(i)))*dtheta(i,k);
        Rdeb(i,k) = sqrt(Ld^2 + (Rcom(i,k))^2 - 2 * Ld * Rcom(i,k) * cos(psi(i,k)));
        Rtet(i,k) = sqrt(Lt^2 + (Rcom(i,k))^2 + 2 * Lt * Rcom(i,k) * cos(psi(i,k)));

        VR(i,k) = dRcom(i,k);
        vRotTet(i,k) = dtheta(i,k) * Rtet(i,k);
        vRotDeb(i,k) = dtheta(i,k) * Rdeb(i,k);
        vTetCom(i,k) = Lt * dpsi(i,k);
        vDebCom(i,k) = Ld * dpsi(i,k);

        phi1(i,k) = asin((Rcom(i,k) * sin(psi(i,k)))/Rdeb(i,k)) - pi/2;
        lambda1(i,k) = pi/2 - phi1(i,k) - psi(i,k);
        phi2(i,k) = asin((Rcom(i,k) / Rtet(i,k)) * sin(pi - psi(i,k)));
        lambda2(i,k) = psi(i,k) - phi2(i,k);

        VRadDeb(i,k) = - vDebCom(i,k) * cos(phi1(i,k)) + VR(i,k) * cos(lambda1(i,k));
        VNormDeb(i,k) = vRotDeb(i,k) + vDebCom(i,k) * sin(phi1(i,k)) + VR(i,k) * sin(lambda1(i,k));
        VRadTet(i,k) = - vTetCom(i,k) * sin(phi2(i,k)) + VR(i,k) * cos(lambda2(i,k));
        VNormTet(i,k) = vRotTet(i,k) + vTetCom(i,k) * cos(phi2(i,k)) - VR(i,k) * sin(lambda2(i,k));

        VTotDeb(i,k) = sqrt(VRadDeb(i,k)^2 + VNormDeb(i,k)^2);
        VTotTet(i,k) = sqrt(VRadTet(i,k)^2 + VNormTet(i,k)^2);
    end
end

%PSI PLOT
o = [];
figure;
yyaxis left
plot(theta/(2*pi),psi(:,1));
xlabel('Orbits'); t1 = ylabel('Rotation Angle $\psi$ [rad]');
   hold on;
yyaxis right
plot(theta/(2*pi),dpsi(:,1)); grid on;
```

```
xlabel('Orbits'); t2 = ylabel('Rotation Velocity $\dot{\psi}$ [rad/s]');
tl = title('$\psi$ and $\dot{\psi}$ vs orbits');
set(tl, 'Interpreter', 'latex'); set(t1, 'Interpreter', 'latex'); set(t2, 'Interpreter', 'latex');

figure;
yyaxis left
o(:,1) = plot(theta/(2*pi),psi);
xlabel('Orbits'); t1 = ylabel('Rotation Angle $\psi$ [rad]'); hold on;
yyaxis right
o(:,2) = plot(theta/(2*pi),dpsi); grid on;
xlabel('Orbits'); t2 = ylabel('Rotation Velocity $\dot{\psi}$ [rad/s]');
legend(o(:,1), 'e = 0', 'e = 0.05', 'e = 0.1', 'e = 0.15');
tl = title('$\psi$ and $\dot{\psi}$ vs orbits');
set(tl, 'Interpreter', 'latex'); set(t1, 'Interpreter', 'latex'); set(t2, 'Interpreter', 'latex');

%RADIUS PLOT
figure;
plot(theta/(2*pi),Rcom / 1000 - (Re / 1000)); grid on;
legend('e = 0', 'e = 0.05', 'e = 0.1', 'e = 0.15');
xlabel('Orbits'); ylabel('Orbit height [km]');
title('CoM orbit height vs orbits');

%DEBRIS VELOCITIES PLOT
o = [];
figure;
o(:,1) = plot(theta/(2*pi),vDebCom / 1000, '-', 'color', [0, 0.5, 0]); hold on;
o(:,2) = plot(theta/(2*pi),vRotDeb / 1000, '-', 'color', [0.8500, 0.3250, 0.0980]); hold on;
o(:,3) = plot(theta/(2*pi),VR / 1000, '-', 'color', [0.4940, 0.1840, 0.5560]); grid on;
legend(o(1,:), 'VDebCom', 'VRotDeb', 'VR');
xlabel('Orbits'); ylabel('Velocities [km/s]');
title('Debris velocities vs orbits');

figure;
o(:,1) = plot(theta/(2*pi),VRadDeb / 1000, 'k'); hold on;
o(:,2) = plot(theta/(2*pi),VNormDeb / 1000, 'b'); hold on;
o(:,3) = plot(theta/(2*pi),VTotDeb / 1000, 'r'); grid on;
legend(o(1,:), 'Vradial', 'Vnormal', 'Vtotal');
xlabel('Orbits'); ylabel('Velocities [km/s]');
title('Debris radial, normal and total velocities vs orbits');

```

```
%TETHER'S BODY VELOCITIES PLOT
figure;
o(:,1) = plot(theta/(2*pi),vTetCom / 1000, '-', 'color', [0, 0.5, 0]); hold on;
o(:,2) = plot(theta/(2*pi),vRotTet / 1000, '-', 'color', [0.8500, 0.3250, 0.0980]); hold on;
o(:,3) = plot(theta/(2*pi),VR / 1000, '-', 'color', [0.4940, 0.1840, 0.5560]); grid on;
legend(o(1,:), 'VTetCom', 'VRotTet', 'VR');
xlabel('Orbits'); ylabel('Velocities [km/s]');
title('Tethers body velocities vs orbits');

figure;
o(:,1) = plot(theta/(2*pi),VRadTet / 1000, 'k'); hold on;
o(:,2) = plot(theta/(2*pi),VNormTet / 1000, 'b'); hold on;
o(:,3) = plot(theta/(2*pi),VTotTet / 1000, 'r'); grid on;
legend(o(1,:), 'Vradial', 'Vnormal', 'Vtotal');
xlabel('Orbits'); ylabel('Velocities [km/s]');
title('Tethers body radial, normal and total velocities vs orbits');

%TRANSFER ORBIT CALCULATIONS
for k=1:length(e)
    for i = 1:length(theta)
        adeb(i,k) = (mu * Rdeb(i,k)) / (2*mu - (VTotDeb(i,k))^2*Rdeb(i,k));
        atet(i,k) = (mu * Rtet(i,k)) / (2*mu - (VTotTet(i,k))^2*Rtet(i,k));
    end
    [A] = islocalmin(adeb);
    Minimum = find(A(:,k) == 1);

    ReleasePosition(k) = Minimum(8); %Of all the valleys of a_deb, this value represents the one that is chosen to be the release instant
    VNormDebRelease(k) = VNormDeb(ReleasePosition(k),k);
    VTotDebRelease(k) = VTotDeb(ReleasePosition(k),k);
    VNormTetRelease(k) = VNormTet(ReleasePosition(k),k);
    VTotTetRelease(k) = VTotTet(ReleasePosition(k),k);

    psirelease(k) = psi(ReleasePosition(k),k);

    adebrelease(k) = (mu * Rdeb(ReleasePosition(k),k)) / (2*mu - (VTotDebRelease(k)^2)*Rdeb(ReleasePosition(k),k));
    pdeb(k) = (VNormDebRelease(k)*Rdeb(ReleasePosition(k),k))^2 / mu;
    edeb(k) = sqrt(1 - pdeb(k)/adebrelease(k));
    atetrelease(k) = (mu * Rtet(ReleasePosition(k),k)) / (2*mu - (VTotTetRelease(k)^2)*Rtet(ReleasePosition(k),k));
```

```
157     ptet(k) = (VNormTetRelease(k)*Rtet(ReleasePosition(k),k))^2 /
            mu;
158     etet(k) = sqrt(1 - ptet(k)/atetrelease(k));
159
160     for i = 1:length(theta)
161         Rnewdeb(i,k) = pdeb(k) / (1 + edeb(k) * cos(theta(i)+
                theta(ReleasePosition(k))));
162         Rnewtet(i,k) = ptet(k) / (1 + etet(k) * cos(theta(i)+
                theta(ReleasePosition(k))));
163         dthetadeb(i,k) = sqrt( (mu*(1 + edeb(k)*cos(theta(i)+
                theta(ReleasePosition(k))))) / (Rnewdeb(i,k)^3) );
164         dthetatet(i,k) = sqrt( (mu*(1 + etet(k)*cos(theta(i)+
                theta(ReleasePosition(k))))) / (Rnewtet(i,k)^3) );
165         dRnewdeb(i,k) = pdeb(k) * (1/(1+edeb(k)*cos(theta(i)+
                theta(ReleasePosition(k))))^2) * (edeb(k)*sin(theta(i)
                +theta(ReleasePosition(k)))) * dthetadeb(i,k);
166         dRnewtet(i,k) = ptet(k) * (1/(1+etet(k)*cos(theta(i)+
                theta(ReleasePosition(k))))^2) * (etet(k)*sin(theta(i)
                +theta(ReleasePosition(k)))) * dthetatet(i,k);
167         VTotDeb2(i,k) = sqrt(dRnewdeb(i,k)^2 + (dthetadeb(i,k)*
                Rnewdeb(i,k))^2);
168         VTotTet2(i,k) = sqrt(dRnewtet(i,k)^2 + (dthetatet(i,k)*
                Rnewtet(i,k))^2);
169
170         adeb2(i,k) = (mu * Rnewdeb(i,k)) / (2*mu - (VTotDeb2(i,k)
                )^2*Rnewdeb(i,k));
171         atet2(i,k) = (mu * Rnewtet(i,k)) / (2*mu - (VTotTet2(i,k)
                )^2*Rnewtet(i,k));
172
173         orbits(i,k) = theta(i)/(2*pi) + theta(ReleasePosition(k))
                /(2*pi);
174     end
175 end
176
177 o = [];
178 figure;
179 o(:,1) = plot(theta/(2*pi),adeb / 1000);
180 xlabel('Orbits'); ylabel('Semi-major axis [km]'); hold on;
181 plot(theta/(2*pi),adeb2(:,1) / 1000,'-', 'color', [0, 0.4470,
        0.7410],'LineWidth',1.5); hold on;
182 plot(theta/(2*pi),adeb2(:,2) / 1000,'-', 'color', [0.8500,
        0.3250, 0.0980],'LineWidth',1.5); hold on;
183 plot(theta/(2*pi),adeb2(:,3) / 1000,'-', 'color', [0.9290,
        0.6940, 0.1250],'LineWidth',1.5); hold on;
184 plot(theta/(2*pi),adeb2(:,4) / 1000,'-', 'color', [0.4940,
        0.1840, 0.5560],'LineWidth',1.5); grid on;
185 legend(o(:,1), 'e = 0', 'e = 0.05', 'e = 0.1', 'e = 0.15');
186 title('Possible and final semi-major axis of the debris');
```

```
187
188 o = [];
189 figure;
190 o(:,1) = plot(theta/(2*pi),atet / 1000);
191 xlabel('Orbits'); ylabel('Semi-major axis [km]'); hold on;
192 plot(theta/(2*pi),atet2(:,1) / 1000,'-', 'color', [0, 0.4470,
    0.7410],'LineWidth',1.5); hold on;
193 plot(theta/(2*pi),atet2(:,2) / 1000,'-', 'color', [0.8500,
    0.3250, 0.0980],'LineWidth',1.5); hold on;
194 plot(theta/(2*pi),atet2(:,3) / 1000,'-', 'color', [0.9290,
    0.6940, 0.1250],'LineWidth',1.5); hold on;
195 plot(theta/(2*pi),atet2(:,4) / 1000,'-', 'color', [0.4940,
    0.1840, 0.5560],'LineWidth',1.5); grid on;
196 legend(o(:,1), 'e = 0', 'e = 0.05', 'e = 0.1', 'e = 0.15');
197 title('Possible and final semi-major axis of the tethers body');
198
199 figure;
200 for k=1:length(e)
201     plot(orbits(:,k),(Rnewdeb - Re)/1000); grid on;
202     legend('e = 0', 'e = 0.05', 'e = 0.1', 'e = 0.15');
203     xlabel('Orbits'); ylabel('Orbit height [km]');
204     xlim([orbits(1,k) orbits(1,k)+5])
205     title('New orbit heights of the debris after release');
206 end
207
208 figure;
209 for k=1:length(e)
210     plot(orbits(:,k),(Rnewtet - Re)/1000); grid on;
211     legend('e = 0', 'e = 0.05', 'e = 0.1', 'e = 0.15');
212     xlabel('Orbits'); ylabel('Orbit height [km]');
213     xlim([orbits(1,k) orbits(1,k)+5])
214     title('New orbit heights of the tethers body after release');
215 end
216
217
218
219 %------- Varying tether's length -------
220
221 clc;clear;close all;
222 syms y(x);
223 %THETA = x, PSI = y
224
225 G = 6.674e-11;
226 Me = 5.972e24;
227 mu = G * Me;
228 rad = pi/180;
229 Re = 6371000;
230
```

```
231 %ORBIT INTERVAL
232 x0 = 0;
233 xf = 5 * 2*pi;
234 xinterval = (x0:rad*1:xf);
235
236 %INITIAL ANGLES
237 y0 = 0.2;
238 dy0 = 0;
239 initialconditions = [y0; dy0];
240
241 %RADIUS PERIGEE
242 rp = 3000000 + Re;
243
244 %MASSES AND LENGTHS
245 Md = 100;
246 Mt = 1000;
247 Lt = 120;
248 for k=2:4
249     Lt(k) = Lt(k-1) + 20;
250 end
251 Ld = (Mt / Md) * Lt;
252
253 %ECCENTRICITY
254 e = 0.1;
255
256 %VELOCITIES
257 [theta, Y] = ode45(@(theta, Y) Differential(theta,Y,e),xinterval,
        initialconditions);
258 psi = Y(:,1);
259 dpsi = Y(:,2);
260 for k=1:length(Lt)
261     for i=1:length(theta)
262         Rcom(i,k) = (rp*(1+e)) / (1 + e* cos(theta(i)));
263         dtheta(i,k) = sqrt((mu*(1+e*cos(theta(i)))) / ((Rcom(i,k)
                )^3));
264         dRcom(i,k) = rp * (1+e) * (1/(1+e*cos(theta(i)))^2)*(e*
                sin(theta(i)))*dtheta(i,k);
265         Rdeb(i,k) = sqrt(Ld(k)^2+(Rcom(i,k))^2-2*Ld(k)*Rcom(i,k)*
                cos(psi(i)));
266         Rtet(i,k) = sqrt(Lt(k)^2+(Rcom(i,k))^2+2*Lt(k)*Rcom(i,k)*
                cos(psi(i)));
267
268         VR(i,k) = dRcom(i);
269         vRotTet(i,k) = dtheta(i,k) * Rtet(i,k);
270         vRotDeb(i,k) = dtheta(i,k) * Rdeb(i,k);
271         vTetCom(i,k) = Lt(k) * dpsi(i);
272         vDebCom(i,k) = Ld(k) * dpsi(i);
273
```

```
274         phi1(i,k) = asin((Rcom(i,k) * sin(psi(i)))/Rdeb(i,k)) -
                pi/2;
275         lambda1(i,k) = pi/2 - phi1(i,k) - psi(i);
276         phi2(i,k) = asin((Rcom(i,k) / Rtet(i,k)) * sin(pi - psi(i
                )));
277         lambda2(i,k) = psi(i) - phi2(i,k);
278
279         VRadDeb(i,k) = - vDebCom(i,k) * cos(phi1(i,k)) + VR(i,k)
                * cos(lambda1(i,k));
280         VNormDeb(i,k) = vRotDeb(i,k) + vDebCom(i,k) * sin(phi1(i,
                k)) + VR(i,k) * sin(lambda1(i,k));
281         VRadTet(i,k) = - vTetCom(i,k) * sin(phi2(i,k)) + VR(i,k)
                * cos(lambda2(i,k));
282         VNormTet(i,k) = vRotTet(i,k) + vTetCom(i,k) * cos(phi2(i,
                k)) - VR(i,k) * sin(lambda2(i,k));
283         VTotDeb(i,k) = sqrt(VRadDeb(i,k)^2 + VNormDeb(i,k)^2);
284         VTotTet(i,k) = sqrt(VRadTet(i,k)^2 + VNormTet(i,k)^2);
285     end
286 end
287
288 %PSI PLOT
289 figure;
290 yyaxis left
291 plot(theta/(2*pi),psi);
292 xlabel('Orbits'); ylabel('Rotation Angle [rad]'); hold on;
293 yyaxis right
294 plot(theta/(2*pi),dpsi); grid on;
295 xlabel('Orbits'); ylabel('Rotation Velocity [rad/s]');
296 lg = legend('Rotation Angle $\psi$', 'Rotation Velocity $\dot{\
    psi}$');
297 tl = title('$\psi$ and $\dot{\psi}$ vs orbits');
298 set(lg, 'Interpreter', 'latex'); set(tl, 'Interpreter', 'latex');
299
300 %RADIUS PLOT
301 figure;
302 plot(theta/(2*pi),Rcom / 1000 - (Re / 1000)); grid on;
303 xlabel('Orbits'); ylabel('Orbit height [km]');
304 title('CoM orbit height vs orbits');
305
306 %DEBRIS VELOCITIES PLOT
307 o = [];
308 figure;
309 o(:,1) = plot(theta/(2*pi),vDebCom / 1000, '-', 'color', [0, 0.5,
      0]); hold on;
310 o(:,2) = plot(theta/(2*pi),vRotDeb / 1000, '-', 'color', [0.8500,
      0.3250, 0.0980]); hold on;
311 o(:,3) = plot(theta/(2*pi),VR / 1000, '-', 'color', [0.4940,
    0.1840, 0.5560]); grid on;
```

```
312 legend(o(1,:), 'VDebCom', 'VRotDeb', 'VR');
313 xlabel('Orbits'); ylabel('Velocities [km/s]');
314 title('Debris velocities vs orbits');
315
316 figure;
317 for k=1:length(Ld)
318     o(:,1) = plot(theta/(2*pi),VRadDeb(:,k) / 1000, 'k'); hold on
        ;
319     o(:,2) = plot(theta/(2*pi),VNormDeb(:,k) / 1000, 'b'); hold
        on;
320     o(:,3) = plot(theta/(2*pi),VTotDeb(:,k) / 1000, 'r'); grid on
        ;
321     legend(o(1,:), 'Vrad', 'Vnormal', 'Vtotal');
322     xlabel('Orbits'); ylabel('Velocities [km/s]');
323     title('Debris radial, normal and total velocities vs orbits')
        ;
324 end
325
326 %TETHER'S BODY VELOCITIES PLOT
327 figure;
328 o(:,1) = plot(theta/(2*pi),vTetCom / 1000, '-', 'color', [0, 0.5,
    0]); hold on;
329 o(:,2) = plot(theta/(2*pi),vRotTet / 1000, '-', 'color', [0.8500,
    0.3250, 0.0980]); hold on;
330 o(:,3) = plot(theta/(2*pi),VR / 1000, '-', 'color', [0.4940,
   0.1840, 0.5560]); grid on;
331 legend(o(1,:), 'VTetCom', 'VRotTet', 'VR');
332 xlabel('Orbits'); ylabel('Velocities [km/s]');
333 title('Tethers body velocities vs orbits');
334
335 figure;
336 o(:,1) = plot(theta/(2*pi),VRadTet / 1000, 'k'); hold on;
337 o(:,2) = plot(theta/(2*pi),VNormTet / 1000, 'b'); hold on;
338 o(:,3) = plot(theta/(2*pi),VTotTet / 1000, 'r'); grid on;
339 legend(o(1,:), 'Vrad', 'Vnormal', 'Vtotal');
340 xlabel('Orbits'); ylabel('Velocities [km/s]');
341 title('Tethers body radial, normal and total velocities vs orbits
   ');
342
343 %TRANSFER ORBIT CALCULATIONS
344 for k=1:length(Ld)
345     for i = 1:length(theta)
346         adeb(i,k) = (mu * Rdeb(i,k)) / (2*mu - (VTotDeb(i,k))^2*
            Rdeb(i,k));
347         atet(i,k) = (mu * Rtet(i,k)) / (2*mu - (VTotTet(i,k))^2*
            Rtet(i,k));
348     end
349     [A] = islocalmin(adeb);
```

```
350     Minimum = find(A(:,k) == 1);
351
352     ReleasePosition(k) = Minimum(5);
353     VNormDebRelease(k) = VNormDeb(ReleasePosition(k),k);
354     VTotDebRelease(k) = VTotDeb(ReleasePosition(k),k);
355     VNormTetRelease(k) = VNormTet(ReleasePosition(k),k);
356     VTotTetRelease(k) = VTotTet(ReleasePosition(k),k);
357
358     psirelease(k) = psi(ReleasePosition(k));
359
360     adebrelease(k) = (mu * Rdeb(ReleasePosition(k),k)) / (2*mu -
            (VTotDebRelease(k)^2)*Rdeb(ReleasePosition(k),k));
361     pdeb(k) = (VNormDebRelease(k)*Rdeb(ReleasePosition(k),k))^2 /
            mu;
362     edeb(k) = sqrt(1 - pdeb(k)/adebrelease(k));
363     atetrelease(k) = (mu * Rtet(ReleasePosition(k),k)) / (2*mu -
            (VTotTetRelease(k)^2)*Rtet(ReleasePosition(k),k));
364     ptet(k) = (VNormTetRelease(k)*Rtet(ReleasePosition(k),k))^2 /
            mu;
365     etet(k) = sqrt(1 - ptet(k)/atetrelease(k));
366
367     for i = 1:length(theta)
368         Rnewdeb(i,k) = pdeb(k) / (1 + edeb(k) * cos(theta(i)+
                theta(ReleasePosition(k))));
369         Rnewtet(i,k) = ptet(k) / (1 + etet(k) * cos(theta(i)+
                theta(ReleasePosition(k))));
370         dthetadeb(i,k) = sqrt( (mu*(1 + edeb(k)*cos(theta(i)+
                theta(ReleasePosition(k))))) / (Rnewdeb(i,k)^3) );
371         dthetatet(i,k) = sqrt( (mu*(1 + etet(k)*cos(theta(i)+
                theta(ReleasePosition(k))))) / (Rnewtet(i,k)^3) );
372         dRnewdeb(i,k) = pdeb(k) * (1/(1+edeb(k)*cos(theta(i)+
                theta(ReleasePosition(k))))^2) * (edeb(k)*sin(theta(i)
                +theta(ReleasePosition(k)))) * dthetadeb(i,k);
373         dRnewtet(i,k) = ptet(k) * (1/(1+etet(k)*cos(theta(i)+
                theta(ReleasePosition(k))))^2) * (etet(k)*sin(theta(i)
                +theta(ReleasePosition(k)))) * dthetatet(i,k);
374         VTotDeb2(i,k) = sqrt(dRnewdeb(i,k)^2 + (dthetadeb(i,k)*
                Rnewdeb(i,k))^2);
375         VTotTet2(i,k) = sqrt(dRnewtet(i,k)^2 + (dthetatet(i,k)*
                Rnewtet(i,k))^2);
376
377         adeb2(i,k) = (mu * Rnewdeb(i,k)) / (2*mu - (VTotDeb2(i,k)
                )^2*Rnewdeb(i,k));
378         atet2(i,k) = (mu * Rnewtet(i,k)) / (2*mu - (VTotTet2(i,k)
                )^2*Rnewtet(i,k));
379
380         orbits(i,k) = theta(i)/(2*pi) + theta(ReleasePosition(k))
                /(2*pi);
```

```
    end
end

o = [];
figure;
o(:,1) = plot(theta/(2*pi),adeb / 1000);
xlabel('Orbits'); ylabel('Semi-major axis [km]'); hold on;
plot(theta/(2*pi),adeb2(:,1) / 1000,'-', 'color', [0, 0.4470,
    0.7410],'LineWidth',1.5); hold on;
plot(theta/(2*pi),adeb2(:,2) / 1000,'-', 'color', [0.8500,
    0.3250, 0.0980],'LineWidth',1.5); hold on;
plot(theta/(2*pi),adeb2(:,3) / 1000,'-', 'color', [0.9290,
    0.6940, 0.1250],'LineWidth',1.5); hold on;
plot(theta/(2*pi),adeb2(:,4) / 1000,'-', 'color', [0.4940,
    0.1840, 0.5560],'LineWidth',1.5); grid on;
legend(o(:,1), 'Ltet=80m, Ldeb=800m', 'Ltet=100m, Ldeb=1000m', '
    Ltet=120m, Ldeb=1200m', 'Ltet=140m, Ldeb=1400m');
title('Possible and final semi-major axis of the debris');

o = [];
figure;
o(:,1) = plot(theta/(2*pi),atet / 1000);
xlabel('Orbits'); ylabel('Semi-major axis [km]'); hold on;
plot(theta/(2*pi),atet2(:,1) / 1000,'-', 'color', [0, 0.4470,
    0.7410],'LineWidth',1.5); hold on;
plot(theta/(2*pi),atet2(:,2) / 1000,'-', 'color', [0.8500,
    0.3250, 0.0980],'LineWidth',1.5); hold on;
plot(theta/(2*pi),atet2(:,3) / 1000,'-', 'color', [0.9290,
    0.6940, 0.1250],'LineWidth',1.5); hold on;
plot(theta/(2*pi),atet2(:,4) / 1000,'-', 'color', [0.4940,
    0.1840, 0.5560],'LineWidth',1.5); grid on;
legend(o(:,1), 'Ltet=80m, Ldeb=800m', 'Ltet=100m, Ldeb=1000m', '
    Ltet=120m, Ldeb=1200m', 'Ltet=140m, Ldeb=1400m');
title('Possible and final semi-major axis of the tethers body');

figure;
for k=1:length(Ld)
    plot(orbits(:,k),(Rnewdeb - Re)/1000); grid on;
    legend('Ltet=80m, Ldeb=800m', 'Ltet=100m, Ldeb=1000m', 'Ltet
        =120m, Ldeb=1200m', 'Ltet=140m, Ldeb=1400m');
    xlabel('Orbits'); ylabel('Orbit height [km]');
    xlim([orbits(1,k) orbits(1,k)+5])
    title('New orbit heights of the debris after release');
end

figure;
for k=1:length(Ld)
    plot(orbits(:,k),(Rnewtet - Re)/1000); grid on;
```

```
418     legend('Ltet=80m, Ldeb=800m', 'Ltet=100m, Ldeb=1000m', 'Ltet
            =120m, Ldeb=1200m', 'Ltet=140m, Ldeb=1400m');
419     xlabel('Orbits'); ylabel('Orbit height [km]');
420     xlim([orbits(1,k) orbits(1,k)+5])
421     title('New orbit heights of the tethers body after release');
422 end
423
424
425
426 %------- Varying radius of the perigee -------
427
428 clc;clear;close all;
429 syms y(x);
430 %THETA = x, PSI = y
431
432 G = 6.674e-11;
433 Me = 5.972e24;
434 mu = G * Me;
435 rad = pi/180;
436 Re = 6371000;
437
438 %ORBIT INTERVAL
439 x0 = 0;
440 xf = 5 * 2*pi;
441 xinterval = (x0:rad*1:xf);
442
443 %INITIAL ANGLES
444 y0 = 0.2;
445 dy0 = 0;
446 initialconditions = [y0; dy0];
447
448 %RADIUS PERIGEE
449 rp = 2000000 + Re;
450 for k=2:4
451     rp(k) = rp(k-1) + 1000000;
452 end
453
454 %MASSES AND LENGTHS
455 Md = 100;
456 Mt = 1000;
457 Lt = 120;
458 Ld = (Mt / Md) * Lt;
459
460 %ECCENTRICITY
461 e = 0.1;
462
463 %VELOCITIES
464 [theta, Y] = ode45(@(theta, Y) Differential(theta,Y,e),xinterval,
```

```
    initialconditions);
psi = Y(:,1);
dpsi = Y(:,2);
for k=1:length(rp)
    for i=1:length(theta)
        Rcom(i,k) = (rp(k)*(1+e))/(1+e*cos(theta(i)));
        dtheta(i,k) = sqrt((mu*(1+e*cos(theta(i)))) / ((Rcom(i,k)
            )^3));
        dRcom(i,k) = rp(k)*(1+e)*(1/(1+e*cos(theta(i)))^2)*(e*sin
            (theta(i)))*dtheta(i,k);
        Rdeb(i,k) = sqrt(Ld^2+(Rcom(i,k))^2-2*Ld*Rcom(i,k)*cos(
            psi(i)));
        Rtet(i,k) = sqrt(Lt^2+(Rcom(i,k))^2+2*Lt*Rcom(i,k)*cos(
            psi(i)));

        VR(i,k) = dRcom(i,k);
        vRotTet(i,k) = dtheta(i,k) * Rtet(i,k);
        vRotDeb(i,k) = dtheta(i,k) * Rdeb(i,k);
        vTetCom(i,k) = Lt * dpsi(i);
        vDebCom(i,k) = Ld * dpsi(i);

        phi1(i,k) = asin((Rcom(i,k) * sin(psi(i)))/Rdeb(i,k)) -
            pi/2;
        lambda1(i,k) = pi/2 - phi1(i,k) - psi(i);
        phi2(i,k) = asin((Rcom(i,k) / Rtet(i,k)) * sin(pi - psi(i
            )));
        lambda2(i,k) = psi(i) - phi2(i,k);

        VRadDeb(i,k) = - vDebCom(i,k) * cos(phi1(i,k)) + VR(i,k)
            * cos(lambda1(i,k));
        VNormDeb(i,k) = vRotDeb(i,k) + vDebCom(i,k) * sin(phi1(i,
            k)) + VR(i,k) * sin(lambda1(i,k));
        VRadTet(i,k) = - vTetCom(i,k) * sin(phi2(i,k)) + VR(i,k)
            * cos(lambda2(i,k));
        VNormTet(i,k) = vRotTet(i,k) + vTetCom(i,k) * cos(phi2(i,
            k)) - VR(i,k) * sin(lambda2(i,k));
        VTotDeb(i,k) = sqrt(VRadDeb(i,k)^2 + VNormDeb(i,k)^2);
        VTotTet(i,k) = sqrt(VRadTet(i,k)^2 + VNormTet(i,k)^2);
    end
end

%PSI PLOT
figure;
yyaxis left
plot(theta/(2*pi),psi);
xlabel('Orbits'); ylabel('Rotation Angle [rad]'); hold on;
yyaxis right
plot(theta/(2*pi),dpsi); grid on;
```

```
502 xlabel('Orbits'); ylabel('Rotation Velocity [rad/s]');
503 lg = legend('Rotation Angle $\psi$', 'Rotation Velocity $\dot{\
    psi}$');
504 tl = title('$\psi$ and $\dot{\psi}$ vs time');
505 set(lg, 'Interpreter', 'latex'); set(tl, 'Interpreter', 'latex');
506
507 %RADIUS PLOT
508 figure;
509 plot(theta/(2*pi),Rcom / 1000 - (Re / 1000)); grid on;
510 legend('hper = 2000km', 'hper = 3000km', 'hper = 4000km', 'hper =
     5000km');
511 xlabel('Orbits'); ylabel('Orbit height [km]');
512 title('CoM orbit height vs orbits');
513
514 %DEBRIS VELOCITIES PLOT
515 o = [];
516 figure;
517 o(:,1) = plot(theta/(2*pi),vDebCom / 1000, '-', 'color', [0, 0.5,
     0]); hold on;
518 o(:,2) = plot(theta/(2*pi),vRotDeb / 1000, '-', 'color', [0.8500,
     0.3250, 0.0980]); hold on;
519 o(:,3) = plot(theta/(2*pi),VR / 1000, '-', 'color', [0.4940,
    0.1840, 0.5560]); grid on;
520 legend(o(1,:), 'VDebCom', 'VRotDeb', 'VR');
521 xlabel('Orbits'); ylabel('Velocities [km/s]');
522 title('Debris velocities vs orbits');
523
524 figure;
525 o(:,1) = plot(theta/(2*pi),VRadDeb / 1000, 'k'); hold on;
526 o(:,2) = plot(theta/(2*pi),VNormDeb / 1000, 'b'); hold on;
527 o(:,3) = plot(theta/(2*pi),VTotDeb / 1000, 'r'); grid on;
528 legend(o(1,:), 'Vrad', 'Vnormal', 'Vtotal');
529 xlabel('Orbits'); ylabel('Velocities [km/s]');
530 title('Debris radial, normal and total velocities vs orbits');
531
532 %TETHER'S BODY VELOCITIES PLOT
533 figure;
534 o(:,1) = plot(theta/(2*pi),vTetCom / 1000, '-', 'color', [0, 0.5,
     0]); hold on;
535 o(:,2) = plot(theta/(2*pi),vRotTet / 1000, '-', 'color', [0.8500,
     0.3250, 0.0980]); hold on;
536 o(:,3) = plot(theta/(2*pi),VR / 1000, '-', 'color', [0.4940,
    0.1840, 0.5560]); grid on;
537 legend(o(1,:), 'VTetCom', 'VRotTet', 'VR');
538 xlabel('Orbits'); ylabel('Velocities [km/s]');
539 title('Tethers body velocities vs orbits');
540
541 figure;
```

```
542 o(:,1) = plot(theta/(2*pi),VRadTet / 1000, 'k'); hold on;
543 o(:,2) = plot(theta/(2*pi),VNormTet / 1000, 'b'); hold on;
544 o(:,3) = plot(theta/(2*pi),VTotTet / 1000, 'r'); grid on;
545 legend(o(1,:), 'Vradial', 'Vnormal', 'Vtotal');
546 xlabel('Orbits'); ylabel('Velocities [km/s]');
547 title('Tethers body radial, normal and total velocities vs orbits
    ');
548
549 %TRANSFER ORBIT CALCULATIONS
550 for k=1:length(rp)
551     for i = 1:length(theta)
552         adeb(i,k) = (mu * Rdeb(i,k)) / (2*mu - (VTotDeb(i,k))^2*
              Rdeb(i,k));
553         atet(i,k) = (mu * Rtet(i,k)) / (2*mu - (VTotTet(i,k))^2*
              Rtet(i,k));
554     end
555     [A] = islocalmin(adeb);
556     Minimum = find(A(:,k) == 1);
557
558     ReleasePosition(k) = Minimum(3);
559     VNormDebRelease(k) = VNormDeb(ReleasePosition(k),k);
560     VTotDebRelease(k) = VTotDeb(ReleasePosition(k),k);
561     VNormTetRelease(k) = VNormTet(ReleasePosition(k),k);
562     VTotTetRelease(k) = VTotTet(ReleasePosition(k),k);
563
564     psirelease(k) = psi(ReleasePosition(k));
565
566     adebrelease(k) = (mu * Rdeb(ReleasePosition(k),k)) / (2*mu -
          (VTotDebRelease(k)^2)*Rdeb(ReleasePosition(k),k));
567     pdeb(k) = (VNormDebRelease(k)*Rdeb(ReleasePosition(k),k))^2 /
          mu;
568     edeb(k) = sqrt(1 - pdeb(k)/adebrelease(k));
569     atetrelease(k) = (mu * Rtet(ReleasePosition(k),k)) / (2*mu -
          (VTotTetRelease(k)^2)*Rtet(ReleasePosition(k),k));
570     ptet(k) = (VNormTetRelease(k)*Rtet(ReleasePosition(k),k))^2 /
          mu;
571     etet(k) = sqrt(1 - ptet(k)/atetrelease(k));
572
573     for i = 1:length(theta)
574         Rnewdeb(i,k) = pdeb(k) / (1 + edeb(k) * cos(theta(i)+
              theta(ReleasePosition(k))));
575         Rnewtet(i,k) = ptet(k) / (1 + etet(k) * cos(theta(i)+
              theta(ReleasePosition(k))));
576         dthetadeb(i,k) = sqrt( (mu*(1 + edeb(k)*cos(theta(i)+
              theta(ReleasePosition(k))))) / (Rnewdeb(i,k)^3) );
577         dthetatet(i,k) = sqrt( (mu*(1 + etet(k)*cos(theta(i)+
              theta(ReleasePosition(k))))) / (Rnewtet(i,k)^3) );
578         dRnewdeb(i,k) = pdeb(k) * (1/(1+edeb(k)*cos(theta(i)+
```

```
            theta(ReleasePosition(k))))^2) * (edeb(k)*sin(theta(i)
            +theta(ReleasePosition(k))) * dthetadeb(i,k);
        dRnewtet(i,k) = ptet(k) * (1/(1+etet(k)*cos(theta(i)+
            theta(ReleasePosition(k))))^2) * (etet(k)*sin(theta(i)
            +theta(ReleasePosition(k))) * dthetatet(i,k);
        VTotDeb2(i,k) = sqrt(dRnewdeb(i,k)^2 + (dthetadeb(i,k)*
            Rnewdeb(i,k))^2);
        VTotTet2(i,k) = sqrt(dRnewtet(i,k)^2 + (dthetatet(i,k)*
            Rnewtet(i,k))^2);

        adeb2(i,k) = (mu * Rnewdeb(i,k)) / (2*mu - (VTotDeb2(i,k)
            )^2*Rnewdeb(i,k));
        atet2(i,k) = (mu * Rnewtet(i,k)) / (2*mu - (VTotTet2(i,k)
            )^2*Rnewtet(i,k));

        orbits(i,k) = theta(i)/(2*pi) + theta(ReleasePosition(k))
            /(2*pi);
    end
end

o = [];
figure;
o(:,1) = plot(theta/(2*pi),adeb / 1000);
xlabel('Orbits'); ylabel('Semi-major axis [km]'); hold on;
plot(theta/(2*pi),adeb2(:,1) / 1000,'-', 'color', [0, 0.4470,
    0.7410],'LineWidth',1.5); hold on;
plot(theta/(2*pi),adeb2(:,2) / 1000,'-', 'color', [0.8500,
    0.3250, 0.0980],'LineWidth',1.5); hold on;
plot(theta/(2*pi),adeb2(:,3) / 1000,'-', 'color', [0.9290,
    0.6940, 0.1250],'LineWidth',1.5); hold on;
plot(theta/(2*pi),adeb2(:,4) / 1000,'-', 'color', [0.4940,
    0.1840, 0.5560],'LineWidth',1.5); grid on;
legend(o(:,1), 'hper = 2000km', 'hper = 3000km', 'hper = 4000km',
    'hper = 5000km');
title('Possible and final semi-major axis of the debris');

o = [];
figure;
o(:,1) = plot(theta/(2*pi),atet / 1000);
xlabel('Orbits'); ylabel('Semi-major axis [km]'); hold on;
plot(theta/(2*pi),atet2(:,1) / 1000,'-', 'color', [0, 0.4470,
    0.7410],'LineWidth',1.5); hold on;
plot(theta/(2*pi),atet2(:,2) / 1000,'-', 'color', [0.8500,
    0.3250, 0.0980],'LineWidth',1.5); hold on;
plot(theta/(2*pi),atet2(:,3) / 1000,'-', 'color', [0.9290,
    0.6940, 0.1250],'LineWidth',1.5); hold on;
plot(theta/(2*pi),atet2(:,4) / 1000,'-', 'color', [0.4940,
    0.1840, 0.5560],'LineWidth',1.5); grid on;
```

```
609 legend(o(:,1), 'hper = 2000km', 'hper = 3000km', 'hper = 4000km',
        'hper = 5000km');
610 title('Possible and final semi-major axis of the tethers body');
611
612 figure;
613 for k=1:length(Ld)
614     plot(orbits(:,k),(Rnewdeb - Re)/1000); grid on;
615     legend('hper = 2000km', 'hper = 3000km', 'hper = 4000km', '
            hper = 5000km');
616     xlabel('Orbits'); ylabel('Orbit height [km]');
617     xlim([orbits(1,k) orbits(1,k)+5])
618     title('New orbit heights of the debris after release');
619 end
620
621 figure;
622 for k=1:length(Ld)
623     plot(orbits(:,k),(Rnewtet - Re)/1000); grid on;
624     legend('hper = 2000km', 'hper = 3000km', 'hper = 4000km', '
            hper = 5000km');
625     xlabel('Orbits'); ylabel('Orbit height [km]');
626     xlim([orbits(1,k) orbits(1,k)+5])
627     title('New orbit heights of the tethers body after release');
628 end
```